Thermal Conductivity Measurement at Ultra Low Temperatures

by

Issam Alkhesho

A thesis
presented to the University of Waterloo
in fulfillment of the
thesis requirement for the degree of
Master of Science
in
Physics

Waterloo, Ontario, Canada, 2010

I hereby declare that I am the sole author of this thesis. This is a true copy of the thesis, including any required final revisions, as accepted by my examiners.

I understand that my thesis may be made electronically available to the public.

Abstract

Thermal Conductivity studies can provide fundamental information regarding the symmetry of the superconducting energy gap.

To perform this kind of experiment, we need to use a very low temperature environment. Also a special mount has been to designed and constructed for the thermal conductivity measurements. This mount will allow holding the sample in different directions with respect to the applied magnetic field.

The results are consistent with Wiedemann-Franz law to within 2.5%. We also discuss a series of thermal conductivity experiments to shed additional light on the symmetry of the superconducting order parameter in the unconventional superconductor $PrOs_4Sb_{12}$.

Acknowledgements

I would like to thank all the people who made this possible, specially my advisor Robert Hill for his great support and guidances during this program and also I admire his patience and knowledge regarding this research. I also would like to thank My committee member Professor Walter Duley for his great support and encouragement.

I thank the department of physics for permitting me this opportunity to endeavour in the pursuance of my study.

Dedication

This is dedicated to the one I love, My wife Munera for her support and to my lovely kids, Rawan, Lana, and Andre.

Table of Contents

List of Figures

Chapter 1

Introduction

When a chunk of matter becomes superconducting, its resistance doesn't just become very small, it really becomes zero. This is very remarkable property in such could be applied to make the loss of transmitting electric power through a conductor almost zero. This happens when the material is extremely cooled down to a very low temperature called T_c, at the same temperature the same material will repels any external magnetic field, this superconducting property has many applications, for example, in nowadays technology superconducting magnets are some of the most powerful electromagnets known, they are used in MRI and NMR machines, they can provide high magnetic fields as well as they can work in a persistent mode for long time without loosing any current at all. Not surprisingly, its difficult and expensive to cool materials down to these low temperatures, for superconductors to be used on a large scale for their exceptional properties, their operating temperatures need to be much higher. Many materials have been discovered to have superconducting properties below 21K, a complete satisfactory theory explains the phase transformation from normal state to superconducting state has been proposed using BCS theory. It provides a full explanation about the superconducting state, this theory shows the mechanism of the coupling between the electron pairing is mediated by phonons. However, for long time, it was believed that according to the BCS theory there can't be any high temperature superconductor material until the discovery of the superconductivity in a lanthanum-based cuprate pervoskite materials, this discovery raised T_c to 30K, but by replacing lanthanum with yttrium, T_c went up to 92K, in which liquid nitrogen the inexpensive cryogenic liquid can be used to cool them down. This discovery opened a wide hope and prompted the researchers to concentrate more on finding material that could exhibit superconductivity at more higher temperatures even at room temperatures. However, understanding how thinks work is just as important as inventing a new technology, many theories and explanations have been proposed to explain the high T_c superconducting phenomena, but a complete model that is entirely understood has not been proposed

yet. One of the most powerful methods to understand the high T_c superconducting state is by studying the order symmetry parameter in the superconducting phase, this could be done by more investigation about the type and the shape of the energy gap.

The majority of superconductors have a conventional s-wave energy gap. But, also an unconventional superconductivity with a gap symmetries other than s-wave has been found such as the heavy fermion compounds. Several unusual features have been reported concerning the superconducting state of $PrOs_4Sb_{12}$. These later studies revealed the presence of nodes and lowering of symmetry of the gap [14]. The presence of these nodes in the gap structure is very related to the pairing interaction of the electrons. Although, the total picture about the presence of these nodes is believed to be a pairing mechanism "other than phonons" interaction instead of a conventional electron-phonon mediated interaction, yet, the intrinsic nature of $PrOs_4Sb_{12}$ has not been clearly established and a complete model has not been proposed specially regarding the nodes nature and locations. One way to distinguish whether the superconductor has nodes or not is by measuring its thermal conductivity [9]. At very low temperature analysis become more clear because the contribution of electrons and phonons to the thermal conductivity measurements can be separated. As for a superconductor, this low temperature is limited and has to be within the range of ($\frac{T}{T_C}$<0.1), because the lower the temperature the less contribution from the qusiparticles to the thermal conductivity, and any contribution would be from phonons only, also at this regime the only factor that limits the mean free path of the heat carriers is the impurities and the sample boundaries. Therefore, lowering T as much as its possible would help in measuring any small residual electronic contribution, then an explanation for the gap shape could be revealed whether the sample has fully opened s-shape gap, or it has a d-shape gap with nodes.

To get access to low temperatures, dilution fridge is needed because it can provide low temperatures as low as 10 mK continuously. In this research, installing a dilution fridge will be shown with all considerations that needs to be taken care of, especially the isolation issue from the sources of noise which make the set-up vibration free. Also by conducting a fundamental tests on a known materials would provide a clear picture about the accuracy of the interested experiments. Thermal conductivity of silver has been measured and compared with the Wiedemann Franz law, other experiments on studying the temperature sensors have been carried over during this research. In chapter two a review on the theory of thermal conductivity will be detailed. In chapter three details about constructing and installing the dilution fridge will be shown. While in chapter four and five some experimental results and observations will be discussed.

Chapter 2

Review of Theory for Thermal Conductivity

2.1 Introduction

Heat can be transmitted through solids via electrical carriers, phonons, electromagnetic waves, spin waves or other excitations. In metals electrons carry the majority of the heat, while in insulators phonons are the dominant heat transporter. At very low temperatures, the total thermal conductivity κ will be to the sum of all the components representing various excitations, i.e., $\kappa = \sum_{ex} \kappa_{ex}$, where (ex) denotes an excitation.

In the coming section calculating the total thermal conductivity of a material will be shown, that is by implicitly making the assumption that electrons and phonons are the main heat carriers. Although, there are other possible excitations in the structure of metals and in the magnetic insulators such as the spin waves, under certain circumstances, contribute a small additional term, we shall not consider these small contributions.

On the other hand, the thermal conductivity of superconductors may be given in a simple term from the viewpoint of the two-fluid model and the Bardeen-Cooper-Schrieffer (BCS) theory. The property of the superconducting states are such that carriers are not scattered by phonons or by impurities. The specific heat of these superconducting electrons is zero, hence, they cannot contribute to the heat transport. And as the temperature is reduced below T_c fewer normal electrons can carry heat, so the thermal conductivity becomes less than its when the metal is in the normal state. Therefore, in some superconductors that are usually called "conventional superconductors", their superconducting state is isotropic and it could be explained by the BCS theory, will not have a contribution from the electronic conductivity part, hence, the energy gap between the superconducting and the normal state will have a simple spherical shape "fully gaped". Whereas in

some other superconductors that are called an "unconventional superconductors", their state can't be explained using the BCS theory, they would show some contribution from the electronic conductivity part, and hence, the energy gap will have a low value at some points called the "nodes".

2.2 The Kinetic Theory

Following the solid state physics text books, [44] [2] [28], according to this theory the thermal conductivity κ is defined as

$$\kappa = -\frac{\dot{Q}}{\nabla T} \tag{2.1}$$

Where $\dot{Q}$ is the heat flow rate or heat flux across a unit cross section, ∇T is the temperature gradient across the sample. Using the concepts of this theory a relation that shows the proportionality between thermal conductivity κ, specific heat C_v, and the mean free path ℓ can be deduced. In order to explore how those parameters are related to each other, we will start with a more fundamental property, the density of states (DOS) of a system which describes the number of states at each energy level that are available to be occupied, also it characterizes the electronic properties of a solid. A high DOS at a specific energy level means that there are many states available for occupation. A DOS of zero means that no states can be occupied at that energy level. To calculate the DOS ($g(E)$) we need to find the number of states N per unit sample volume V at an energy E inside an interval $[E, E + dE]$. The general form of ($g(E)$) of a system is given as:

$$g(E) = \frac{1}{V}\frac{dN}{dE} \tag{2.2}$$

$g(E)$ is often combined with a probability distribution that gives the likelihood of occupation of a particular state. The product of the ($g(E)$) and the probability distribution function is the number of occupied states per unit volume at a given energy for a system in thermal equilibrium. There are two common distribution functions: The Fermi-Dirac probability distribution function is used to find the probability that a fermion occupies a specific quantum state in a system at thermal equilibrium. Fermions are particles which obey the Pauli Exclusion Principle [no two identical fermions particles with half-integer spin e.g. (electrons, protons, neutrons) may occupy the same quantum state simultaneously]. The distribution function in equilibrium can be written as:

$$f_{FD}(E) = \frac{1}{\exp(\frac{E-\mu}{k_B T} + 1)} \tag{2.3}$$

μ is the chemical potential, often referred to as the Fermi level or Fermi energy and written as E_F.

The second distribution function considered is the Bose-Einstein probability distribution function. This is used to find the probability that a boson occupies a specific quantum state in a system at thermal equilibrium. Bosons are particles which do not obey the Pauli Exclusion Principle, e.g. (phonons and photons). In equilibrium, the distribution function can be written as:

$$f_{BE}(E) = \frac{1}{\exp(\frac{\hbar\omega_{\vec{k}}}{k_B T} - 1)} \tag{2.4}$$

These two distribution, in conjunction with DOS, can be used to calculate properties such as the internal energy U, specific heat capacity C_v of the heat carriers (phonons or electrons), and thermal conductivity κ. The relationships between these properties and the product of the $g(E)$ and the probability distribution are [44]:

$$U = \int Ef(E)g(E)dE \tag{2.5}$$

$$C_v = \frac{\partial}{\partial T}\int Ef(E)g(E)dE \tag{2.6}$$

$$\kappa = \frac{1}{d}\frac{\partial}{\partial T}\int Ef(E)g(E)v(E)\ell(E)dE \tag{2.7}$$

where d=3 is dimensionality (the factor 1/3 comes from the fact that the heat flow is in one direction), v is the velocity of the heat carriers and ℓ is mean free path. Combining equations (2.6) and (2,7) we obtain a relationship between thermal conductivity and specific heat,

$$\kappa = \frac{1}{3}C_v v\ell \tag{2.8}$$

We now consider the relationship in Eq.(2.8) for different heat carriers.

2.3 Phonon thermal conductivity

Thermal energy can be stored in the vibrational normal mode of the crystal, therefore one can transport thermal energy through the lattice using theses modes. At low temperatures the fact that the allowed energies of a normal mode are quantized is of critical importance, and would make the description of this transport more convenient when using the language of phonon. According to Eq.(2.8), if we would like to calculate the lattice thermal conductivity, we need to calculated the phonon specific heat first. To do so we need to use the Debye model. The assumption has been made in this theory is that the atomic system

is assumed to be an elastic continuum in which only certain frequencies are allowed to propagate or to be excited and maintained. These frequencies will be those which are able to set up a standing waves, any others will die rapidly. Also, the average phonon velocity υ approximately equals to the velocity of sound [41]. For a quantum harmonic oscillator of angular frequency ω, a mode of vibration would have on average

$$<n> = \frac{1}{\exp^{(\frac{\hbar\omega}{k_B T})} - 1} \tag{2.9}$$

phonons associated with it at temperature T, then $<n>$ is called the "phonon occupancy" of the mode. A solid with N atoms would have 3N vibrational modes each with an energy $<E>$ and phonon occupancy $<n>$. Because, in a solid, the particular direction of propagation of the vibration of any wave length in which the standing wave conditions are satisfied, there will be other directions in which a standing wave with the same value of the wave length could be maintained. Each of these vibrations associated with a different direction is called a mode, and for each direction there will be three modes corresponding to the two transverse and one longitudinal vibrations which can be excited. The number of modes in a frequency range between ω and $\omega + d\omega$ is $(g(\omega).d\omega)$ and each of these modes is considered as being due to a separate oscillator which will have a mean energy at temperature T given by

$$\bar{U} = \frac{1}{2}\hbar\omega + \frac{\hbar\omega}{\exp^{\frac{\hbar\omega}{k_B T}} - 1} \tag{2.10}$$

Thus the internal energy of the system will be

$$U = \int_0^{\omega_{max}} \bar{U} g(\omega).d\omega \tag{2.11}$$

where ω_{max} is the maximum frequency which is excited. Such a frequency must exist because otherwise the energy of the system would become infinity. In the Debye theory the actual distribution function is given by

$$g(\omega)d\omega = 4\pi(\frac{1}{v_\ell^3} + \frac{2}{v_t^3})V\omega^2 d\omega \tag{2.12}$$

where v_ℓ and v_t are the velocities of the longitudinal and transverse waves in the medium, V is the volume. This theory also predicts that the modes which are able to be excited are assumed to be those of the lowest possible frequencies up to the maximum number of 3N. The maximum frequency of oscillation ω_{max} (later on is denoted by ω_D) is determined by ensuring that when Eq.(2.12) is integrated between 0 and ω_{max} it will give 3N modes, i.e.,

$$3N = \frac{4}{3}\pi(\frac{1}{v_\ell^3} + \frac{1}{v_t^3})V\omega_{max}^3 \tag{2.13}$$

Using Eq.(2.13) a substitution can be made for bracketed term in (2.12) to obtain

$$g(\omega).d\omega = \frac{9N}{\omega_{max}^3}\omega^2 d\omega \tag{2.14}$$

By substituting equations (2.10) and (2.14) in (2.11), the temperature-dependent energy is equal to

$$U = \frac{9N}{\omega_{max}^3}\int_0^{\omega_D} \frac{\hbar\omega^3 d\omega}{[\exp^{(\frac{\hbar\omega}{k_B T})} - 1]} \tag{2.15}$$

where this upper limit can be expressed in terms of a Debye characteristic temperature:

$$\Theta_D = \frac{\hbar\omega}{k_B} = \frac{\hbar v_s}{k_B}(\frac{6\pi^2 N}{V})^{\frac{1}{3}} \tag{2.16}$$

v_s is the velocity of sound, Θ_D is a measure temperature below which phonons begin to "freeze out". By changing the dimensionless variable ($x = \frac{\hbar\omega_{max}}{k_B T}$), and ($x_{max} = \frac{\Theta_D}{T}$), then substituting them into equation(2.15) the resulting lattice vibrational energy per unit volume is

$$U = [\frac{9Nk_B T^4}{\Theta_D^3}]\int_0^{\frac{\Theta_D}{T}} \frac{x^3 dx}{e^x - 1} \tag{2.17}$$

Differentiating with respect to T, one would obtain the specific heat

$$C_v = (\frac{\partial U}{\partial T})_v = [\frac{9Nk_B T^3}{\Theta_D^3}]\int_0^{\frac{\Theta_D}{T}} \frac{x^4 e^x dx}{(e^x - 1)^2} \tag{2.18}$$

At high temperatures much larger than Θ_D, i.e. when $(k_B T/\hbar)$ is large compared with all the phonon frequencies, or when every normal mode is in a highly excited state, the integral $[\frac{1}{e^x - 1} = \frac{1}{x}[1 - \frac{x}{2} + ...]]$, then $x = \frac{\hbar\omega}{k_B T} \ll 1$, the energy becomes 3RT and this yields to the Dulong and Petit value for the specific heat of 3R.

At low temperatures (about $\frac{\Theta_D}{10}$), equation(2.18) may be simplified to [2]

$$C_{ph}(T) = \frac{12}{5}\pi^4 N_o k_B(\frac{T}{\Theta_D})^3 = 1944(\frac{T}{\Theta})^3(\frac{Joule}{mole.K}) \equiv \beta T^3 \tag{2.19}$$

we obtained the well known T^3 phonon or the lattice specific heat expression.

Referring to Eg.(2.8), v_s is considered constant at low T (T $\ll \frac{\Theta_D}{10}$) [The characteristic velocity of phonons is the velocity of the sound v_s, this is the velocity with which

"vibrations" or "phonons" move through the lattice [44]. Typical values for solids are $v_s = (3-5) * 10^3 \frac{cm}{sec}$ [32]], therefore

$$\kappa_{ph} \propto T^3 \ell_{ph}(T) \qquad at \qquad T \ll \frac{\Theta_D}{10} \tag{2.20}$$

In a perfectly harmonic crystal, phonon thermal conductivity in Eq.(2.20) would have an infinite value, because the phonon states are stationary states and therefore if a distribution of phonons has been established, it will remain unaltered in a course of time. But the reality is different, these phonons encounter many types of scattering "thermal resistances" and hence limiting the thermal conductivity of the material, particularly by affecting the term ℓ_{ph}. The main scattering processes limiting the thermal conductivity are phonon-phonon (which is absent in the harmonic approximation), phonon- defect, electron-phonon, electron-impurity. To calculate the total thermal resistance one needs to follow "Matthiessen's rule" which simplifies the problem by assuming that one scattering process is not influenced by others which are occurring in the same time. According to this rule the resistance of various scattering process may be calculated separately and their sum would give the total thermal resistivity [35]. The total phonon thermal resistivity W_{ph}will be the sum of a number of resistivities,

$$W_{ph} = W_{Um} + W_i + W_b + W_d \tag{2.21}$$

W_{Um} is the resistivity due to interaction of phonons with one another "umklapp process", where in an ideal pure crystal for the over most temperature range will determine the thermal resistance. W_i is the resistance due to scattering by point defects (impurity atom, isotopes, etc.), W_b is resistance due to scattering by the boundaries of the specimen or the crystallites, and W_d is the resistance due to scattering by dislocations.

At low temperatures (T$\ll \Theta_D$), the number of thermally excited phonons is small, and they are no longer important for scattering (due to the exponential suppressed in the umklapp processes), the phonon which carry heat are scattered by crystal defect or by crystal boundaries. Because at low temperatures the dominant phonon wavelength is larger than the size of the lattice imperfections, phonon-boundary scatter W_b is the important process. Since ℓ is temperature independent at theses temperatures, therefore, κ then is given by the temperature dependence of the specific heat and decreases strongly with temperature as T^3, also, it depends on the size of the specimen. Large amount of impurities and dislocations will also decrease the conductivity, see figure 2.1.

However, one needs to point out that, all the scattering mechanism that has been discussed above which are operative in insulators, will be still operative in metal crystals. In addition, there is one mechanism in metals which tends to dominate all the others, this is the scattering of the phonons by the conduction electrons and it gives rise to a phonon

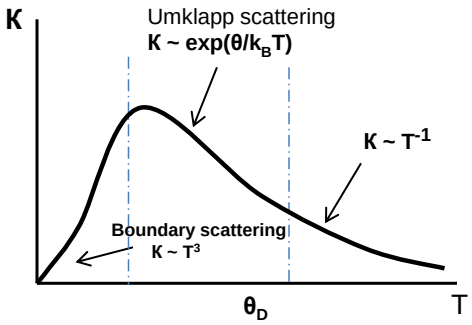

Figure 2.1: Representation of the low- temperature thermal conductivity of isolators, it shows a steep exponential rise in the conductivity due to the reduction in the number of umklapp-processes, followed by a decrease due to the T^3 boundary scattering term, which usually occurs at the range $\dfrac{\Theta_D}{10}$. from [35].

resistivity $W_{(ph,e)}$, which is given by

$$W_{ph,e} = ET^{-2} \tag{2.22}$$

this temperature dependence is because of the following reason: The mean free path ℓ of the phonons will be proportional to the number of electrons with which they can interact. The only electrons with which this is possible are those whose energy lies within k_BT of the Fermi energy ξ_F, and the proportion of these electrons to the total number present will be of the order $\frac{k_BT}{\xi_F}$. Hence, the number of electrons available for scattering will be proportional to T and therefore ℓ will vary as T^{-1}. If one assumes that the phonon velocity υ is constant and that C_v is proportional to T^3, then, from the kinetic theory $W_{ph,e}$ is proportional to T^{-2}.

2.4 Electron thermal conductivity

In order to calculate the electron thermal conductivity, again we need to find the electron specific heat first using equations (2.2),(2.3),(2.6), we will follow [2],[41],[3]. Also the free electron model will be assumed, which is the simplest way to represent the electronic structure of metals. At T = 0K this function is a step function that sharply divides the occupied states from the unoccupied states, with the Fermi energy playing marked line between the two. At $E<E_F$, all available single-electron states are fully occupied while for $E>E_F$ all states are empty, thus Fermi energy is the highest occupied energy level. Using

the single-electron approximation, apart from their distribution function, one also needs to know the number of energy states per unit volume in a unit energy interval, i.e., the DOS. The density of electrons per unit volume is

$$n = \int_0^\infty g(E)f(E,T)dE \tag{2.23}$$

n=$\frac{N}{V}$ and N is the number of electrons at temperature T. When electrons are heated from absolute zero temperature to some finite T, their internal energy is increased by

$$U(T) = \int_0^\infty E.g(E).f(E,T).dE - \int_0^{E_F^0} E.g(E).dE \tag{2.24}$$

the second integral in Eq.(2.24) represents the internal energy of electrons U(0) at T=0K due to Pauli exclusion principle [41]. The electronic specific heat will be

$$C_e = \frac{dU}{dT} = \int_0^\infty (E - E_F).g(E)\frac{df(E,T)}{dT}dE \tag{2.25}$$

Since we are only interested in temperatures for which $k_BT \ll E_F$ the derivative $\frac{df}{dT}$ is large only at the energies which lie very close to the Fermi energy. Therefore, we can ignore the variation of $g(E)$ under the integral and take it outside the integrand at the Fermi energy, so that

$$C_e = g(E)\int_0^\infty (E - E_F).\frac{df(E,T)}{dT}dE \tag{2.26}$$

Another approximation will be used as well, which is by ignoring the variation of the chemical potential with the temperature and assume that $\mu = E_F$. This is a good approximation at room temperature and below [2], thus

$$\frac{f(E,T)}{dT} = \frac{E - E_F}{k_BT^2}\,\frac{e^{(E-E_F)/k_BT}}{[e^{(E-E_F)/k_BT}+1]^2} \tag{2.27}$$

Eq.(2.25) can, then, be rewritten as

$$C_e = g(E_F)\int_0^\infty \frac{(E-E_F)^2}{k_BT^2}\,\frac{e^{(E-E_F)/k_BT}}{[e^{(E-E_F)/k_BT}+1]^2} = g(E_F)\int_{\frac{-E_F}{k_BT}}^\infty \frac{x^2(k_BT)^3}{k_BT^2}\,\frac{e^x}{(e^x+1)^2}dx \tag{2.28}$$

Taking into account that $E_F \gg k_BT$, we can put the low integration limit to minus infinity [28] and obtain

$$C_e = k_B^2Tg(E_F)\int_{-\infty}^{+\infty}\frac{x^2e^x}{(e^x+1)^2}dx = \frac{\pi^2}{3}k_B^2Tg(E_F) \tag{2.29}$$

Where $x = (E - E_F)/k_BT$. For a free electron gas the DOS becomes, (details are given in Appendix III)

$$g(E) = \frac{(2m)^{\frac{3}{2}}}{2\pi^2\hbar^3}E^{\frac{1}{2}} \tag{2.30}$$

and the density of electrons per unit volume will be expressed as

$$n = \frac{2}{3}g(E_F)E_F \tag{2.31}$$

with the definition of the Fermi temperature $T_F = \frac{E_F}{k_B}$, the heat capacity of electrons per unit volume can be obtained as

$$C_e = \frac{\pi^2}{2}nk_B\frac{T}{T_F} \tag{2.32}$$

Whereas the specific heat per mole of the substance [2] since it contains ZN_A conduction electrons (where Z is the valence and) and occupies a volume (ZN_A/n) will be equal to

$$C_e = \frac{\pi^2}{2}ZR\frac{T}{T_F} \equiv \gamma T \quad valid\,at \;\; k_BT \ll E_F \tag{2.33}$$

Again referring to Eg.(2.8), the thermal conductivity due to conduction electrons will be

$$\kappa_e \propto T\ell_e(T) \tag{2.34}$$

Usually, in metal, this electronic thermal conductivity is considerably larger than the phonon thermal conductivity because the Fermi velocity of conduction electrons is much larger than the sound velocity. Fermi velocity is determined by the kinetic Fermi energy E_F, typical values [2] are

$$v_F = \frac{\hbar}{m_e}\left(\frac{3\pi^2N_A}{V_m}\right)^{\frac{1}{3}} \;\; = \;\; 10^7 - 10^8 \;\; \frac{cm}{sec} \gg v_s \tag{2.35}$$

Where $\hbar = \frac{h}{2\pi}$, m_e is mass of electron, N_A is number of atoms per mole "Avogadro's number", and V_m is the molar volume.

At low temperatures, the number of phonons is again small, the dominant scatter would be from the defects and impurities. As a result the electronic contribution will go through a maximum with value and position strongly depends on the perfection of the metal, the defects will give rise to a mean free path ℓ which is temperature independent. Using the kinetic formula introduced earlier, providing that the specific heat of electrons is proportional to T and assuming the velocity to be constant, the thermal conductivity is proportional to T,

$$\kappa_e \propto T \tag{2.36}$$

Figure 2.2-a shows the thermal conductivity for a typical metal, also it shows the experimental results for some materials.

Conclusion

From the above and from the previous section results one would arrive at the following equation for the total specific heat of a metal at low temperatures, (low means small compared to the Debye temperature),

$$C = \gamma T + \beta T^3 \tag{2.37}$$

where γ and β are constants. And in conclusion, we see that κ is related to the temperature via the dependence of the specific heat on temperature, hence, the total thermal conductivity at low temperature can be written as,

$$\kappa_{total} = \kappa_e + \kappa_{ph} = AT + BT^3 \tag{2.38}$$

2.5 Wiedemann-Franz law

In metals, most of the heat actually is carried by electrons, and since these electrons carry charge, hence theses carriers carry both heat and charge. Therefore At low temperatures there must be clearly a mathematical relationship between the electrical and thermal conductivities. This may be obtained very simply from the expressions we have already presented. Following [41], one can deduce this relationship, the thermal conductivity is given in Eq.(2.8) by $\kappa = \frac{1}{3} C_v v \ell$, and by using Eq.(2.30) for the electron specific heat, $v_e^2 = \frac{2E_F}{m}$ for the electron velocity (where $E_F = T_F k_B$), and $\sigma = \frac{ne^2\tau}{m}$ for the electrical conductivity (where, $\tau = \ell/v$), we would obtain

$$\kappa = \frac{1}{3}(\frac{\pi^2}{2} N_A k_B \frac{T}{E_F})(\frac{2E_F}{m})^{\frac{1}{2}} \ell \tag{2.39}$$

then

$$\frac{\kappa}{\sigma T} = \frac{\pi^2}{3}(\frac{k_B}{e})^2 \;\equiv\; L_o = 2.44 \times 10^{-8} \;\; \frac{Watt.\Omega}{K^2}. \tag{2.40}$$

This relationship is commonly referred to as the Wiedemann-Franz law. L_o is usually called the Lorenz number [43]. It shows that all metals have the same electronic thermal conductivity to electrical conductivity ratio, and this ratio is proportional to absolute temperature. Furthermore, Eg.(2.39) is independent of the scattering mechanism and the band structure of the electrons as long as the scattering is elastic, other wise, this law will fail. Typically this is valid at very low temperatures ($T \ll \Theta_D$) (0 to 10K) [3] and at high temperatures only, else where is not valid. Figure 2.2-b illustrates the temperature dependence of Lo.

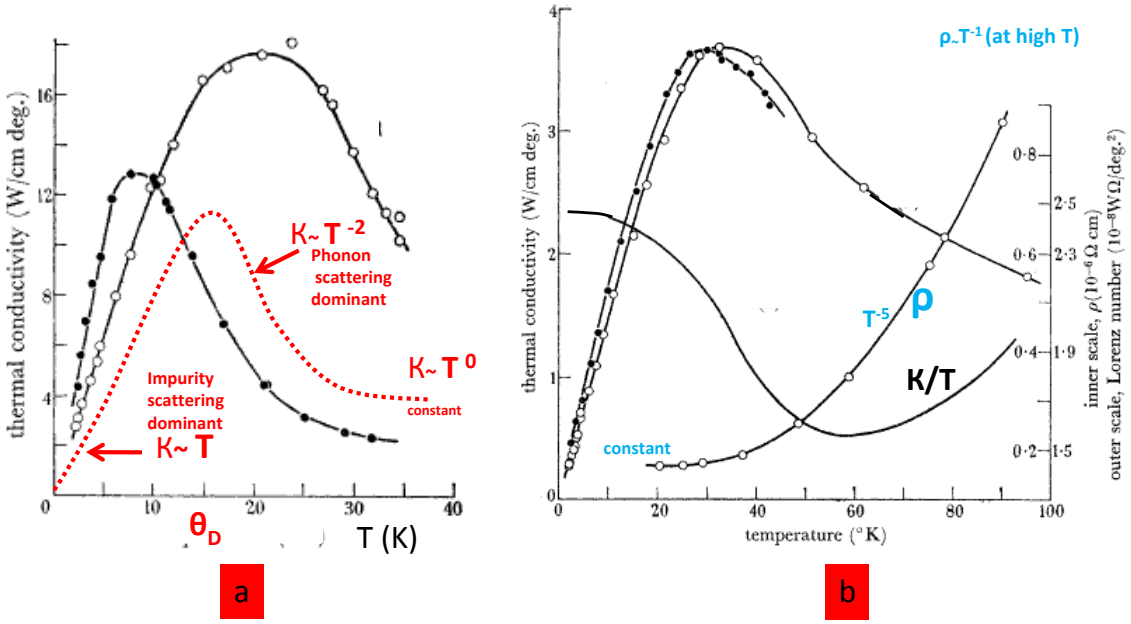

Figure 2.2: a) [red dots] Electronic thermal conductivity for typical metal along with experimental results of the measured electronic thermal conductivity for two different metals (black circles) and (white circles), note that the peak occurs below 10 K where the electron-phonon scatter process will have no effect because the phonons will have long wave length at low T (they cannot see the electrons), the electron will only scatter with impurities in an elastic collision. b) [black dots] Experimental results of the electronic thermal conductivity for tungsten compared with the calculated values [white curlicues] with the temperature dependence of the resistivity and κ/T term plots. From κ/T plot note that this term is constant at very low temperature (where the W-F law is valid) because in that range the impurity scattering is dominant and the resistivity is constant, therefore both the heat and charge conductivity are affected. As T is increased the electron scatter will be inelastic with a little effect on the charge conductivity but affects the thermal conductivity, therefore κ/T will decrease to a minimum value depends on the sample purity, hence, the W-F is not valid. At very high temperatures, charge conductivity is proportional to T^{-1} due to classic scatter with phonons, and the heat conductivity is constant, hence, the W-F law will be valid again. from [34]

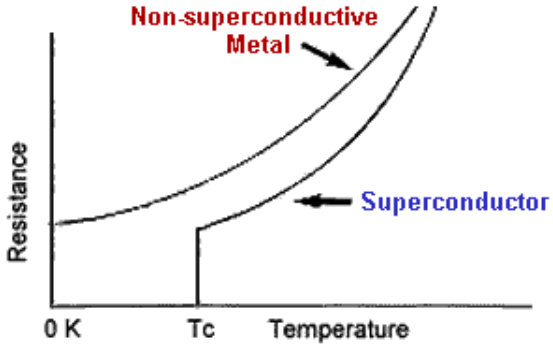

Figure 2.3: Resistance of a superconductor material goes to zero in discontinuously at T_c compared to a non superconductive material where the resistance has a finite value even at T=0.

2.6 Thermal conductivity of Superconductors

2.6.1 Superconductivity: Overview and Phenomenology

Zero Resistance

A superconductor is a perfect conductor of charge, but poor conductor of heat. Most, but not all, conductors of electrical current, when cooled sufficiently in the direction of absolute zero K become superconductors. The superconducting state itself is one in which there is zero electrical resistance. This means that current flowing through a superconducting circuit does not experience I^2R heating, and the current can flow indefinitely, this property happens discontinuously at certain temperature T_c (defined as the "critical temperature" for that superconductor), see figure 2.3.

Meissner Effect

Now we know that when a material is in the superconducting phase, it exhibits zero resistivity. Thus, the induced currents persist, because there are no scattering mechanisms to dissipate the currents, therefore the internal field in the material also persists, and the total magnetic field inside the cylinder remains at zero, which means the sample became perfectly diamagnetic. This zero magnetic field inside the superconducting material is referred to as the Meissner effect. It is another fundamental property of superconductors, see figure 2.4.

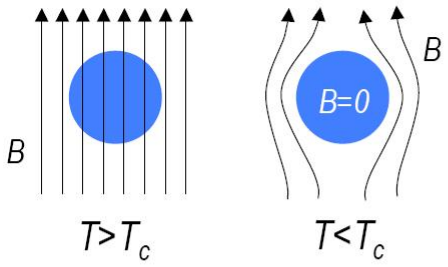

Figure 2.4: Meissner- Ochsenfeld effect. (Left picture) When the external magnetic field exceeds the threshold field strength, the superconducting material behaves like a normal conductor. (Right picture)When the material is in superconducting state the field is expelled from the superconductor. The superconductor produces its own field such that completely cancels the external magnetic flux.

Conventional Superconductor-Electron Pairing (BCS theory)

In 1957 the underlying microscopic theory of superconductivity in metals was unveiled by J. Bardeen, L.N. Cooper and J.R. Schrieffer [26] in the now famous BCS theory. BCS theory suggests the superconductivity as a microscopic effect caused by a "condensation" of pairs of electrons into a boson-like state, the electrons team up in "Cooper pairs". This process is called phonon-mediated coupling because of the sound packets generated by the flexing of the crystal lattice. The essential point is that below T_c the binding energy of a pair of electrons causes the opening of a gap in the energy spectrum at E_F (the Fermi energy), separating the pairs states from the "normal" single electron states. The mechanism behind the weak attractive force binding the cooper pairs was actually first suggested by Herbert Frolich [23]. He proposed that the same mechanism responsible for much of the electrical resistivity in metals (i.e., the interaction of conduction electrons with lattice vibrations) leads to a state of superconductivity. In simple terms, an electron interacts with the lattice by virtue of the Coulomb attraction it feels for the metallic ions. The result is a deformation of the lattice (i.e. a phonon). A second electron in the vicinity of the deformed lattice correspondingly lowers its energy, resulting in an electron-electron attraction via a phonon. This bound state is a configuration of electrons in which states of electrons of equal but opposite momentum and spin are both either occupied or unoccupied. The instability of the Fermi sea against the formation of these pairs causes a gap of order of $k_B T_c$, it is the minimum energy required to create a single-electron (hole) excitation from the superconducting ground state. Thus the binding energy of a cooper pairs is two times the energy gap $\Delta(T)$. BCS theory estimates the zero-temperature energy gap $\Delta(0)$

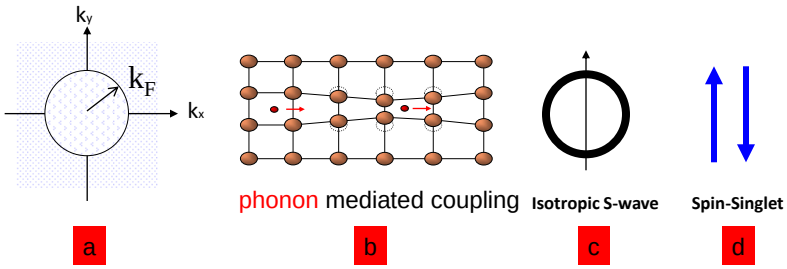

Figure 2.5: BCS symbols for a conventional superconductor. a) In metals the Fermi surface separates the filled from empty states at T=0 and for simplicity it is drawn as a spherical shape. b) Schematic of phonon mediated coupling which is the mechanism behind formation the electron pairs. c) The instability of the Fermi sea against the formation of these electron pairs causes a gap of $k_B T_c$ with no angular dependence, which implies an s-wave shape. d) The spin part of the wave function is therefore antisymmetric and the electron pairs are in spin singlet state.

[40] as,

$$E_g(0) = 2\Delta(0) = 3.528\ k_B T_c \quad for \quad T \ll T_c \tag{2.41}$$

and

$$\frac{\Delta(T)}{\Delta(0)} = 1.74\ (1 - \frac{T}{T_c})^{\frac{1}{2}} \quad at \quad T \approx T_c \tag{2.42}$$

So that the energy gap approaches zero continuously as $T \to T_c$, otherwise it will be finite over the entire Fermi surface. Under ideal circumstances, the magnitude of the gap is the same at all points on the Fermi surface and for simplicity its assumed to be spherical, see figure 2.5. Superconductors which obey Eq.(2.48) are considered to be weakly-coupled, in reference to the weak interaction energy between electrons in a cooper pair. Furthermore, the wave functions corresponding to cooper pairs are spatially symmetric like an atomic s-orbital with angular momentum L=0. That is to say, the wave function of a pair is unchanged if the positions of the electrons are exchanged. This immediately implies that the spin part of the wave function is antisymmetric in accordance with the Pauli exclusion principle. In particular, the electron pairs are in a spin-singlet state s=0 with anti-parallel spins which is the rule among low-temperature superconductors,[24].

Response to Magnetic Field

Superconductor materials are classified into two type depending on their response to the external magnetic field:

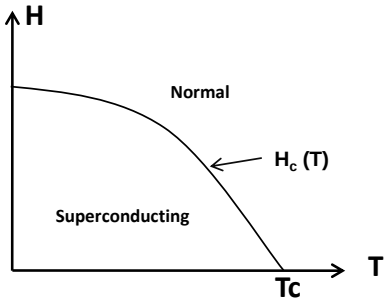

Figure 2.6: Type I superconductor, the phase boundary between the superconducting and normal state. The boundary is given by the curve

Type I: The Type I category of superconductors is mainly comprised of simple metals and metalloids, they exhibit a very sharp transition to a superconducting state at T_c. Below a critical field $H_c(T)$ that increases as T falls below T_c, there is no penetration of flux, when the applied field exceeds $H_c(T)$ the entire specimen reverts to the normal state and the filed penetrates perfectly, see figure 2.6.

Type II: The Type II category of superconductors is comprised of metallic compounds and alloys (includes all high-temperature superconductors). This category of superconductors was identified by L.V. Shubnikov when he found two distinct critical magnetic fields (known as Hc_1 and Hc_2) in $PbTi_2$, see figure 2.7. Type II superconductors differ from Type I in that their transition from a normal to a superconducting state is gradual across a region of "mixed state" behaviour [1]. Below a lower critical $H_{c1}(T)$ there is no penetration of flux, when the applied field exceeds an upper critical field $H_{c2}(T)>H_{c1}(T)$, the entire specimen reverts to the normal state and the field penetrates perfectly [2]. When the applied field strength is between $H_{c1}(T)$ and $H_{c2}(T)$, there is a partial penetration of flux and the sample develops a rather complicated microscopic structure of both normal and superconducting regions, known as the mixed state [29]. Since a Type II will allow some penetration by an external magnetic field into its surface, this creates some rather novel microscopic phenomena like superconducting "stripes" and "lattice vortices" [40], see figure 2.8.

Unconventional Superconductors

In 1986, "high-temperature superconductivity" was discovered (i.e. superconductivity at temperatures considerably above the previous limit of about 30 K; up to about 130 K),

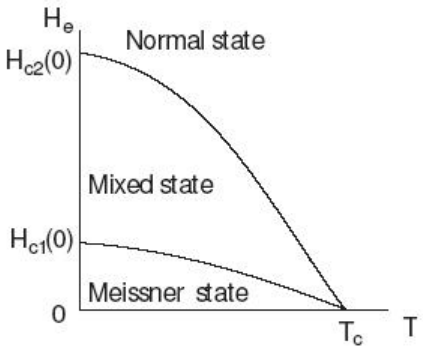

Figure 2.7: Type II superconductor with an existence of a mixed state between Hc_1 and Hc_2. Above H$_{c1}$, magnetic flux from external fields is no longer completely expelled, and the superconductor exists in a mixed state. Above the higher magnetic flux H$_{c2}$, the superconductivity is completely destroyed, and the material exists in a normal state.

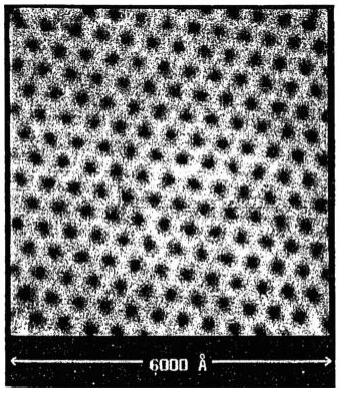

Figure 2.8: Magnetic vortices in $NbSe_2$ defined by scanning tunnelling microscopy. from[1]

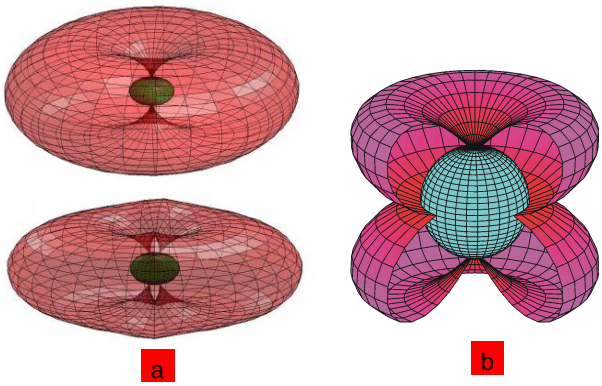

Figure 2.9: a) 3 dimensional illustration of the Fermi surface with the energy gap function in an unconventional superconductors. In (a) it shows the energy gap function with point nodes at the polars, whereas in (B) the energy gap has d-wave with a combination of point nodes and a line nodes. from [17]

this type of superconductivity is defined as one that lies outside the scope of the simplest BSC model, therefore they are called an unconventional [40]. The difference between the conventional and unconventional superconductors can be in the gap symmetry other than s-wave, and the type of interactions which give rise to the formation of cooper pairs is most likely due to e-coupling instated of a phonon coupling, this type of pairing and the condensation happens at high T_c. A high T_c "superconductors" and a heavy fermions superconductors for example might have a d-wave gap symmetry, the mechanism behind the paring is still unknown but certainly is not a simple phonon mechanism. Hence, the symmetry of the order parameter in unconventional superconductors comparing to BCS superconductors is reduced so that there might be gap-less even for the pure specimens. The nodal structure on the Fermi surface of unconventional superconductors can be series of line nodes or point nodes, figure 2.9 shows a superconducting gap with nodes.

This thesis examines the gap symmetry which has implications regrading the paring mechanism too, the probe for this examination is by measuring the thermal conductivity as discussed earlier in the previous sections as well as in the following section, see figure 2.11-a.

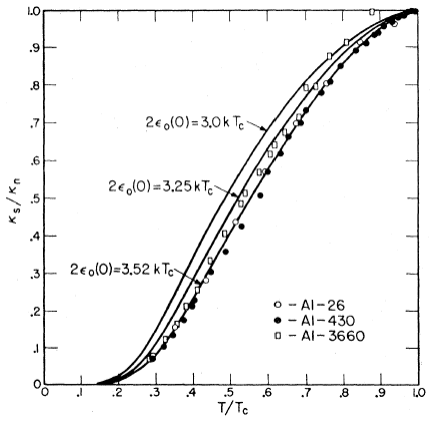

Figure 2.10: The ratio of superconducting to normal thermal conductivity vs $\frac{T}{T_c}$ for Aluminium. from [37]

2.6.2 Thermal conductivity in Conventional (Fully gaped) S/C

In a superconducting metals some of the electrons are paired to what is called a "Cooper pairs". They all sit in the same low-energy state of zero entropy which is separated by an energy gap ΔE from the states of the single, unpaired electrons. The cooper pairs cannot leave this ground state to carry heat unless they are broken up into single electrons. Therefore in a superconducting state only the remaining unpaired electrons can carry heat [9], their number decreases exponentially with T, i.e., as e^{-E/k_BT}, where

$$\kappa_{e,s} \propto Te^{-E/k_BT} \tag{2.43}$$

with ΔE = 1.76 k_BT for most elemental superconductors. Hence, the electronic thermal conductivity of superconductor decreases very rapidly with decreasing T. The mean free path of phonons is limited by electron-phonon scattering, then the thermal conductivity of phonons will increase upon entering the superconducting state. So the competition between decreasing κ_e and increasing κ_{ph} will determine the overall dependence of thermal conductivity on temperature [38]. At low temperatures the electronic thermal conductivity of a superconducting metals can even become smaller than its lattice conductivity, see figure 2.10. In the limit of zero temperature, electronic heat conduction in a fully gaped superconductor goes to zero, as there are no thermally-excited quasiparticles to carry heat (the pairs in the condensate carry no heat). This shows up as a thermal conductivity $\kappa(T)$ whose linear term $\frac{\kappa}{T}$ goes to zero as the temperature $T \to 0$, see figure 2.11-a.

2.6.3 Thermal conductivity in Unconventional (Nodal gap) S/C

In reference [13], the electronic thermal conductivity in unconventional superconductors with line nodes has been calculated. A clean superconductor with an order parameter that vanishes along a line on the Fermi surface, is a linear function of the excitation energy, $N(\in) = N_F \frac{\in}{\Delta_0}$ for $\in < \Delta_0$. Because of impurity atoms, the density of states is approximately constant and non zero below an energy level, γ which is interpreted as the bandwidth of qusiparticle states bound to impurities. For an order parameter with a line of nodes, the bandwidth, γ, and the density of bound states at zero energy, $N(0)$, are finite for any finite concentration of impurities, [30], [9]. There is considerable evidence that some of the heavy fermions superconductors have an order parameter with a line of zeros on the Fermi surface. It has been discussed in [30] that the component of the electronic thermal conductivity tensor corresponding to quasiparticles in the vicinity of line nodes are determined by the same scattering rate as the electrical conductivity and are universal in the limit T$\rightarrow$ 0. The thermal conductivity in this vicinity can be expressed as:

$$\kappa \sim N_F(\frac{\gamma}{\Delta_0})k_B^2 T\nu_F^2(\frac{\hbar}{\gamma}) \sim N_F\nu_F^2 k_B^2 T(\frac{\hbar}{\Delta_0}) \tag{2.44}$$

Note that in Eq.(2.41) $\kappa \sim$T so that $\frac{\kappa}{T} \longrightarrow 0$ as T$\longrightarrow$0 in contrast with the fully gaped expressed in Eg.(2.40) which indicates that $\kappa \sim \exp(\mathrm{T})$.

Having establishing that fact, κ is distinguishable between a fully gapped and a nodal superconductor that is by measuring the interception of the term $\frac{\kappa_o}{T}$, see figure2.11-a.

2.6.4 Magnetic field dependency of κ

As shown in figure 2.11-b, applying magnetic field can provided information on the gap structure. So in the limit of T$\rightarrow$ 0, the field will be a way to excite quasiparticles in type II, even at T=0, and probe the excitation spectrum at finite energy. In an s-wave superconductor at the same temperature limit, the quasiparticles are localized in states within the vortex core and any conduction perpendicular to the magnetic field would be due to tunnelling between adjacent vortices which will leads to a slow rise in the $(\frac{\kappa_o}{T})$value vs H. This slow growth of $(\frac{\kappa_o}{T})$ as a function of field at H$\ll$H$_c$ is a typical signature of a node-less gap or an s-wave superconductor.

In a superconductor with a nodes, there are delocalized states outside the vortex cores even at T = 0 and these dominate the transport in the vortex state. In this case, the effect of a magnetic field is to shift the low energy states and thus excite more quasiparticles. This shift has two mechanisms: First, Doppler shift which yields to a H$^{\frac{1}{2}}$ growth in quasiparticles

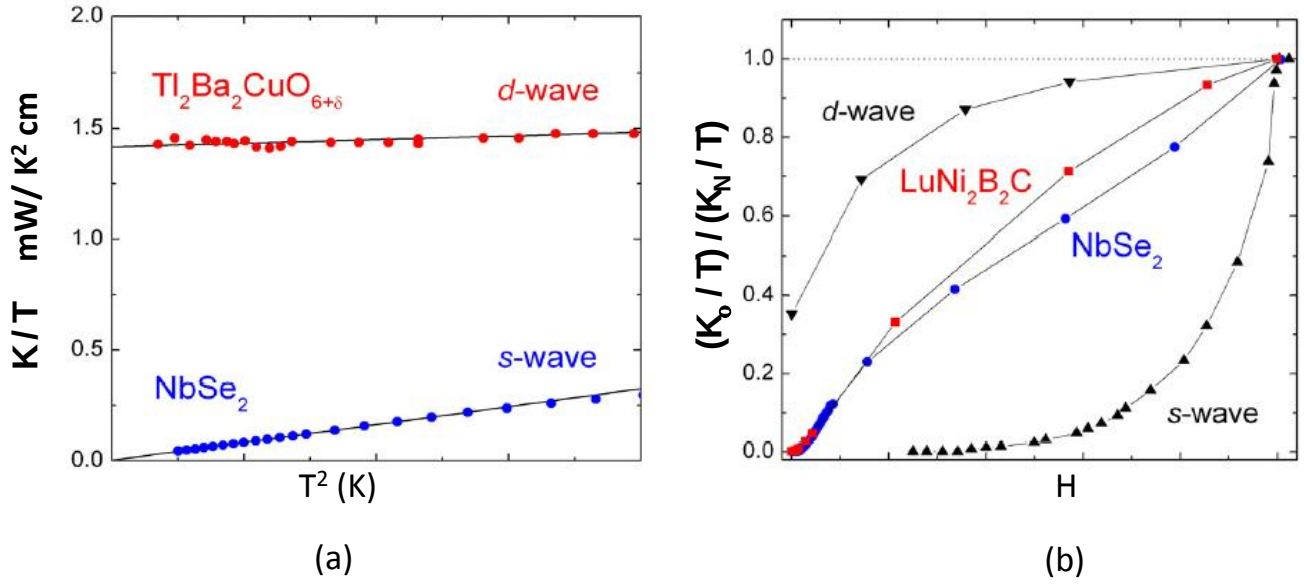

Figure 2.11: (a): Thermal conductivity of s-wave and d-wave superconductor, note the large residual linear term in the d-wave superconductor. (b):The residual linear term κ/T vs magnetic field H. from [9]

density of states. Second, the shift due to a spin coupling which yields to a linear growth in the density of states. At low fields, the first shift dominates causes $(\frac{\kappa_o}{T})$ to rise rapidly in sub-linear manner.

Chapter 3

Experimental details

Nowadays, there are many cryostats available covers a wide temperature range, for example, flow cryostats, closed systems with experimental chambers or cold fingers attachment, and multi property liquid cooled cryostats. Even if these cryostats are adequate for different kind of measurements, it is useful to understand the difference requirements and the limitations that are imposed by different property measurements. It is difficult for one system to suit all possible physical measurements on substance at all low temperatures. The complexity of such an apparatuses would be considerable, knowing the fact that a little extra difficulty in construction may allow a much wider temperature range and increased accuracy. However, a decision to choose one of all these available systems would primarily depend upon what range of temperature we do need.

3.1 Cooling Techniques

Different techniques could be used to get to the low temperatures. In order to choose one, the experiment type and its properties (specially the required temperature) are the important criteria that would decide in choosing the proper technique. Figure 3.1 shows an overview of the range of temperatures can be attained using different techniques. Its obvious from this figure that every refrigeration process lower than 10K uses liquid helium in either the final or the pre-cooled stage. The low temperatures are obtained by evaporating ^{4}He, or ^{3}He or by circulating a mixture of ^{3}He-^{4}He. Although, using the evaporation method with ^{3}He can achieve temperatures 0.3K, but with this process it cannot be done continuously, it is a single shot cooling for a few hours, then needs to be repeated again after a period of time. However, it is very important to point out the fact that the dilution ^{3}He-^{4}He refrigerators are the most practical and popular cooling techniques in the

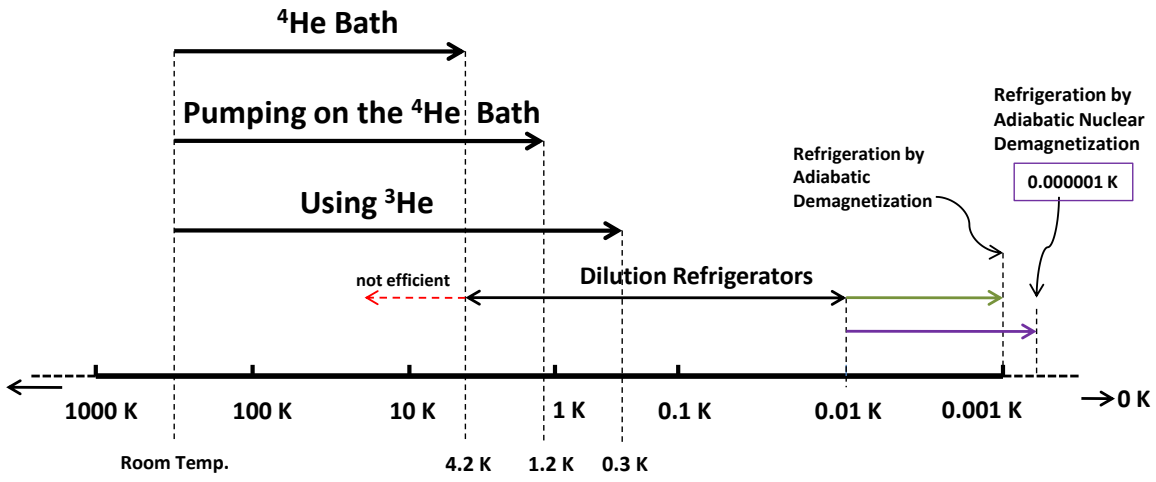

Figure 3.1: The temperature ranges drawn in logarithmic scale that could be attainable using different cooling techniques.

millikelvin range, because they can run continuously and that the cooling power at low temperatures is considerable.

3.2 Liquid helium properties and its Isotopes

In 1908 Kamerlings-Onnes succeeded in liquefying helium at 4.2 K, this opened up new avenues of research of ultra low temperatures. Helium gas when is cooled to a critical temperature of 2.17 K (called its Lambda point), a remarkable discontinuity in heat capacity occurs, the liquid density drops, and a fraction of the liquid becomes a zero viscosity "superfluid". Superfluidity arises from the fraction of helium atoms which has condensed to the lowest energy state. The common stable helium isotope is ^{4}He, its nucleus contains two protons and two neutrons, each with anti parallel nuclear spin orientation [4], therefore the total nuclear spin of ^{4}He is zero; it is a Bose particle or a Boson. While on the other hand the rare helium isotope ^{3}He constitutes a fraction $1 \sim 2 * 10^{-7}$ of helium gas from natural gas sources and about $1.3 * 10^{-6}$ of the helium gas in the atmosphere, its nucleus contains two protons and one neutron. An important property of ^{3}He which distinguishes it from the more common ^{4}He, is that its nucleus is a Fermion since it contains an odd number of spin 1/2 particles. The mass difference makes the boiling point 3.2K instead of 4.2K, because of the larger zero-point energy for the lighter atom. ^{4}He is obtained from natural gas sources, however, obtaining ^{3}He by separating it from ^{4}He is very costly and is impractical. The other method of separating is done using the diffusion processes from Tritium [19].

Both ^{3}He and ^{4}He Isotopes have low boiling points and critical temperatures, and they don't become solid under their own vapour pressure even when cooled close to absolute zero [39], one has to apply at least about 25.4 bar or 34.4 bar for $T \to 0$K, respectively, to get these two isotopes in their solid state. The origin of these observations is essentially due to the light weight of helium, the unavoidable shuffling keeps it from forming an orderly crystal. The binding forces between the atoms are very weak, they are van der Waals forces and are weak because of closed electronic s-shell of helium.

3.3 Types of Liquid He Cryostats

3.3.1 Introduction

Two important properties that determines whether a liquid is suitable for use as a refrigerant is the latent heat, L, and the vapour pressure P_{vap} [32]. For ^{4}He the latent heat is only one third of its value of the corresponding other liquids, see figure 3.2-(a and c). Due to

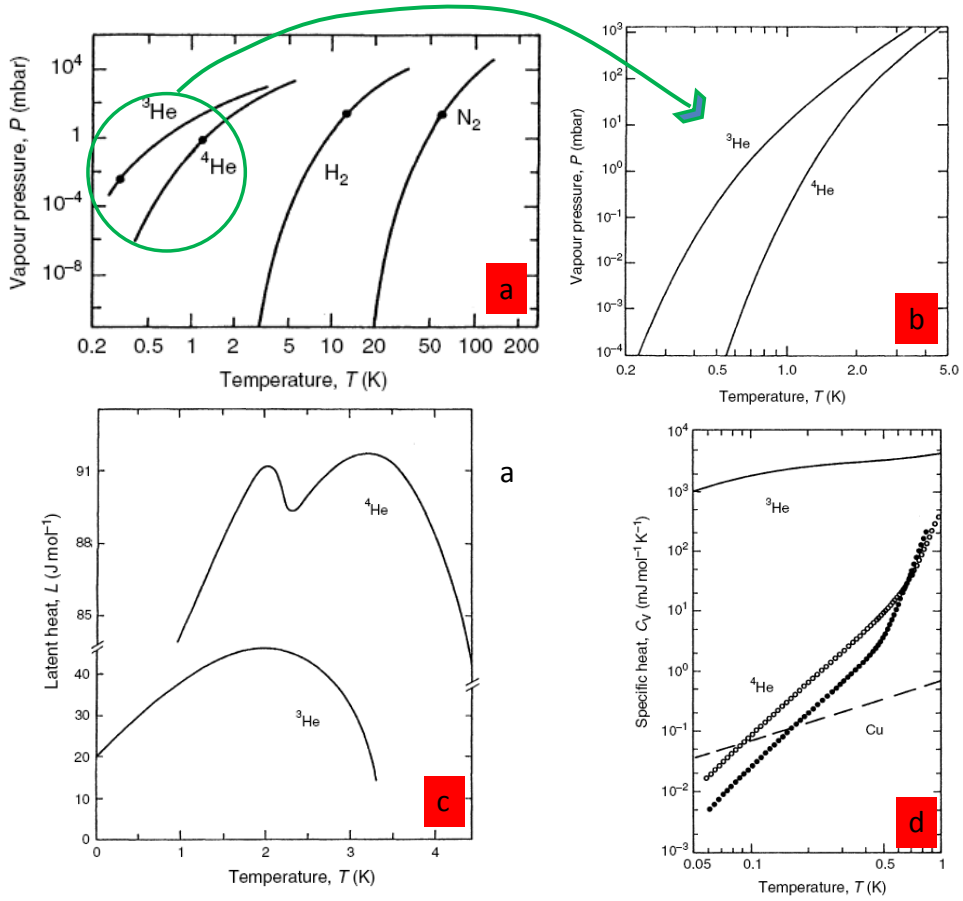

Figure 3.2: (a) Vapour pressure of various cryoliquids. (b) Vapour Pressures of liquid ^{3}He and liquid ^{4}He. (c) Latent heats of evaporation of ^{3}He and ^{4}He. Note the change of vertical scale. (d) Specific heat of Liquid ^{4}He at vapour pressure (27.58cm^3/mol,o) and about 22 bar (23.55 cm^3/mol,•) compared to the specific heats of liquid ^{3}He and of Cu. from [32].

this small value, liquid He baths have a rather small cooling power (it is very easy to evaporate them). Therefore all low temperatures experiments require efficient shielding against introduction of heat from the surroundings which could be from radiation, heat along the support of the experiments, or heat due to measurement. In the following sections, the use of liquid helium in different types of cryostats will be discussed.

3.3.2 Helium - 4 Cryostat

The idea with using this type of cryogenics is to emerge the experiment in special dewar contains liquid helium to cool it down to 4.2 K. The heat of evaporation for helium transforming from the liquid to the gaseous phase is about 82.4 J/mol (20.6 J/gm) [31] at its boiling temperature of 4.2 K, this is rather small number compare to the enthalpy of helium gas between 4.2 K and 77 K, which is about 64 (kJ/ℓit) [32]. As a result, it's very important to use the enthalpy of the cold helium after the liquid has undergoes the transition to the gaseous state when cooling the equipment, and the gas should leave the cryostat with temperature as close as possible to room temperature. On the other hand, pre-cooling with liquid nitrogen from 300 K to 77 K will save a large amount of liquid helium. Liquid Nitrogen has 60 times the latent heat of evaporation of liquid helium, its about an order magnitude cheaper. Beside, at 77 K most of the heat capacity of the materials to be refrigerated will be removed already.

Cryostat with temperature for $1.3<T<4.2$ K

The vapour pressure P varies with temperature T according to

$$\frac{dp}{dT} = \frac{\Delta S}{\Delta V} = \frac{L}{T\Delta V} \tag{3.1}$$

L is the latent heat of evaporation, S is the entropy, V is the volume, see figure 3.2-c. From this dependence, in the 1 K range, vapour pressure of all substances are extremely low except for helium. Also one can pump the vapour above the liquid helium bath to obtain temperatures below the normal (1 bar) boiling point. This technique is known as evaporative cooling it is used to obtain temperatures down to approximately 1 kelvin. In the dilution refrigerators a small vessel is filled with liquid helium, usually it is a few cubic centimetres in size with a pickup-tube extending into the primary liquid helium bath of the dewar. When a vessel containing liquid helium is connected to a vacuum pump, the vapour pressure above the liquid surface drops, thereby allowing the more energetic helium molecules to evaporate out of the liquid. As the particles evaporate and are pumped away from the liquid, they carry heat energy with them, so the remaining fluid tends to cool,

this vessel is called the 1K pot, In section (3.4.3) more details about this vessel and its position in the Oxford dilution fridge will be given.

a) **pumping on the main bath**

One can just pump the vapour above the liquid ^{4}He bath away to decrease its temperature. This is very uneconomical because 40% of the liquid has to be evaporated to cool it from 4.2 K to 1.3 K. Due to the large change of its specific heat in this temperature range, for example, at about 1.5 K the specific heat of 1 gm of ^{3}He or ^{4}He is of the order 1J/K [32], whereas the specific heat of 1 gm of Cu is only about 10^{-5} J/K at this temperature, see figure3.2-(d).

On the other hand, the specific heat of solids is rather small in this temperature range, to cool them from 4.2 to 1.3 K we have to evaporate only a small fraction of liquid ^{4}He. It's therefore much more efficient to leave the main part of the liquid at its normal boiling point of 4.2 K and just pump on a small fraction of it in a separate container to reach the lower temperature for the experiment.

b) **continuously operating ^{4}He evaporation cryostat**

In such a refrigerator a small fraction of the liquid from the main 4.2 K bath flows through a suitable flow impedance into a small vessel of several cm^3 located in a vacuum can inside the cryostat. Through the central tube we pump on the liquid arriving in this evaporation vessel. Figure 3.3 is a schematic of a continuous ^{4}He cryostat. The liquid from

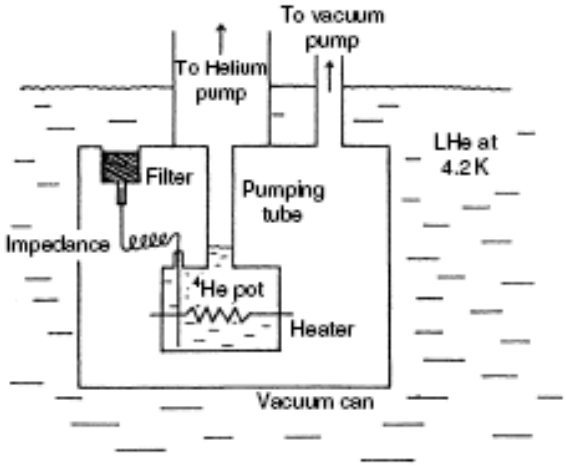

Figure 3.3: Schematic of continuously operating ^{4}He. from [32].

the main bath at 1 Bar isenthalpically expanded through the impedance and will arrive at

lower temperature in the evaporation vessel. Almost half of the heat of evaporation is used for cooling the liquid, the other half can be utilized to fill up the inner vessel with liquid and to cool something else. This vessel will continue to fill until the level of the liquid is at certain height at which the heat transferred from the main helium bath through this column of liquid, plus the heat from the experiment, just balance the cooling power of the refrigerator available from the latent heat of evaporation. This technique of using an impedance to control the flow of liquid helium could be fixed (by using a certain length of a capillary tube), or variable impedance (by using an adjustable needle valve). Each method has its own advantageous and its disadvantageous. To show a comparison between these two methods, in fixed impedance, no control could be provided to the Liquid flow, hence the base temperature would be fixed at a certain point. Whereas, using the variable impedance, one can change the rate of the flow of the liquid Helium, this would provide more power to remove more high energetic molecules, hence lowering down the base temperature. On the other hand, the disadvantageous of using the variable impedance is through adding an extra mechanical parts to the system which would add more complication, beside arising the problems of blocking the valve by accumulating the moistures or the impurities, as well as the mechanical problems. The problem of blocking the flow could be existed in the fixed impedance method too.

3.3.3 Helium - 3 Cryostat

The temperature range accessible with the liquid ^{4}He bath is typically 4.2 - 1.3 K, but this temperature can be extended to about 0.3 K if the rare isotope ^{3}He is used instead of the common isotope ^{4}He. The main reason is that ^{3}He has a substantially larger vapour pressure than ^{4}He at the same temperature, the ratio $P3/P4$ is 74 at 1 K but about 10^4 at the 0.5 K [32]. A further advantage of using liquid ^{4}He at temperatures below their normal boiling point is due to the fact that the specific heat of liquid ^{3}He varies much less between, for example, 2 and 0.5 K than the specific heat of ^{4}He does. One therefore has to evaporate only about 20% of ^{3}He to cool this liquid from 1.5 to 0.3 K by using its own heat of evaporation. Furthermore, the specific heat of liquid ^{3}He is larger than the specific heat of liquid ^{4}He below 1.5 K, resulting in a large heat reservoir in this temperature range. Finally liquid ^{3}He is not super-fluid in the temperature range of concern in this research, therefore it does not have the heat transfer problems sometimes arising from the super-fluid film flow of liquid ^{4}He. However, there are two rather serious disadvantageous of using liquid ^{3}He. First, its latent heat of evaporation is substantially smaller than that of liquid ^{4}He, hence this will not allow using it in a continuous cooling systems, it can be used in a single pulse mode cooling systems. Second, and more important, ^{3}He is much more expensive than ^{4}He. One can only use ^{3}He in a closed gas handling and cryogenic system.

3.3.4 ^{3}He -^{4}He Dilution Refrigerators

The principle of operation of the dilution refrigerator was originally proposed by H. London in 1951. When a mixture of the two stable isotopes of helium is cooled below a critical temperature it separates into two phases [15]. The lighter "concentrated phase" is rich in ^{3}He and the heavier "dilute phase" is rich in ^{4}He. Since the enthalpy of the ^{3}He in the two phases is different, it is possible to obtain cooling by "evaporating ^{3}He" from the concentrated phase into the dilute phase. The dilution refrigerator can reach temperatures of the order of a few millikelvin (mK) above absolute zero continuously. This is the only method by which it can be achieved.

Phase Diagram and Solubility

^{4}He is a Bose liquid which undergoes a transition to superfluid. The superfluidity has two consequences; first, ^{3}He may flow through liquid ^{4}He with little impedance; second, the refrigerator must be completely leak tight. On the other hand, ^{3}He is a Fermi fluid which is highly viscous. At dilution fridge temperatures superfluid ^{4}He may be considered to be in its ground state with very little entropy, whilst ^{3}He has a large entropy [31]. As the phase diagram of the ^{3}He-^{4}He mixtures in figure 3.4 shows, the miscibility of the two isotopes is very limited. The reason for this limiting concentration lies in the quantum fluid behaviour of the liquid, but the utility of it is that at the lowest temperatures ^{3}He dissolves in ^{4}He. Between 2.87K and 0.867K a superfluid can only exist under a maximal amount of ^{3}He which increases with decreasing temperature. But below 0.867K an interesting effect leads to a split up into two phases. The superfluid phase of ^{4}He contains 6.6% of the lighter isotope and is therefore called diluted phase. The ^{3}He almost behaves like a perfect gas in a mechanical vacuum with no mutual friction between the atoms, but sensitive to pressure. On the other hand a concentrated phase of almost pure ^{3}He forms. As an effect of different densities the concentrated phase floats on top of the diluted phase, additionally the ^{3}He atoms in the concentrated phase have lower enthalpy than in the diluted phase. But if a ^{3}He crosses the phase boundary to the diluted phase, its enthalpy must increase, this energy can be taken from a surrounding system and is the basic cooling principle in dilution refrigerators. As a result, the flow rate of ^{3}He across the phase boundary may be kept high even at the lowest temperatures and very high cooling powers may be achieved. This is in contrast to an evaporative refrigerator in which the rapidly diminishing vapour pressure reduces the number of atoms moving into the vapour and thus stops further cooling taking place.

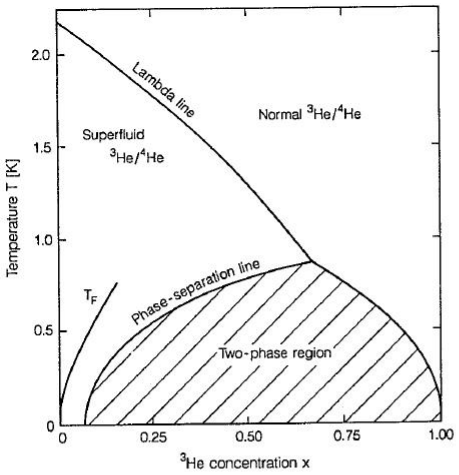

Figure 3.4: Phase diagram of liquid at saturated vapour pressure. The diagram shows the lambda line for the super-fluid transition of ^{4}He, the phase separation line of the mixtures below which they separate into ^{4}He- rich and a ^{3}He- rich phase, and the line of the Fermi temperatures T_F of the ^{3}He component. from [32].

3.4 Kelvinox Cryomagnetic System Components

3.4.1 Introduction

The ^{3}He/^{4}He dilution refrigerators has now become a standard laboratory instrument for the production of ultra low temperatures for a variety of research purposes, specially to perform experiments in the millikelvin temperature range. The dilution refrigerator consist of two main parts, the main bath ^{4}He dewar, and the dilution unit insert (where the insert must be mounted in the dewar). Figure 3.5 shows the entire cryomagnetic system installation used in this research. There are three main parts to a dilution unit insert: the Still, the Mixing Chamber, and between them, the Heat Exchangers (more details about each one of them will be given in the next section). Figure 3.6 illustrates the important parts of a dilution unit insert. Oxford Instruments is one of the world largest suppliers of these dilution refrigerators where they combine in their products the dilution refrigerator and superconducting magnet systems in one integrated unit in order to obtain the extreme condition of ultra low temperature and high magnetic field for a variety of research applications. In this type of refrigerators, always it involves pumps and vacuum environment. These pumps are used to circulate the gas mixture by removing it from the fridge and compress it to a certain pressure, then pass it through filters to remove impurities and return it to the cryostat. Indeed, working below the atmospheric pressure

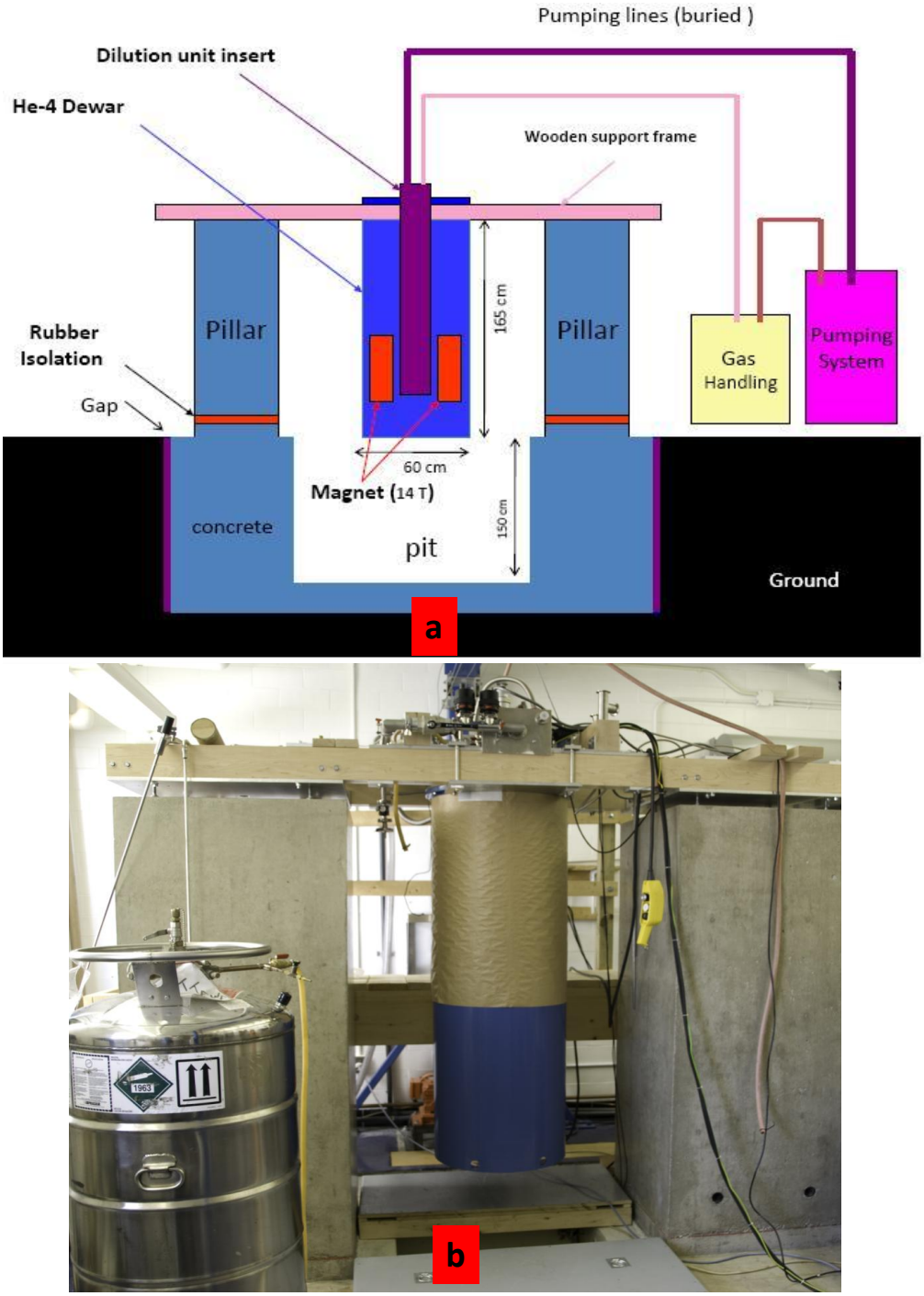

Figure 3.5: a) Schematic picture of the main parts of the Oxford dilution refrigerator. b) Real picture of the entire Oxford cryomagnetic system installation.

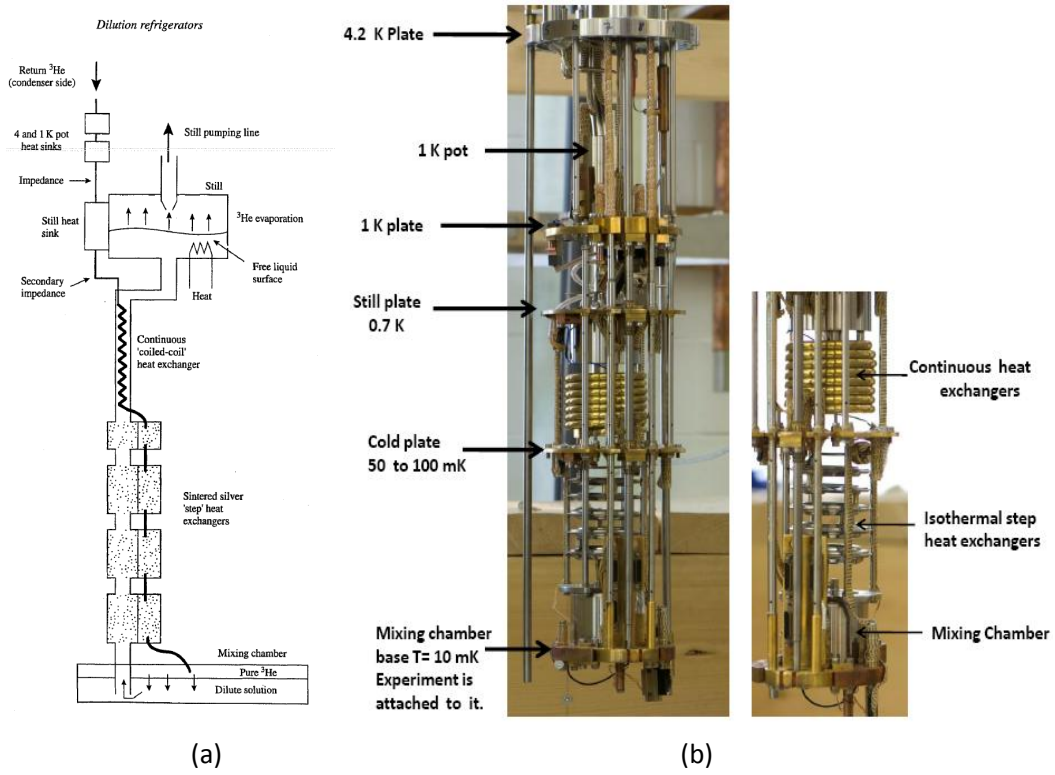

Figure 3.6: a) Schematic of ^{3}He-^{4}He dilution refrigerator, from [31]. b) The Oxford dilution unite insert real picture, it shows the different stages with corresponding temperature at that point.

is very crucial because in case of any kind of leak is developed in the system, no gas mixture (the most expensive part) will be lost, however, it will contaminate but cleaning the gas mixture is not difficult, it can be done easily. Appendix I has more details about this subject.

The other important issue needs to be taken care off is the method of installation. There are several factors involves in optimizing the functionality of the fridge which eventually would have a huge impact on the precision of the measurement performed on it. Vibration is the most crucial factor which needs to be taken care of very carefully, mechanical and acoustical vibrations can be serious source of heat leakage in most experiments at ultralow temperatures. Heating can occur in an otherwise thermally isolated system due to it being mechanically coupled to the building which itself is vibrating from elevators, nearby traffic, unbalanced machinery, from the pumping system, etc. All these issues have been considered while approving the finial design as well as the method of installing the dilution fridge in this research. The dilution fridge used in this research is model (Kelvinox-400 D. R.), appendix II has the design details and dimensions of this cryostat. In the coming sections details for the dewar and the dilution unit insert with all their components will be given.

3.4.2 Magnet and Dewar

An important aspect of cryogenic design is to keep the evaporation rate of the cryoliquid as low as possible by optimizing the cool down process and by minimizing the heat transferred from the warm surroundings parts to the cold parts of the equipment. In general, heat may be transferred by conduction, convection, and radiation. In most low temperature applications, convection is not significant because of the partial evacuation of gas from the interior of the cryostat. Effective heat transfer takes place by conduction through residual low pressure gas, conduction through the solids that interconnect the various parts of the cryostat, and by radiation. The dewar is made of inner stainless steel reservoir, surrounded by a stainless steel jacket that is filled with liquid nitrogen, a vacuum gap isolates the two reservoirs. This liquid nitrogen reservoir is isolated from room temperature by an exterior stainless steel cylinder with a vacuum gap between them as well. This will provide a very good isolation for the ^{4}He from room temperature, hence, will minimize the evaporation rate. The boiling rate of the Oxford dilution fridge is 12 litres of liquid helium per day when its running. Also super insulation has been used to isolate the magnet from any source of heat radiation. The main bath holds 56 litres of ^{4}He, while the nitrogen jacket holds 66 litres of liquid nitrogen with a boiling rate of 13 litres per day when the fridge is running [25]. A helium gas recovery system is used to collect the exhaust gas from the cryostat which is very useful because it will allow the gas to be liquefied and recycled, also this recovery system will prevent air from entering and contaminating the cryostat.

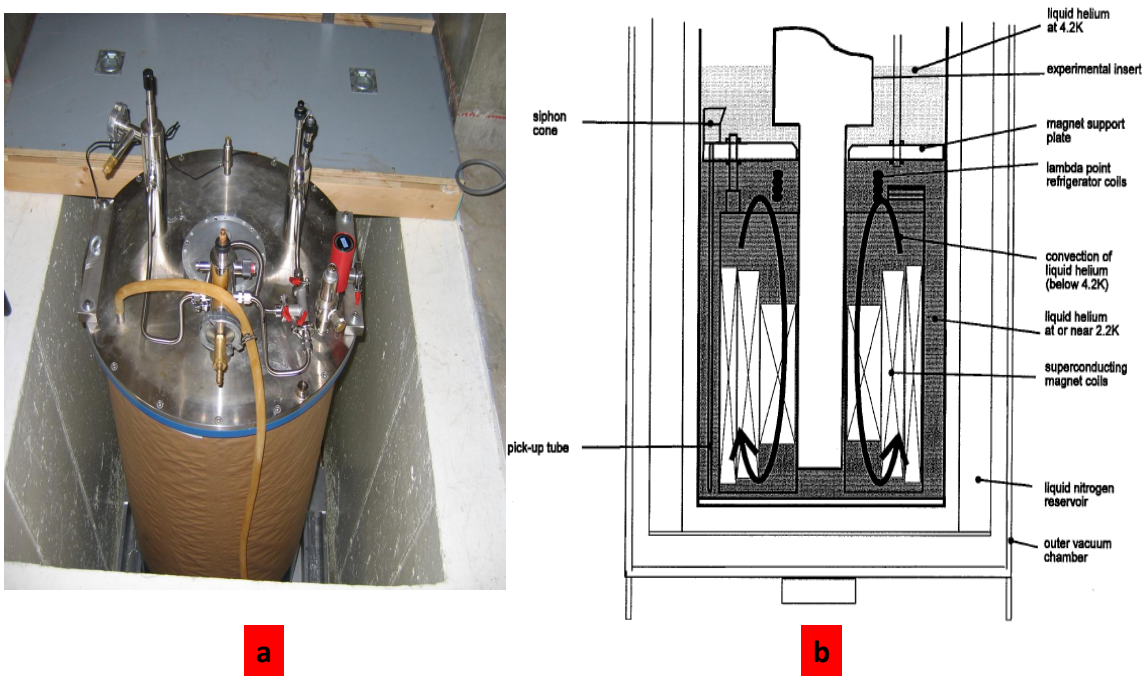

Figure 3.7: (a) Oxford fridge sitting in the pit. (b) Schematic of the superconducting magnet.

The magnet consists of a number of coaxial solenoid sections wound using multi-filamentary superconducting wire [25]. It is constructed using the Magnebond system, an integration of proprietary techniques developed by Oxford Instruments. It gives a structure which is both physically and thermally stable under the large Lorentz forces generated during operation. The magnet type is C14/1652/13, protected by 10 volt resistor diode. These coils are made from the brittle intermetallic compound Nb_3Sn, this material is fragile. The magnet clear bore diameter is 52 mm. It can produce magnetic field from 14 Tesla at 4.2 K to 16 Tesla at 2.2 K, figure 3.7 shows the Oxford dewar. This cryomagntic system is fitted with a superconducting switch which will increase the liquid helium consumption during the field sweep because of the dissipation in the switch heater due to resistive heating in the switch. Therefore, leaving the magnet into "persistent mode" at a constant field for a long time will greatly reduces the helium consumption. In this type of operation, the superconducting circuit is closed to form a continuous loop, and the power supply can then be switched off leaving the magnet "at field".

Additional coils are fitted to the basic winding to modify the shape of the field. "Compensation coils" are used as well to improve the homogeneity at the center of field by reducing the rate at which the field drops at the ends of the coils (due to finite winding

length effects). They are wired in series with the main coils so that they are energised with the magnet. "Shim coils" (or shims) are used to remove residual field gradient; they are wired in series with the main coils to give a basic level correction or independently to give finer adjustment. Shims are either cold superconducting coils or room temperature "normal coil". "Cancellation coils" are fitted to one end (or some times both ends) of a magnet to give a low field region quite close to the center of field. Figure 3.8 shows the magnetic field change with respect to the axial distance. For instance, the mixing chamber in this dilution fridge is 35 cm above the magnet center, the maximum field that could be achieved at this region will be 1 mT according to figure 3.8-c.

3.4.3 Dilution Unit Insert

The Dilution unit insert consists of:

The 1K pot

As it was mentioned earlier in section (3.3.2), the 1k Pot is a vessel of a few cubic centimetres in size with a pipe extended to the liquid helium main bath. A computer controlled needle valve is used in Oxford dilution fridge to allow the helium to flow through this pipe and fill the 1k pot, also it eases controlling the helium level in the pot and hence its temperature. Although a blockage might occur due to accumulation of impurities or due to moistures freezing, operating the 1K pot manually is still available where one can decouple the electrical motor and deal with the valve manually. The 1K pot boil off rate for Oxford system running is 125 cm^3/hour with the Pirani gauge (P2) reading at 11 mbar.

The Still

From (distiller), it is a chamber where liquid ^{3}He is boiled and pumped out back to be condensed and to continue the cooling cycle. If one pumps merely on the surface of a mixture, temperature close to 0.3 K are achieved through evaporation of the ^{3}He. The still needs to be held at around 0.7 K, the simplest way to maintain this criteria (which is been used in this system) is by heating the outside of the still using an external heater. This method has the advantage that a broken heater is simpler to replace and no vacuum seals are required, but the still must be made of a good thermal conductor such as copper, and the internal surface area must be sufficient for good thermal contact to the liquid.

The mixing chamber

The mixing camber is the coldest part of the fridge where the experiments are usually attached. Its purpose is to contain the phase boundary at which the cooling occurs, should the phase boundary leave the mixing chamber, the cooling power will be much reduced. For this reason the chamber should be adequate volume. The mixing chamber also sits in a magnetic field compensated region in order to cancel the effect of the magnetic field on the temperature measurements while the magnet is in operating mode.

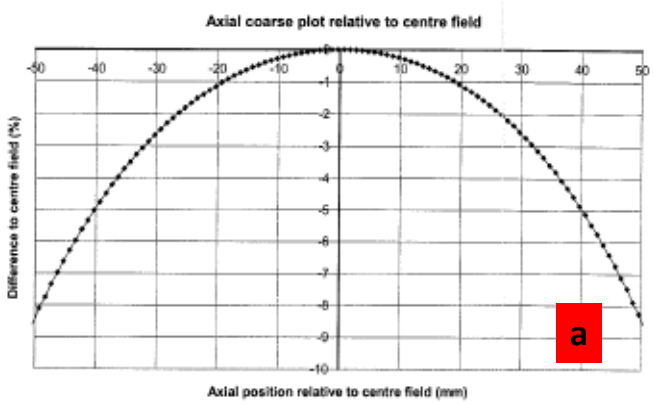

Cancellation coils

Field cancellation region	Volume 50 mm diameter x 50 mm long centred on the base of the mixing chamber
Maximum field in cancellation region	< 100 Gauss

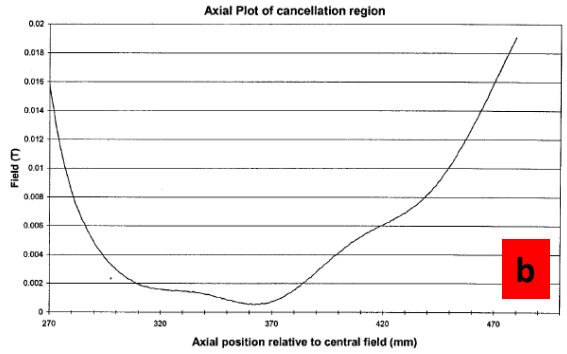

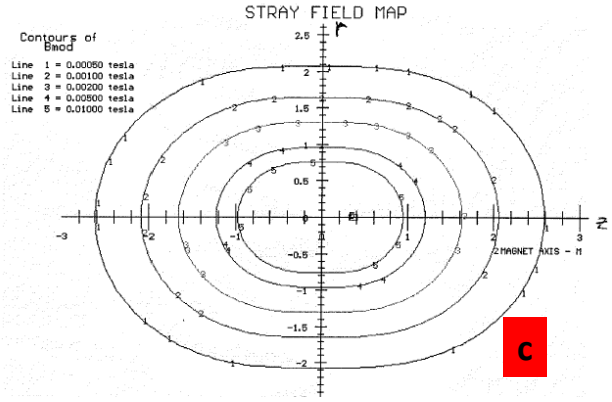

Figure 3.8: a) Percentage change in magnetic field intensity with respect to distance change horizontally from the center of the magnet, the field drops to almost zero close to the skin of the dewar. b) Cancellation region due to cancellation coils used around the mixing chamber, it shows the drop of the field as we move axially out ward the center of the magnet. c) Contour digram of the field where z represents the horizontal distance from the magnet center and r is the vertical distance from the center. from [25]

The heat exchangers

They are perhaps the most important part of the dilution refrigerator, their purpose is to exchange heat between the incoming pure ^{3}He liquid stream and the cold outgoing ^{3}He dilute phase. The are two types of the heat exchangers used in this system made from sintered silver, the continuous and the isothermal step heat exchangers, see figure 3.6-b.

The impedance

The primary flow impedance is situated below the 1K pot and above the still in order that the returning of ^{3}He stream is raised to a pressure high enough to allow it to condense at the temperature of 1K pot, typically (100 mbar) or so. It is prone to being blocked by drifting solids and perhaps pump oil, usually is designed to be replaceable. In Oxford Instruments refrigerators the impedance is a capillary tube about 10 cm long nearly blocked with a wire insert.

The Sorb

A small sorbtion pump is used to evacuate the exchange gas from the IVC. It is mounted on the 1k plate inside the IVC. The advantages of using the sorb are:

1- Exchange gas is removed quickly, typical much less than 1 hour.

2- The mode of operation is simple, with only one heater for sorb control.

3- After the sorb is well proven the risk of leak is small and if there is a small leak the sorb may mask it for long enough to allow the experiment to be completed.

The disadvantages of using the sorb are; there is a risk that small leak may go unnoticed for some time. Also leak testing of the system with the sorb in place is slightly more difficult.

The Shields

All the above mentioned parts are isolated from exposing directly to liquid ^{4}He reservoir by:

1- a radiation shield that protects the tail which holds the samples from the exposing to any external radiation sources that can cause in heat leaking to the mixing chamber, hence, would affect the performance of the fridge.

2- a vacuum can, this provides an evacuated area around the mixing chamber and the samples as well as keeping the liquid ^{4}He away from any contact with the mixing chamber parts, otherwise the fridge would stay at 4 K and will not cool down properly. Indium seal is used to provide a proper seal and an excellent isolation from liquid ^{4}He.

And finally, a fibre glass sliding shield with a sliding seal assembly is used to make pulling out the Insert unit easily from a cold cryostat. This fibre glass shield also allows the helium gas to be recovered and prevents gross contamination of the liquid helium in main bath, this helps inserting the insert part into the dewar easily and at the same time it

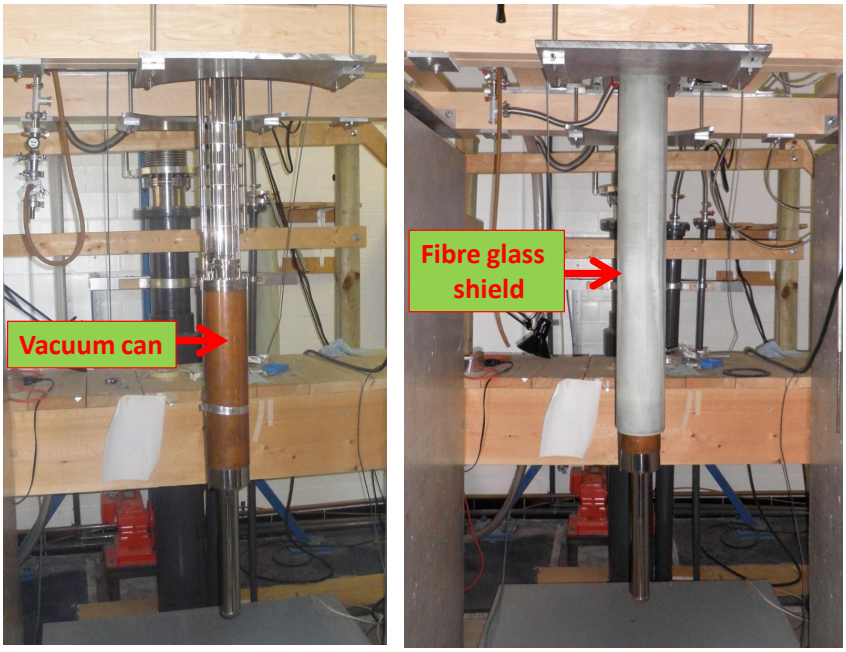

Figure 3.9: The fibre glass shield used with the Oxford dilution unit insert.

provides sealing against the ^{4}He gas while loading and unloading the dilution insert unite, see figure 3.9.

3.4.4 Fridge control and Intelligent Gas Handling System (IGH)

The gas handling system allows circulation and safe handling of ^{3}He/^{4}He mixture, and auxiliary pumping operations. The gas handling system is connected to the cryostat by a set of flexible stainless steel pumping lines attached to PVC pipes. Figure 3.10 shows the gas handling system used with the Oxford dilution fridge. Kelvinox IGH is designed to automate many parts of the operation of Kelvinox system using National Instruments LabView compatible software and "virtual instruments". Remote operation is carried out using serial data link from a computer. The pumping system comprises the mixture into the gas handling system and an automated dilution refrigerator power supply monitors

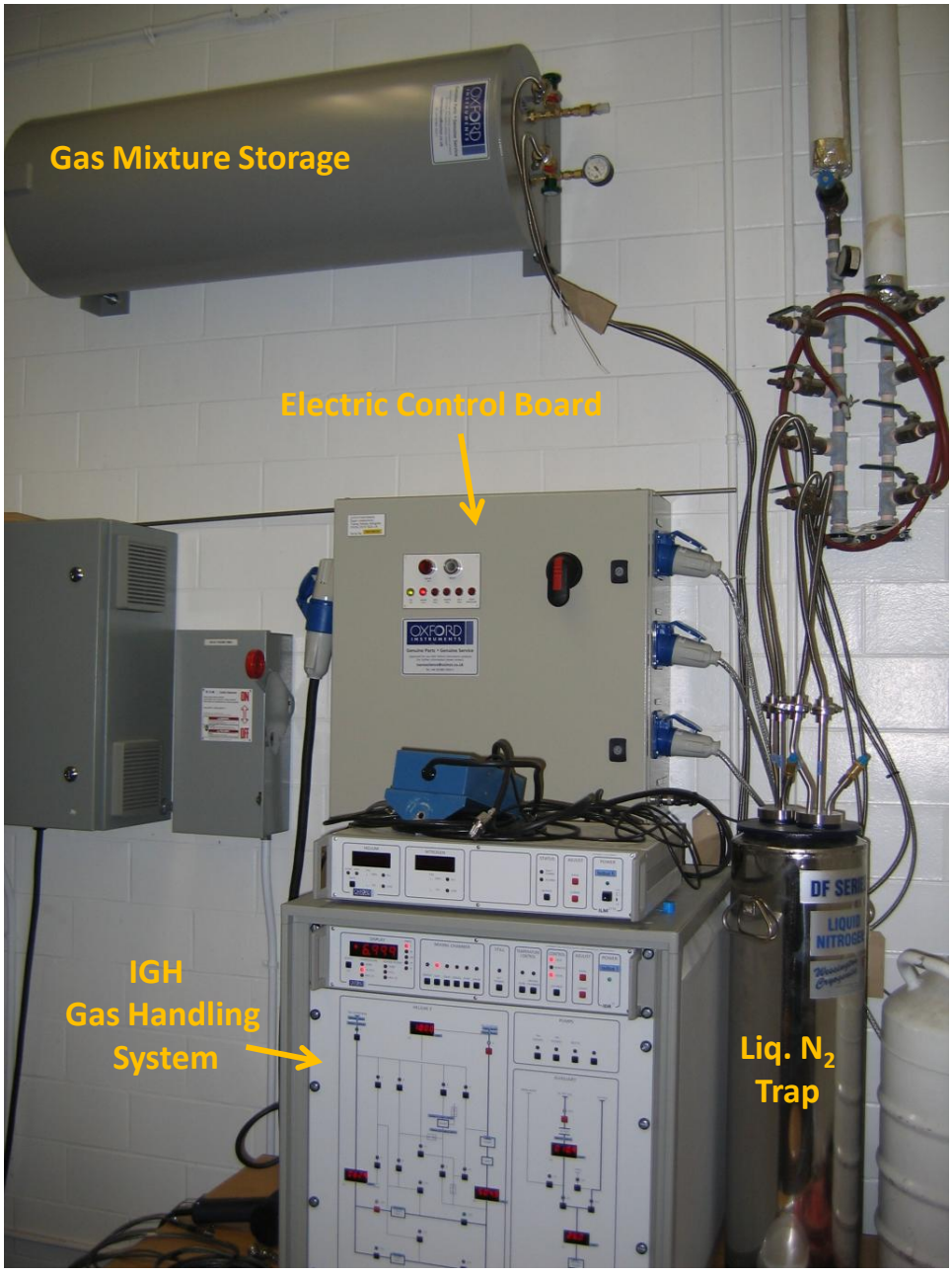

Figure 3.10: Gas handling system and the storage system.

three sensors on the refrigerator (for the 1Kpot, sorb, and the mixing chamber), also it controls the temperature of the exchange gas "sorb" and the amount of heat supplied to the "still heater" and the mixing chamber heater. Other LabView VIs can be run at the same time to control the magnet and the experiment. Two RuO_2 sensors are used to control the fridge temperature, one is not calibrated came with the Oxford power supply, the other one is calibrated but is not controlled by the same power supply. Therefore a new additional heater has been added to the mixing chamber controlled by LakeShore LS-370AC resistance bridge. With this controller we are able to control the fridge temperature to one part in 1000, (more details are given in chapter 5).

^{3}He/^{4}He mixture circulating system

If we suppose the fridge is running at its base temperature which is being made to circulate by the use of room temperature vacuum pumps, and its full with liquid helium. ^{3}He Gas is evaporated from the free liquid surface in the still and returns using the pumps into the IGH system. The ^{3}He is circulated by helium sealed pump, it is cleaned by passing it through an oil mist filter. A pirani gauge is fitted to measure the pressure at the inlet of the rotary pump, and the pump outlet pressure is seen on another gauge. The ^{3}He is purified further by passing it through one of two liquid nitrogen cold traps (77K), this will make sure no impurities or contaminants will be introduced to the system. Then ^{3}He is pumped back to the refrigerator through another liquid helium cold trap to capture any impurity that has passed the nitrogen trap like hydrogen being evaporated from the pumps oil, into the condenser for which the temperature must be low enough and the pressure high enough, typically 100 mbar and 1.6 K is sufficient. The returning gas is cooled first by the surrounding ^{4}He bath around 4 K and then cooled further to around 1.6 K via a 1K pot of pumped ^{4}He which is a small pot usually filled continuously from the surrounding ^{4}He bath and pumped with a rotary pump, it is desirable that the heat of condensation is entirely dumped to the pot and not at lower temperatures. Because of the action of the room temperature pumps, the rest of the dilution unit will be at pressure around 0.1 mabr, therefore, an impedance to the flow needs to be installed to raise the pressure of the incoming gas. This is installed just below the pot so that the incoming ^{3}He condenses at the pot and flows as liquid from thereon down. Secondary impedance is specifically installed at the top of the first heat exchanger at about 0.3 K In order to not let the liquid evaporates again below the "primary" impedance and the rest of the flow path needs to be structured such that a sufficiently high impedance remains so that the pressure drops commensurate with the temperature of the returning ^{3}He. Other part of the ^{3}He is dumped into the still to reduce its temperature to about 0.7 mK, then passes into two sets of heat exchangers, the continuous coiled and the step heat exchangers (both are made from sintered silver) where the liquid ^{3}He temperature drops to 50 mK, down to the mixing chamber where the phase transition occurs. The mixing chamber is cold enough that the liquid gas mixture

separates into two phases, a pure ^{3}He floating on top of the denser ^{4}He, because the ^{4}He contains approximately 6.6% ^{3}He usually is called a gas mixture and the ^{3}He is referred to as dilute solution or the dilute phase where strong bonds between the ^{3}He atoms are broken and new weaker bonds appear between the ^{3}He atom and the dilute phase. The cooling occurs while the ^{3}He atoms form the upper phase evaporate across the phase boundary downwards into the dilute phase [31]. The returning liquid is cooled by the outgoing liquid through heat exchangers between the mixing chamber and the still. Obviously, the still and the mixing chamber must be thermally isolated from each other so that the cold mixing chamber does not suffer a large conductive heat from the still. In order to promote the ^{3}He across the phase boundary, we need to lower the density of ^{3}He in the dilute phase to produce an appropriate chemical potential gradient, it is achieved by taking a pipe from the dilute phase upwards to the still. The still is heated electrically to approximately 0.7 K, in Oxford fridge 5 mW power is used, this enables conventional room temperature vacuum pumps to remove the ^{3}He preferentially, the resulting drop in ^{3}He concentration in the still causes a flow of ^{3}He atoms along the pipe due to concentration gradient and ultimately causes a drop in the dilute phase concentration in the mixing chamber, which is replenished by atoms crossing the phase boundary from the pure phase, then pumped back to the IGH and repeat the cycle again.

When the system is not in use, the mixture is kept in a storage vessel (or a dump). Access to the dump is made through some valves, and the pressure in the dump can be read by another gauge. The dump is outside the IGH system, see figure 3.10.

3.4.5 Sample Position

The experimental apparatus is mounted on the outside of the mixing chamber in vacuum. All connections to room temperature equipment are thermally anchored at various points on the refrigerator to minimize the heat load in the mixing chamber giving the lowest possible base temperature. If the experiment is to be carried out at higher temperatures, the mixing chamber is warmed by applying heat to it directly, and a temperature controller is used to give good stability. One of the most crucial parameters one needs to consider when operating a low temperature dilution fridge is the cost of using liquid helium, therefore finding different ways to minimize this cost is important. One plan to achieve this goal is by running three experiments simultaneously. This means preparing three experimental sample mounts completely. The mounts are bolted to a tail made of pure silver, this tail is attached to the mixing chamber of the dilution fridge. The tail goes to base temperature depending on the quality of the attaching surfaces between the tail base and the mixing chamber, figure 3.11 shows the silver tail. To improve the quality of the contact point between the silver tail and the mixing chamber, we have attached the tail to a block of oxygen free copper which increases the surface areas and enhances the contact quality.

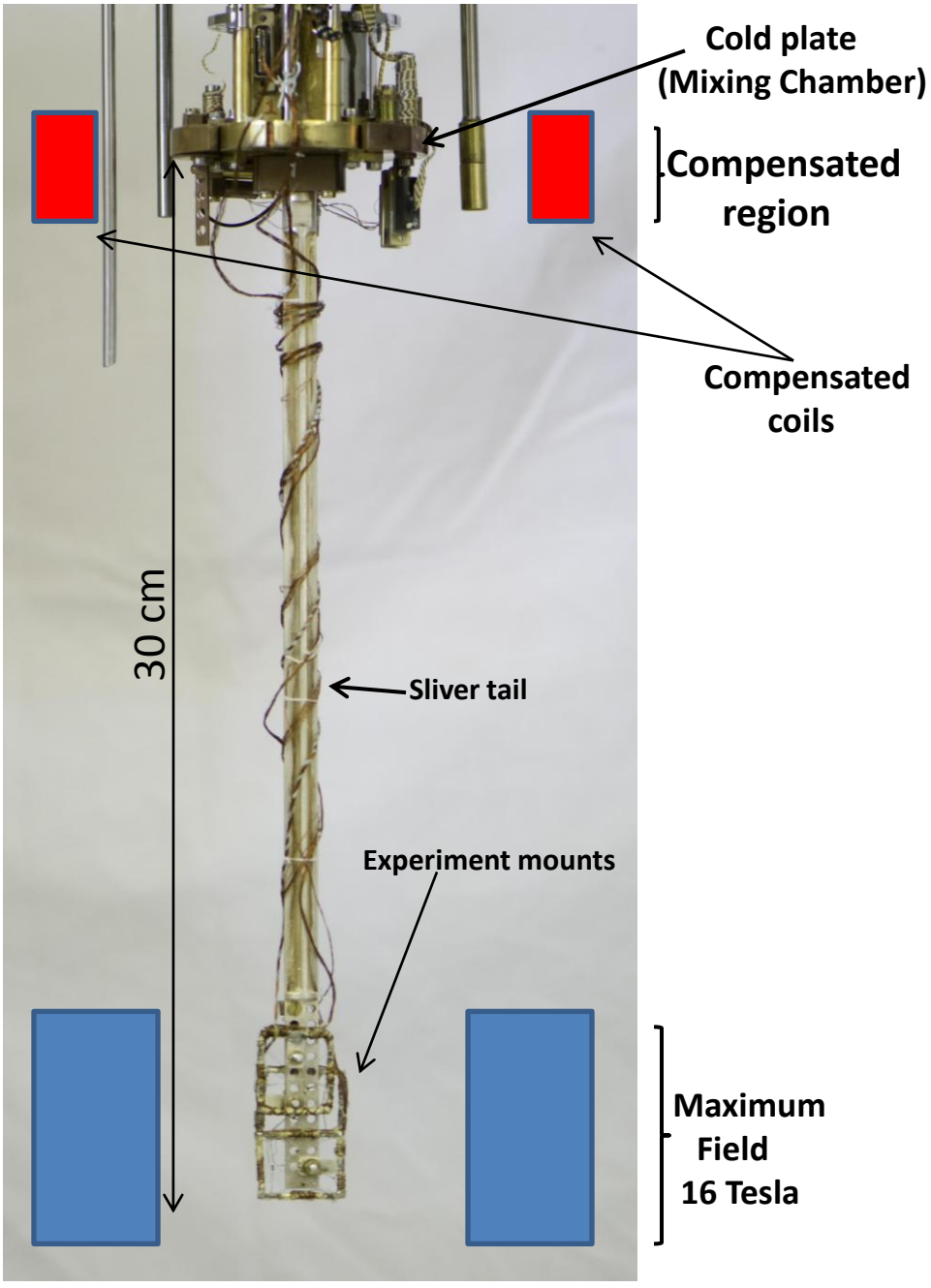

Figure 3.11: The silver tail holding three mounts

The mounts were not attached directly to the mixing chamber because they will not be in the magnetic field center, this is the reason for using this silver tail, it is to extend the position of the sample mounts to be in the center of the magnetic field produced by the superconducting magnet. Silver never becomes a superconductor at very low temperature and has a resistance ratio of RRR = several hundred, it has very low resistance at low temperatures which makes it a good thermal conductor for this purpose.

One sophisticated feature that this cryostat has is the existence of a rotating stage (no picture is shown), details are not given about this facility because we did not used it. With this feature, it makes it possible to rotate the sample mount to different angles with respect to the applied magnetic field direction.

3.5 Installation method and configuration of the Fridge

In the following we detail the procedure features of the fridge installation as shown in Figure(3.7). The most crucial parameter affects the performance of this kind of experiments is the vibration. There are several sources of vibration frequencies that can be transmitted through any configuration, it could be **mechanical** (from the building and the pumps), or **acoustical** (from the noise created by the pumps when they are operational). One has to think in optimizing the fridge set-up in such a vibration free or to the most possible minimum level and that is by isolating the system from the building completely. In this project and in order to achieve this situation we have chosen the set-up method explained in the coming section, further more different materials have been used in this configuration like concrete, aluminium, wood, stainless steel, and rubber. This combination of different materials will prevent the possibilty of the resonance coupling via any path. Two configurations could be used in setting up this Fridge:

First, Dewar is raised and lowered, while the dilution unit insert is fixed.

Second, Dewar remains in the pit and the dilution unit insert is lowered and raised up.

With either methods some advantages and disadvantageous are associated. The main disadvantages of the second methods is, the need of disconnecting the still line in the case of raising or lowering the dilution unit insert, which means contaminating the pipe lines and the need of cleaning and pumping the still line every time during the loading and unloading. However, first method has been considered during the installation of the fridge because it is more controlled and may be used by one person easily.

3.5.1 Pit and Foundation

Because there is a limit in the ceiling hight(330 cm), a pit (90×185×155 cm deep) has been dug in the ground, cast with concrete (no steel beams has been used in any side of the pit in which no attraction might happen in case of operating high magnetic fields), the pit walls are isolated from the building floor and from the sides by a gap of 3cm. The pit provides a convenient hight to allow the liquid He Dewar to be lifted up and slides the dilute part insert of the fridge which is fixed above the dewar, the length of the insert part is 180cm and the dewar hight is 162cm. Trying to construct and install the fridge directly without a pit would make our construction very difficult in this room. A rail and sliding trolley have been manufactured, installed in the pit, the trolley allows the movement (back and forth) of the dewar when is lowered in the pit, which will enable the access to the dilution unit insert when we need to remove the fibre glass, the vacuum, and the radiation cans.

3.5.2 Support Structure

Features of the support structure is shown in figure 3.12.

Pillars

On top of the pit two massive pillars (80×80×180 cm) with a mass of 8 tons each have been cast, they do not sit on the ground directly, instead, a heavy duty rubber matt has been used to provide an extra isolation for the pillars from any vibration might be produced from the building ground, as well as making easy the movement of the pillars in the future if there is a need, see figure 3.12-a.

Wooden frame

On top of the each pillar, there is an aluminium plate sitting on four rubber legs. Theses legs are adjustable to enable the levelling of the plates as well as providing an additional isolation from the pillars, see figure3.12-b. Also this space between the aluminium plates and the top of the pillars could be utilized in the future for using an air springs to hold the plates, which will provide an additional isolation to the system. Two wood beams made from maple wood are bolted to theses two aluminium plates to hold them together as well as providing support to the winch used for lifting the dewar. An extra weight using blocks made from lead (50 Kg each) are placed on top of the aluminium plates to provide an extra stability to the wood bars as well as to absorb any potential vibration source that still has not been absorbed by the pillars, see figure3.12-c.

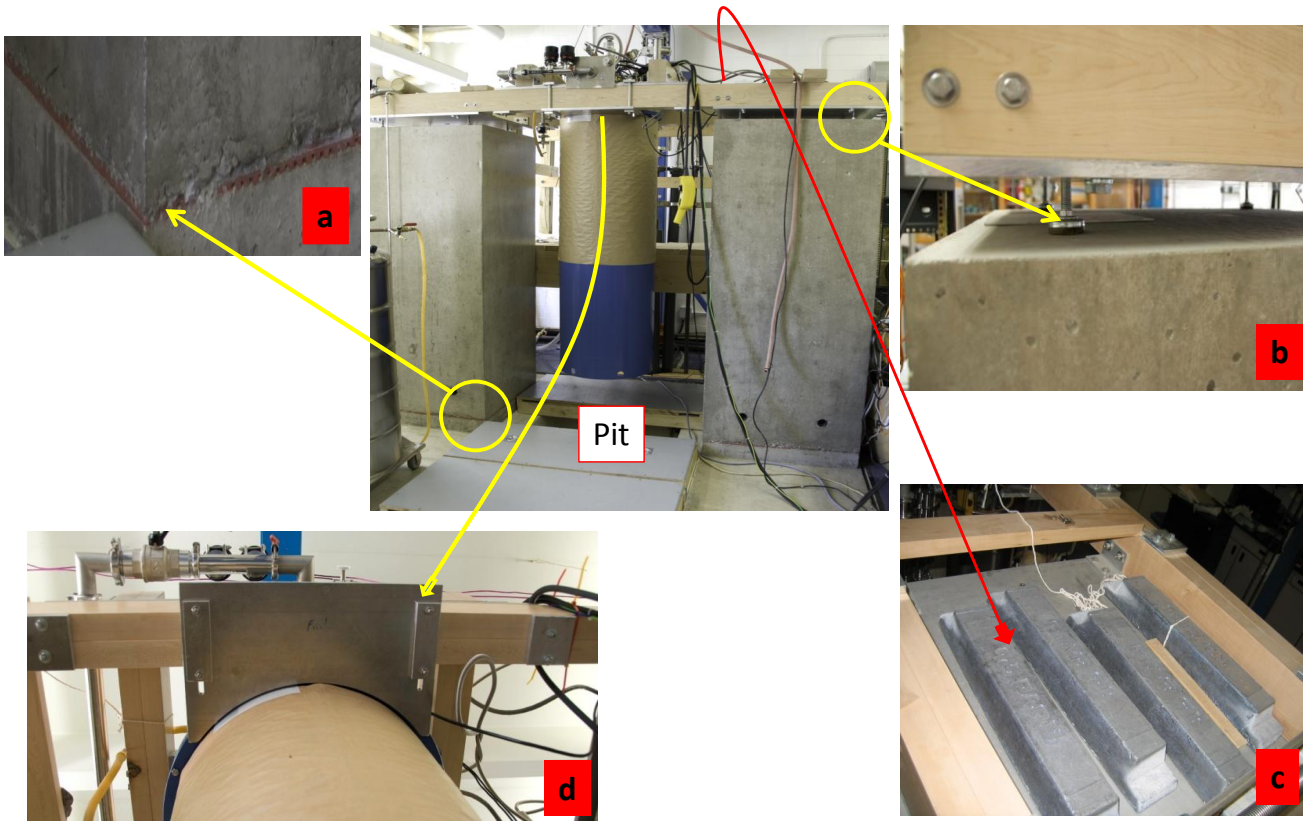

Figure 3.12: a) The Pillar sitting on a heavy duty rubber matt. b) The aluminium plate that sits on the top of the pillar using a rubber legs. c) Lead blocks to provide stability to the wooden frame as well as an extra damping method to any source of noise. d) The moon shape aluminium plate used to hold the dewar.

Dewar holders

Two moon shape aluminium plates are attached to these wood beams to hold the fridge in its final place when its lifted up by sliding in and out underneath the top neck of the dewar, so the tension on the winch cables will be removed (for safety reasons). The moon plates also will provide the fridge a good stability with much less vibration influence, see figure 3.12-d.

Lifting System

Figure 3.13 shows the features and the details of the lifting system parts. The winch system is used in raising and lowering the dewar during the cooling down or the warming up process. Keeping the insert part hanged up on the two pillars and sliding the dewar up or down makes the process very smooth, furthermore, it will keep the samples and the mounts secured from exposing to shocks. The dewar weights almost 125 Kg when its full with helium and nitrogen. The winch consist of an electrical motor, pulleys and aircraft cables, the speed of raising and lowering the dewar is regulated by a controller with a minimum speed of 5 mm/sec.

Once the dewar reaches the designated hight (about 165 cm), the two moon shape aluminium plates slides underneath the dewar top plate, then secured with four stainless steel bolts to the wooden beams. After securing the moon plates the dewar is lowered slowly to let it sit on them in order to remove the tension from the cables.

To lower the dewar some precautions must be taken in order to prevent any risk of mistakes or forgetting to disconnect different attached parts. One needs to make sure the lifting cables are attached properly to the eye rings that are bolted to the dewar, and the superconducting magnet cables and fisher connectors are all disconnected, then finally by disconnecting the recovery line hose the dewar is ready to be lowered. This process will start by lifting the dewar a bit just above the moon shape aluminium plates to make undoing of the secure bolts easy, and slide them outward, the dewar is ready to be lowered slowly and gradually.

3.5.3 Pumping System

Figure 3.14-a shows the sound proof room that contains the pumping system inside it, also it shows the procedures we have considered to minimize the vibrations produced by these pumps. A wide variety of pumps are used to operate dilution refrigerators. The choice of which, depends on factors such as vibration levels, maximum flow rate, cost, and cool down time. The single most important feature of a pump system is that it should be able to

Figure 3.13: a) The winch motor. b) I beam used to hold the pulleys brackets. c) Pulleys bracket. d) The dewar lifted half way using the lifting system.

Figure 3.14: a) The pumps used in dilution fridge, they are acoustically isolated in a special room. b) Three different PVC pipes sizes have been used to connect the pumps to the fridge. c) and d) shows the trench in the ground used to contain the large size PVC pipes with lead bags to dump any introduced vibration. e) Double gimbals design. f) and g) shows the plate used to connect the Pumps to the dilution unit insert.

cope with the circulation rates required whilst maintaining an appropriate low pressure on the still. The next factor is that the system should be completely leak tight. Specifically a sealed rotary pump, powerful, and reliable is required. In Oxford ^{3}He-^{4}He dilution fridge, three types of pumps are used, see figure3.14-a. A small size rotary pump for cleaning the system and pumping out any unwanted molecules or gases, this pump is intended to pump the 1K pot and pump the inner vacuum chamber(IVC) to a rough vacuum. This auxiliary pump may also be used to pump air out of the ^{3}He/^{4}He circulation system, it has a capacity of pumping 14.4 m^3 per hour (0.14 lit/hour). It is also used to clean the liquid nitrogen cold traps, or, to pump the outer vacuum chamber (OVC). However, in most cases a different pump will be used to pump the OVC of the cryostat to high vacuum.

The second pump is large and powerful rotary pump used to circulate the valuable ^{3}He/^{4}He mixture on this system. This pump is fitted with special shaft seals which should give a reliable service for long time, they are leak tight to 10^{-7} mbar. its pumping capacity is 65 m^3 per hour

The third pump is called the roots pump, its pumping capacity is 500 m^3 per hour, it runs depending on the inlet gas mixture pressures. As the ^{3}He rotary pump reaches its maximum pumping capacity, there will be a need from another special and powerful pump to continue the circulation process in a consistent flow. Hence, increasing the pumping speed would result in increasing the cooling power.

To avoid the acoustical noise produced by theses pumps, a special chamber has been built to accommodate them at one corner of the room, 4m far from the fridge. The walls are covered with a special sound proof isolating sheets which lowered the amount of noise produced by these pumps significantly. Since theses pumps are designed to work below 45 C^o surrounding temperature, two powerful fans are used to circulate air inside this small room in order to maintain the internal temperature below 32 C^o always.

Mechanical and acoustical vibrations can be serious source of heat leakage and noise in the measurements at ultra-low temperatures such as the vacuum pumps. The problem of reducing the amplitude of vibrational motion transmitted to the sensitive apparatus is compounded when a pumping line is used to connect the vibrating equipment to the experimental apparatus. To find a suitable method is not always an easy problem to solve particularly when a diameter of the pumping line becomes larger than 6 or 8 cm. In case of small diameter vacuum pumping lines, the usual approach for providing vibration isolation is by holding the metal bellows at some points to a massive objects such as a lead bag. This method is quite effective for damping most vibration, however, this method when applied to large diameter flexible tubing rapidly becomes ineffective due to, first, the metal bellows must be much stiffer because thick walls are needed to support the large force arising from moderate pressure difference, this force scales as the square of the diameter. To compensate for stiffness, the bellows length can be increased but it soon becomes prohibitively long in order to approximate a soft spring. A second problem is that the restoring force increases

with larger diameter bellows. One therefore must provide a comparably greater anchor mass in order to obtain a low resonance frequency. The size of the anchor mass soon becomes very awkward to accommodate around most experimental apparatus.

In our design, three different sizes of PVC plastic pipes have been used to connect the pumps to the fridge. 1, 3, 6, and 8 inches diameters with a short flexible stainless steel bellow at on of the pumps end, see figure3.14-b. These pipes run through a 4m trench long, 75cm deep in the ground, covered by lead bags to dump any vibration, see figure3.14-c and d. In order to connected the pipes that are laid in the trench to the pumps and to the fridge, both ends were extended vertically by a piece of 2m long for each pipe diameter, with theses extensions the length of the three sizes of the used pipes became approximately 10m from the pumps to the fridge. At the fridge side, a stainless steel suspended elbow with a special design has been used, it is called a double gimbal design, see figure3.14-e. The pipes are connected to the dilution unit insert via a spacial plate made for making the the pumps attachment very easy without a need for venting the entire system, see figure3.14-f and g.

3.5.4 Cooling down procedure

The most important factor one need to concern when cooling down efficiently is to have the boiling rate of liquid helium as low as possible. This could be achieved off-course by experience and by doing the transfer procedure slowly. As mentioned in the previous sections, its very important to start cooling the magnet which is the bulkiest part of the fridge first, then the rest parts would cool down quickly. The magnet needs to pre-cooled with liquid nitrogen first from room temperature to 77K, that is by filling the main bath with liquid nitrogen. The magnet resistance reads 165Ω at room temperature, 192Ω at 77K, and 1.3kΩ at 4.2K. Then, by pumping out all the liquid nitrogen out of the main bath to the liquid nitrogen jacket. One needs to make sure getting rid of all that liquid before transferring liquid helium, other wise any left over amount would cause in some difficulties in flushing out the main bath with helium gas, this would be noticed right away once start pumping the main bath and monitoring G3 gage, it should go down quickly (providing no leak is in the system) to 0.4 mbar in four to five minutes. Otherwise, it means either liquid nitrogen is still existed in the bath or there is a leak in the fridge. In our case there is a small leak in the recovery safety valves, to avoid this leak, we used to disconnect the recovery line and use a blank flange instead while we flash out the main bath.

Next step is to prepare and assemble the dilution unit insert. After mounting the tail loaded with experiments, the radiation shield is mounted, one needs to make sure there is no touch between the experiment and the radiation shield at all. Next, the vacuum can is mounted with an indium seal, then the fibre glass shield is attached. The dilution insert

unit is pumped for 4 hours at least and leak checked before introducing the exchange gas. If there is no leak, a 5 cm^3 of exchange gas is used (He gas) to speed up the cooling of the dilution unite insert to 4.2 K while raising the dewar all the way up.

The are two methods of transferring liquid helium to the main bath, either when the dewar is in the pit with the dilution unite insert. Or, when the dewar is raised up with the insert part in. Both ways have their advantageous and disadvantageous, however, with experience one can choose one of them that most suites the existed circumstances. In our case we have found that the most efficient case is to do the transferring while the dewar is in the pit, we transfer an amount of 20% of the maximum level just to keep the magnet covered with liquid helium, then we raise the dewar almost to the point where the fibre glass shield slides into the dewar neck and seals the dewar. Leaving the system for 15 minutes to let the cold helium vapour pass through the fibre glass shield to the recovery system, the dilution unit insert will cool down gradually. Then we start lifting the dewar 5 cm a step every 5 minutes, this process would take about two hours in order to get the dewar up and the entire system cold to 4.2K, however, the slowly lifting up the dewar the more efficient result one can get in terms of the boiling rate.

As a summery of all the preceding sections, and to test the reliance of the design we used to isolate the dilution fridge from the parameter that mostly affects the sensors functionality which is the vibration noise, tests on the thermometers behaviour have been carried over with no magnetic field and with the presence of a magnetic field. Because, with the existing of a vibration, when the magnetic field is applied the effect on the thermometers should be very clear, the magnetic field will cause them to vibrate and produce some heat, this vibration has a negative influence on the resistance values, hence a fluctuation should be noticed. Whereas the magnetic field would have a positive influence on the resistance values in the absence of any vibration, thus, would increase the resistance value due to the magneto resistance effect. In this test, (50, 200 mTesla), 2, and 5 Tesla has been applied while recording the sensor resistance values, see figure 3.15. Its obvious from this plot that no significant difference in the over all performance of the same sensors has been detected except the effect of the thermometer magneto-resistance which has shown a quantitative but not qualitative effect on the measurement results. This will lead to a conclusion that no vibration source is introduced to the experiment, hence, the fridge is isolated properly and any associated fluctuation is independent of the magnetic field. However, this fluctuation could be due to intrinsic noise, electromagnetic interference, eddy current, or due to temperature fluctuations. These sources of noise will be discussed with more details in chapter 4.

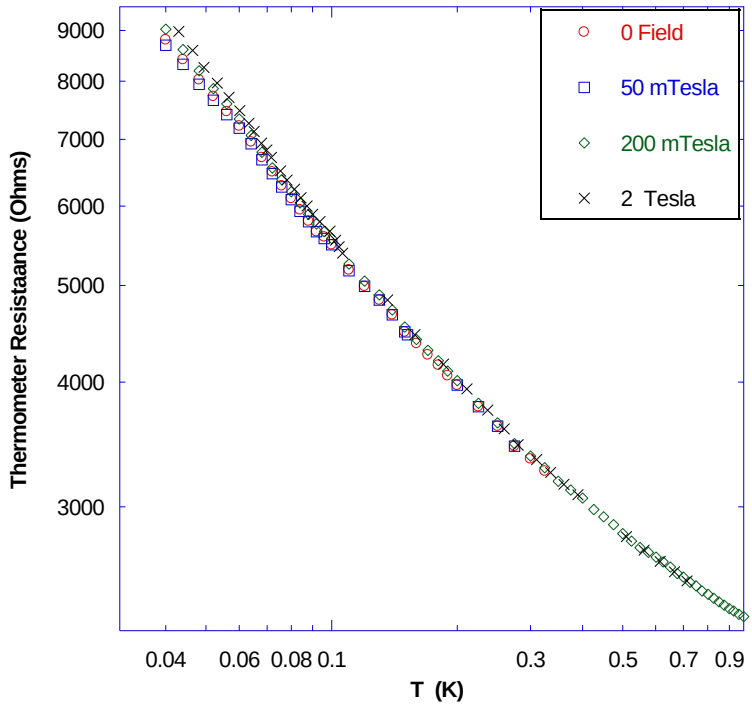

Figure 3.15: Temperature dependence of the sensor resistance with respect to different magnetic fields. The sensors are very delicate and are suspended on the experiment frame using a kapton ribbon thread which makes them vulnerable to vibrations. Since the electrical connections is made via coils, if these coils happened to vibrate in the existence of a magnetic field an induced voltage would generate on these coils, hence, it will have a significant effect on the thermometer readings which makes them warm up due to the produced heat. But from this plot, Its very clear that the magnetic field has no significant impact on the thermometer behaviour, the only change appears on the readings is due to the magneto-resistance of the thermometer in which the resistance values increases.

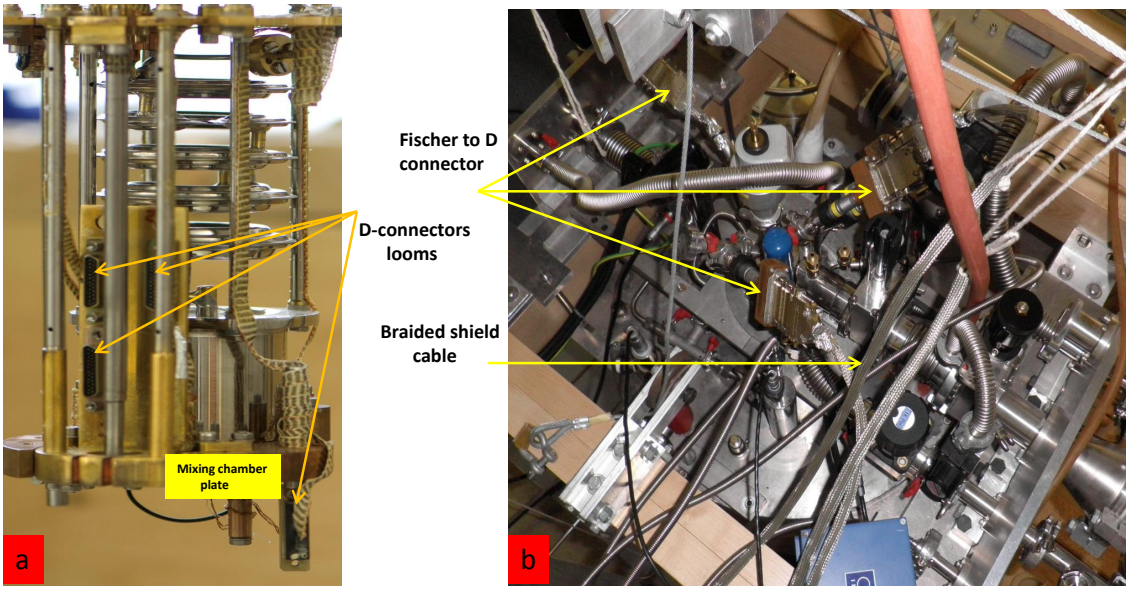

Figure 3.16: a) Mini D-connectors looms at the mixing chamber where the experiment is connected to room temperature through the top connectors. b) Fischer connectors are connected to a copper D-connector adaptors, and are connected to the electronic equipment using braided shields cables.

3.5.5 Experimental Wiring

Figure 3.16 features the details of the wiring connectors of the Oxford dilution fridge. This fridge is designed to provide 4 x 12 twisted pairs of wires made of two different materials, copper/superconductor and constantan wires which provide a variety of experimental options. These wires are rigidly fixed and well shielded to keep RF pick-up signals low. These twisted pairs are separated into four terminals or looms with mini D-connectors at the mixing chamber. From one end they run to the top of the fridge through the dilution unit insert (using a built in channels made specially for this reason) to room temperature with Fischer connectors at the other terminal. These looms are labelled as 1, 2, 3, and 4. Loom 1, 3, and 4 are made of copper/superconducting wire with a 56Ω resistance value, while loom 2 is made from constantan with 150Ω resistance value. In order to avoid the flow of heat from room temperature to the experiment through conduction of these leads wires, they are connected to heat sinks and anchored at different positions before reaching the experiment. If this thermal anchoring is not adequate spurious heating effects can occur. For each loom the twisted pairs run and use the pins 1-2 , 3-4 and so on up to 23-24. In the thermal conductivity measurements one usually needs four wire or two twisted pairs

to measure the sensor resistance, in order to follow one scheme, we have designated 1-2 to represent the voltage V^+ and V^-, 3-4 to represent the current I^+ and I^- respectively, and so froth for the next pairs.

From the room temperature end, these looms are connected to Fischer connectors also labelled as 1, 2, 3, and 4 correspondingly with the other end. A special adaptor has been manufactured to convert the type of connector from the 24 pin Fischer type to the 25 pin D-connector type for convenience. At the room temperature end of this D-connector a filter is attached to reduce the RF noise. This filter is of type SCI 56-725-005 -E with 4000pF capacitor and cut-off frequency of 100MHz. Then a 24 wire cable shielded with a braided metal shield is used to connect the experiments to the bridge resistance. All the electronic devices which connect the experiment to the measurement devices are mounted on a metal rack. Figure 3.17 shows the metal rack used to hold the LR-700 device, the LS-370AC, the heaters voltage supplier, and the BNC connector boards.

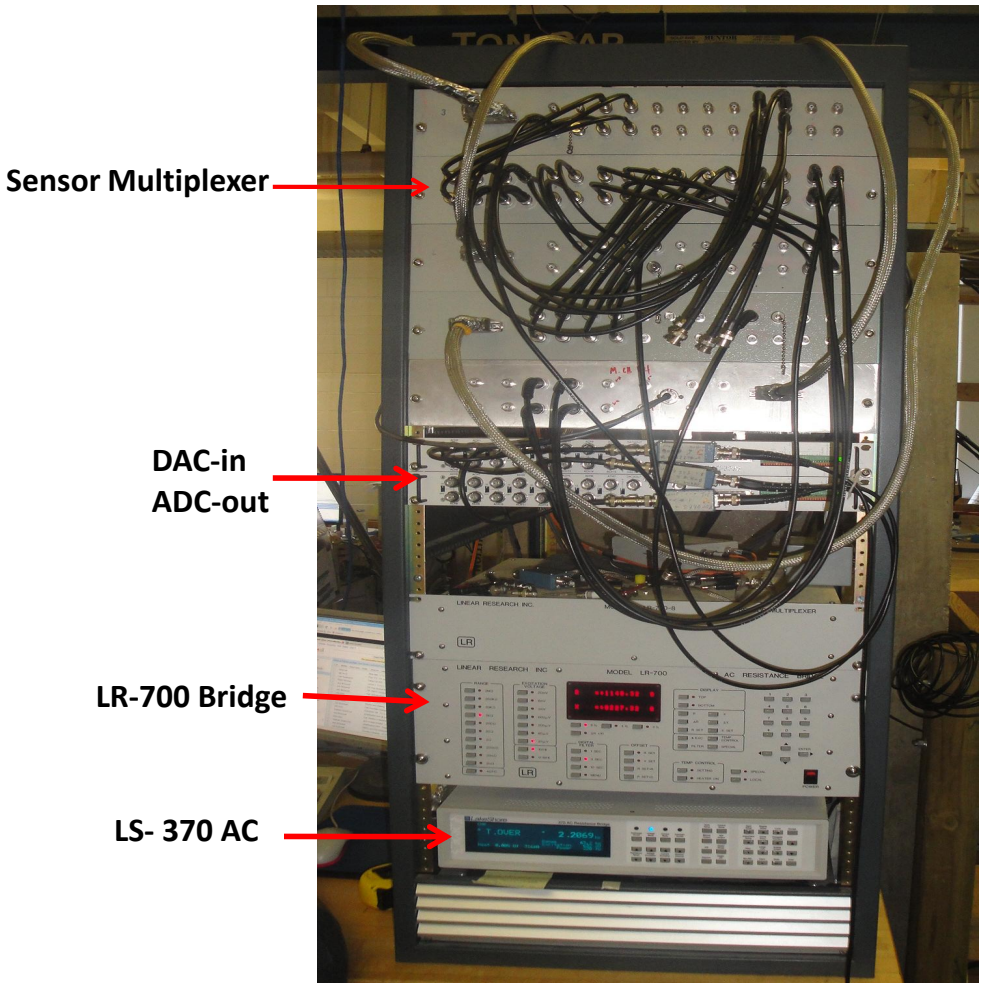

Figure 3.17: The electrical cabinet holds the LR-700, LS-370 resistance bridges with the heater voltage controller

Chapter 4

Thermal Conductivity Measurement

4.1 Introduction

A generic set-up for the measurement of thermal conductivity is shown in figure 4.1a. The main components include a heating device, two thermometers to measure the temperature gradient, and a reference thermometer. Since the thermometers usually used in this kind of measurements are resistors (where the resistance value is converted to temperature later on), therefore a need of using a resistance bridge is a must. The bridge uses current excitation because the controlled current is very stable and predictable where the current can also be scaled easily which is necessary to achieve low excitation. These low excitation currents have low noise and almost no DC component to self heat the measured resistor. Precision resistance measurement uses a four lead method to eliminate the effect of nominal lead resistance, that is by using LR 700 high input impedance bridge (10 MΩ). Excitation current is driven on one pair of leads while the resulting signal voltage is measured on the second pair. Indeed, a thermal conductivity measurement consists mainly of a high precision temperature measurement (to obtain a temperature difference and temperature average). The heat device can take many forms, the goal being to obtain is knowing the amount of heat flowing through the sample. The simplest heater is a resistive element which is in thermal contact with the sample. Joule heating will produce an amount of heat equal to RI^2 when a DC electrical current is applied through this resistance. The heat could also be applied by radiation or by induction, both these methods are harder to implement and to control. There are many methods to measure the temperature gradient across the sample, among these methods the most accurate one is the use of two calibrated thermometers.

Although the measurement of thermal conductivity sounds a very simple one, many considerations must be assumed while designing the experimental set-up. These are: sizes,

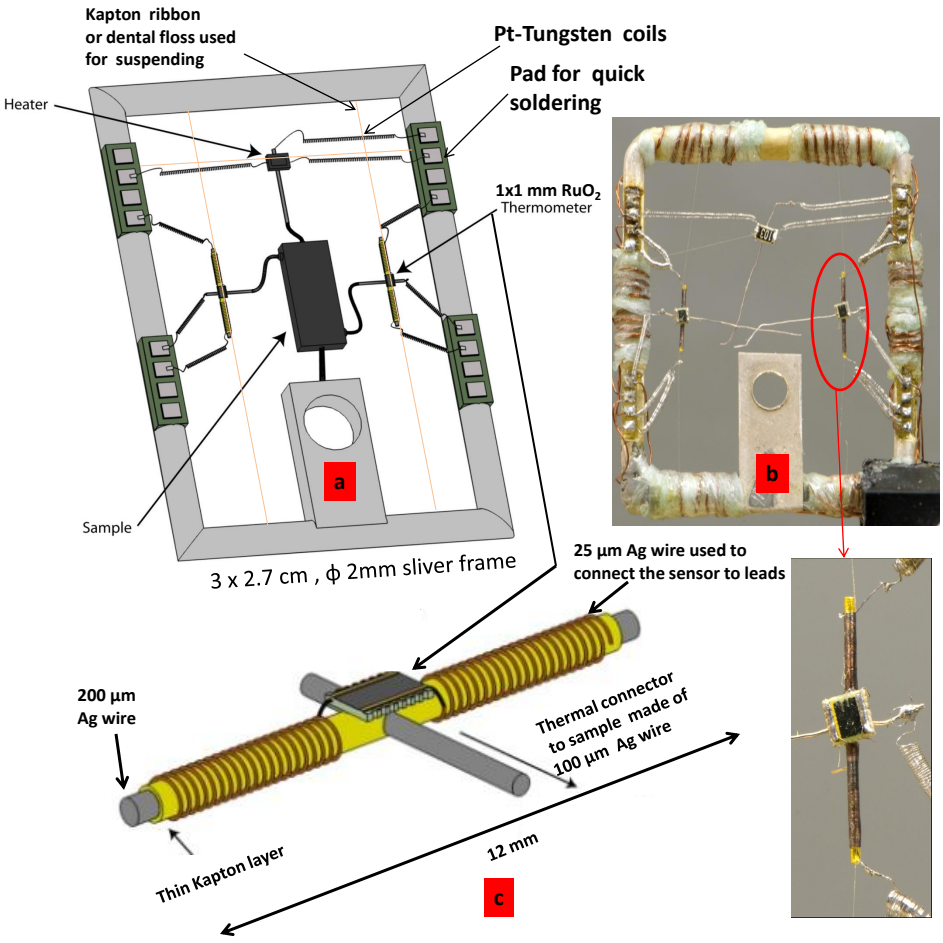

Figure 4.1: a) Schematic of generic thermal conductivity set-up. The main components are heating device to apply heat current, two thermometers to measure the temperature difference ΔT across the sample. Both thermometers and the heater are hanged by Kapton ribbons or a kevlar fibre thread for thermal isolation as well as to provide rigidity to the sensors. b) A real thermal conductivity mount manufactured for this research, note that no real sample is shown on this mount. c) a blow-out picture for the thermometer design. [Courtesy of Joel Vroom]

heat capacity of the components; vibration issues; thermometer temperature; choice of thermometers; and the heat losses probability via the set-up. In this chapter details will be given about the mount design specifications, tests on the thermometers, the thermal conductivity measurement process, and the interface used to control the experiment and the fridge temperature.

4.2 Thermal conductivity mount

Size

Because of the limit space in dilution fridge magnet bore (approximately 5 cm) the frame has to fit this space properly. The thermal conductivity-mount dimensions are 3 x 2.7 cm made of 3mm diameter, its made of a silver wire frame that could be screwed to the sliver tail. This tail is connected to the mixing chamber located inside the dilution unit insert (under vacuum), details were given in section (3.5 - sample position), see figure 4.1b. The size of the thermometers with the heater must be taken into account, further more, the small heat capacity of the materials chosen in this design will all help in getting to the equilibrium state in short time. The response time (the time required to reach a steady state equilibrium to then be able to preform our measurement) is defined as [τ = C * R], C is the total heat capacity of the combination, and R is the resistance of total combination. Both C and R depends on the type of the materials used, for silver C is very small at low temperatures.

The Isolation and the Vibration Issue

The thermometers and the heater must be thermally isolated from the silver frame because all the applied heat essentially has to go through the sample then measured by the thermometers. In the same time the thermometers are electrically isolated from the silver frame because their resistances are electrically measured. Therefore they are suspended on the silver frame using a kapton ribbons thread, or a dental floss, or a kevlar fibres with thickness of 10 to 12 μm. The low thermal conductivity of kapton ribbons or the dental floss is about ($\sim 10^{-5}$ W/cm.K)[32] and about (0.2-0.3$10^{-6}$ W/cm.K) for kevlar fibre [27] will provide an excellent thermal and electrical isolation for thermometers and heaters. In our mount the conductance of the kevlar fibre is about 0.052 $\times 10^{-14} \frac{W}{K}$. In the same time the kevlar fibre will provide rigidity to the thermometers and the heater from vibrating. In order to justify the quality of this isolation, an assess will be provided later in section (4.2.3).

Ease of mounting and dismounting

The other important point that needs to be considered is the ease of mounting and dismounting the sample on the fridge. We have used a block of pure silver (1 x 0.5 x 0.5 mm) with a one side polished surface. It has a threaded hole containing a stud that extends from both side of the block which is used to connect the sample to the cold point. The thermal conductivity mount is bolted very tightly to this block to effectively become one assembly. This design makes dismounting the sample very easy with no need to touch the sample, all one needs to do is remove the mount and replace it with another one that has a sample attached to it already.

4.2.1 Thermometers

One needs to consider the following while choosing the appropriate type of thermometers for the set-up:

Temperature Range

Different thermometers can be chosen depending on the temperatures needed to be covered, for low temperatures the choice arises from the resistance of the thermometer. For example, metal thermometers like Pt-100 is sensitive to about 10 K, while semiconductor thermometers range is between 10 mK and 10 K [32]. In this research thermometers type Ruthenium-Oxide (RuO_2)[33] have been used, they are resistive chips with a high temperature-dependent resistance. Typically, their resistance increases dramatically as the temperature is reduced, in fact, measuring temperature reduces to a simple resistance measurement. They are semiconducting thin film resistors with a surface area of 1.5×1.5 mm^2. The RuO_2 thermometer has a gold substrate to be used for soldering an attachment to it. The thin film is substrated to a thick base made from sapphire, therefore to enhance their temperature response the base has been polished to reduce the thickness, this process was necessary because with a less thickness the heat will transport faster to the thin film, thus, the heat capacity of the combination will be less. Two types of thermometers have been used in this research, a high resistance thermometers with a value of 100kΩ at low temperatures, and a low resistance thermometers with a value of 10kΩ at low temperatures, both types have 1kΩ resistance value at room temperature.

Sensitivity

As for any measurement, it is better to obtain the largest signal to noise ratio to maximize the sensitivity. In this type of experiments sensitivity means the smallest change in T that

we can measure, which is equals to $\propto [\frac{\Delta R}{\Delta T}]$. In other words, the noise dictates the scatter in the thermometer resistance value and hence will determine the scatter in the corresponding temperature.

Low magnetic field dependence

For measurements in the presence of a magnetic field, the thermometers must display a low - or better yet nil- magneto - resistance. Depending on the type of the thermometer, its magneto-resistance may be simple (e.g. Ruthenium oxides) or complicated (e.g. Cernox chips), an important point for the parametrization procedure is (obtaining R(T,H)). In some cases, the thermal conductivity is measured with respect to a rotating magnetic field direction, therefore the thermometers must have an isotopic magneto-resistance (such the case of Ruthenium oxides)[32]. In our case, we can overcome this issue by calibrating the thermometer with respect to a calibrated one each time we run the experiment

Reproducibility

The reproducibility of the thermometers upon thermal cycling is also a point to be considered. Also one can overcome this point by using different fitting according to the new resistance values measured at each run.

Thermometers configuration:

Figure 4.1-c details the thermometers design used in this research. A silver wire of 200μm diameter called a base has been wrapped with a kapton sheet layer (10μm thickness) to provide electrical isolation, in the same time connects it thermally, that is why this sheet has to be as thin as possible. Another sliver wire with 100μm diameter is soldered to a stripped area in the middle of the base, this piece will be used to connect the thermometer to the sample from one end which will provide a thermal contact, and the other end will be used to connect the voltage wires to measure the sample resistance. A 25 μm diameter silver wire is wrapped around the base to provide electrical contact between the thermometer from one end by soldering it to the gold substrate, the other end is soldered to the leads. The thermometer is glued to the stripped area on the base using a G-varnish which has a good thermal conductance. The electrical contact between the thermometer and the experiment leads is made through a coils made from Platinum-Tungsten wires with 25 μm diameter, 10 mm long, the coil resistance is 150Ω. Platinum-Tungsten has a small thermal conductance, this property helps in keeping the sensors thermally isolated, also if one would compare between the heat capacity of Platinum-Tungsten with other materials, it decreases almost down to 100mK without turning back as the other materials

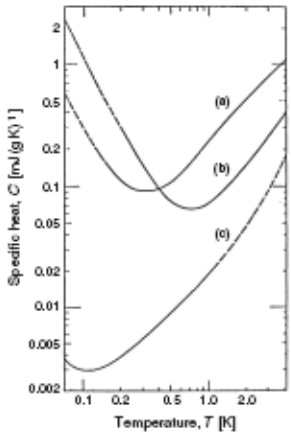

Figure 4.2: Specific heats of (a) Constantan, (b) Cu+Manganin alloy, and (c) Pt alloy. from [32]

does, see figure 4.2. By having the heat capacity small for the combination, getting to the equilibrium state will be quickly because the response time is very small [31]. In section (4.2.3) an assumption of the heat loss in this configuration will be given when heat is applied to the sample.

4.2.2 Heaters

The heaters used in this research are form Vishay Micro-measurements company. They are 10kΩ resistors with a week temperature dependence. The heater is a chip resistance substrated on sapphire base. Using a G-varnish, a piece of 25 μm silver wire is glued to the base of the heater in order to provide a thermal link with the sample from one end, the other end will provide the electrical contact (the I^+) with the sample in order to measure the sample resistance. Two coils of a 25 μm diameter, 10 mm long made from Platinum-Tungsten wires with a 150Ω resistance are used to connect the heater to the experiment leads electrically. A fact that needs to be considered is we must have $R_{Heater} \gg R_{wires}$ in order to make sure all the heat generated will be across the heater not across the connecting wires which are highly thermally resistive. A DAC output (Digital to Analog Converter) is used as a voltage source for the heaters. A current I is applied to the heater which generates heat equal to $\dot{Q} = R_{Heater} I^2 = VI = \frac{V^2}{R_{heater}}$. To measure the value of this voltage an ADC input (Analog to Digital Converter) is used. In this configuration a standard resistance has been connected in series with the heater to reduce the amount of current going into

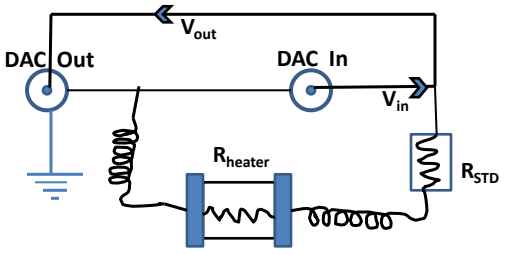

Figure 4.3: Electrical wiring digram used to apply heat to the sample using a heater, DAC is used as a voltage supplier while a ADC is used as a voltmeter to measure the voltage difference in the circuit.

the sample, see figure 4.3. In order to calculate the amount of heat applied to the sample $\dot{Q}$, the heater resistance value is 10640Ω, standard resistance has a value of 565KΩ, then all we need to know is the current flowing in the circuit. In fact, a voltage is applied to this heater via the DAC out unite controlled by a computer software, then the current is calculated from $I = \frac{V}{R_{heater}+R_{std}}$, or

$$I = \frac{V}{(10640 + 565500)} \quad (Amp) \tag{4.1}$$

hence, $\dot{Q} = I^2 \times 10640$ Watts.

4.2.3 Heat losses possibility

The thermal contact problems is ever presented for thermometry at T <1K, therefore we must have a very good thermal contact points between the sample with the thermometers, the heater, and the ground (the fridge), otherwise a temperature gradient will be created across the contact points which in the end will add a significant issues to the measurements. Another crucial parameter one has to consider when measuring thermal conductivity is the heat losses channels. Since we apply an amount of heat through the sample, we have to make sure all that heat is going through the sample, not through other paths. If the heat is travelling through other channels, then how much is the exact amount of heat going across the sample? To answer this question one needs to consider all the possible channels that heat can travel through them. Looking at figure 4.4, the schematic shows the possible paths for heat to flow. Ideally, all the heat generated by the heater must flow through path 1. But, in reality the heat can flow through other paths 2, 3, and 4. In order to have most of the heat flow through the sample, paths 2, 3, 4 must have a much smaller thermal

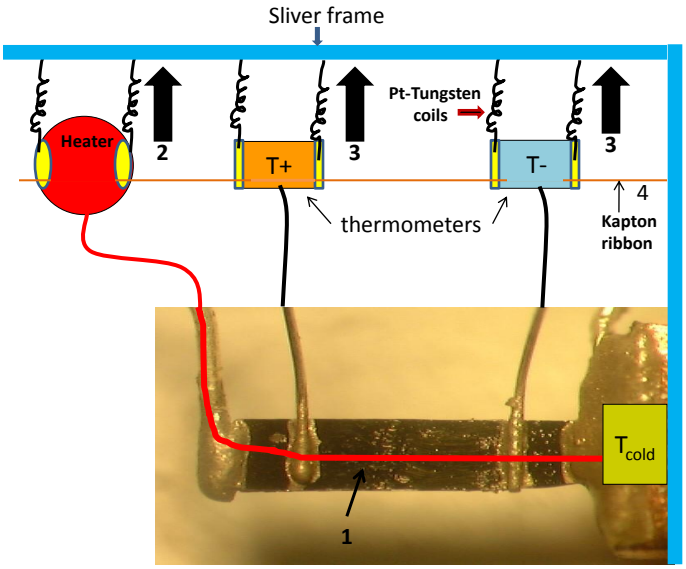

Figure 4.4: Schematic of possible heat losses channels in the thermal conductivity measurement.

conductance comparing to the sample. As a demonstration, one can calculate the amount of heat loss in one Pt-constantan coil and compare it with the amount flowing into the silver piece used to connect the heater with the sample by using the Wiedemann-Franz law principle,

$$G(conductance) = \frac{L_o \times T_{avg}}{R_{sample}} \tag{4.2}$$

For the Pt-constantan coil of R= 150 Ohms, $\Phi = 10$mm, $\ell = 10$mm at T_{avrg}=160mK

$$G_{coil} = \frac{2.44 * 10^{-8} \times 160 * 10^{-3}}{150} = 2.6 \times 10^{-11} \quad (\frac{W}{K}) \tag{4.3}$$

and for the three coils, $G_{3coils} = 7.8 \times 10^{-11} \quad (\frac{W}{K})$

For the silver wire piece of R= 0.44 mOhm, $\Phi = 100\mu$m, $\ell = 10$mm at the same T

$$G_{Ag} = \frac{2.44 * 10^{-8} \times 160 * 10^{-3}}{0.44 * 10^{-3}} = 887.2 \times 10^{-8} \quad (\frac{W}{K}) \tag{4.4}$$

This will yield to $\frac{G_{Ag}}{G_{Ag}+G_{coils}} = 99.9\%$, i.e., 99.9% of the applied heat is going through the sample and only 0.1% is lost via the coils, in which will give 0.1% less in the thermal conductivity measurement providing the temperature gradient is absolutely correct.

4.3 Electrical Resistance Measurements

For measuring the resistance of the thermometers and the sample we used an AC resistance bridge LR-700 from linear research Inc. The bridge uses a signal with 16 Hertz frequency for measuring the resistance and inductance. It measures the sensor resistance every 188 msec regardless the digital filter that is selected. The filtering method used is a straight average giving equal weight to each of the readings in the time period. For example, in the 1 sec filtering mode, 5 readings are averaged together and divided by 5. In order to read the resistance of a temperature sensor, one needs to measure the voltage across the sensor due to a current flowing through it. The heat generated into the system is proportional to the square of this current $P = I^2 R_{sensor}$. At low temperatures, when the resistance of sensors is very large, one needs to use a small current to avoid generating too much heat in the system, in the same time the current should not be too small which would give rise to the noise associated and hence an inaccurate measurements. The amplification noise of LR-700 bridge is approximately $2\frac{nano\ V}{\sqrt{Hz}}$, this is approximately the Johnson noise associated with a 1KΩ resistance at room temperature. The Johnson noise voltage is given by [42]

$$v_n = \sqrt{\bar{v}_n^2}\sqrt{\Delta f} \quad = \sqrt{4k_B T R \Delta f} \tag{4.5}$$

$\bar{v}_n$ is the voltage variance or the mean square, k_B is Boltzmann constant, T is the temperature, R is the resistor, and Δf is the frequency band width. In section (5.1.1) it will be discussed in more details the noise associated with the sensors used in this research.

4.3.1 Temperature dependence of the thermometer resistance

Since the resistance of a semiconductor increases as the temperature is reduced, one would expect to see a continuous increase in the thermometer resistance value as T goes to zero with no saturation, providing that no vibration is introduced and the thermometer is very good thermally anchored. Also the method of grounding the fridge has a direct influence on the thermometer behaviour. Therefore to get to the point where all the above issues have been studied and investigated, we started this research by exploring the temperature dependence of the thermometer very early before mounting the dilution fridge on its final configuration. Its important to be pointed out that these experiments have been performed using the Oxford temperature sensor and controller.

4.3.2 Effect of using a simple damping method and improving the fridge grounding

During the installation of the dilution fridge while it was sitting on the floor, an experiment

to study the effect of vibration produced by the pumps then transmitted to the fridge via the pumping lines has been performed. Also improving the fridge grounding has shown a significant impact on the thermometers resistance value, in figure 4.5 some of these results are displayed. In this figure, the fridge was connected to the pumps through a stainless-steel hoses, the sensor resistance was measured when no arrangement is done, and when weighing the stainless steel hoses with a lead bags. Also the grounding configuration has been improved during this experiment to minimize any source of RF or the grounding loops. Obviously there is a significant effect of using damping method to reduce the noise transmitted by pumps through the stainless steel lines, as well as changing the grounding configuration.

4.3.3 Temperature dependence of the thermometers with respect to the thermal anchoring point

A special mount has been manufactured from pure (Oxygen free) copper, it can hold eight thermometers in the same time with another reference thermometer. The reference sensor job is to indicate if there is a temperature gradient between the mixing chamber (the actual fridge temperature) and the copper mount. Figure 4.6 shows the copper mount where the thermometers are attached directly to the fridge. Definitely the value of there resistances would not be the same, each thermometer will give different resistance value depending on its manufacturing characteristics, however, the quality of increasing in the resistance value must be the same and that is a dramatic increasing as the temperature goes down without any saturation or bending at any certain temperatures, see figure 4.7. Although, not all the eight thermometers responded in the same way, some of them have shown a continuous increase in their resistance value, while others did not. Instead, they have shown a saturation as the temperature is reduced. The reason for this saturation is attributed to the poor thermal contact resulting from manufacturing process, wrapping wires, or from the GE varnish glue. However, the good ones have been chosen to be used for the thermal conductivity mounts later on.

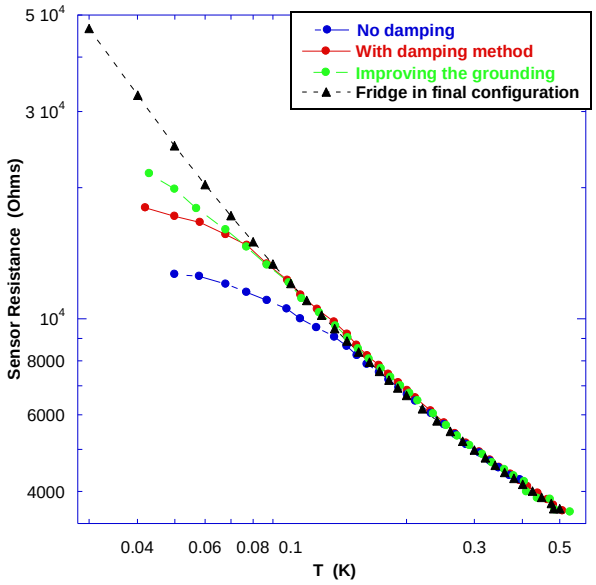

Figure 4.5: Measuring the thermometer resistance in three different situations in comparison with the final configuration for the fridge. The thermometers are semiconductor chips which have the property of a continuous increase in the resistance value as the temperatures is . The plot shows clearly that there is a significant improvement using each method, its obvious how the damping method and enhancing the fridge grounding had improved a lot the thermometer behaviour. Comparing with the results when the fridge is in its final situational, apparently we have got to the situation close to the expected one where the thermometer resistance is increasing continuously as T is lowered.

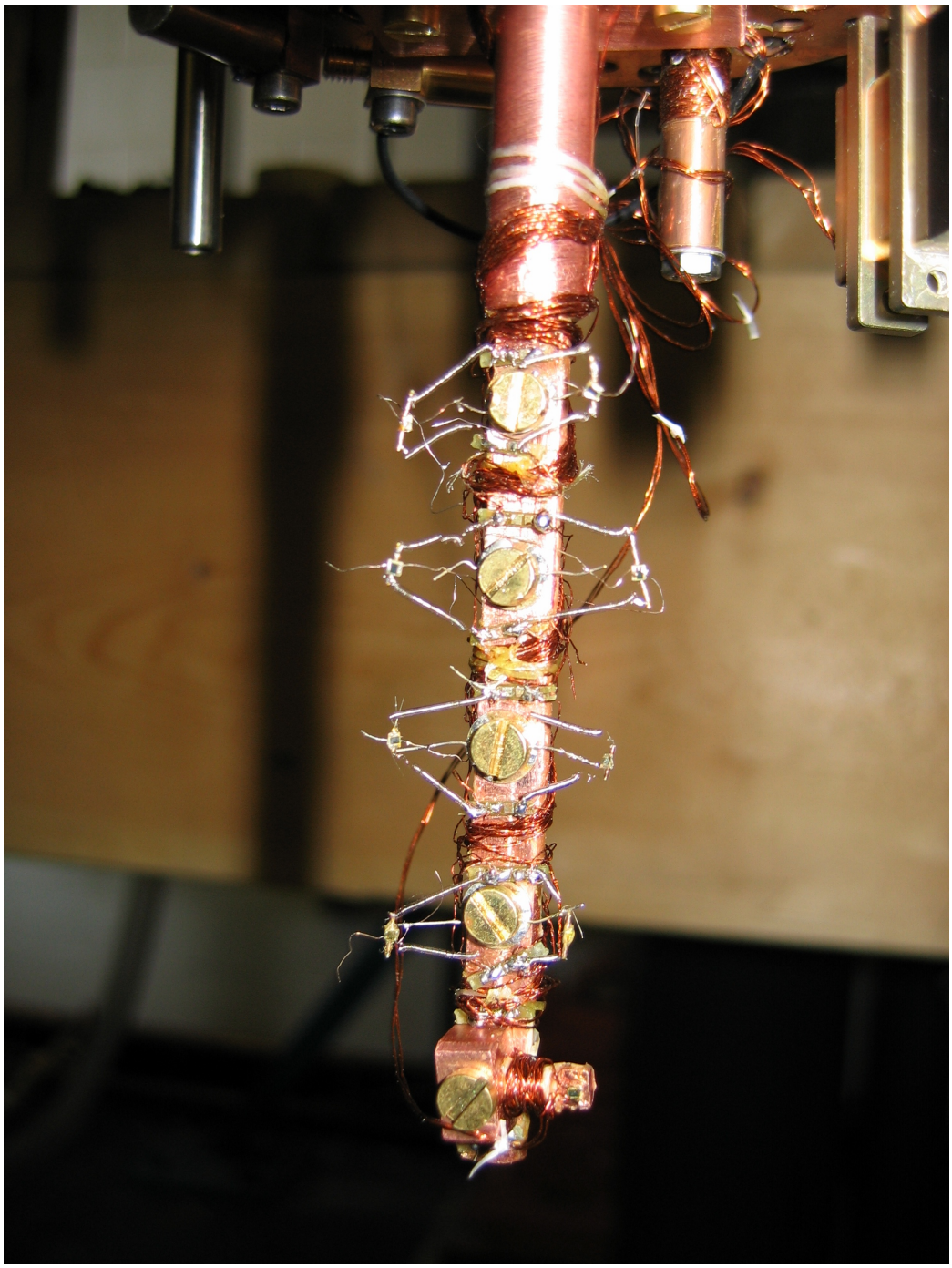

Figure 4.6: Copper mount used to test eight chip sensors.

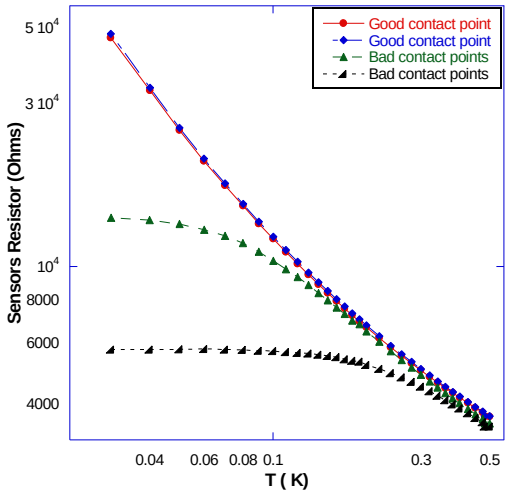

Figure 4.7: The behaviour of thin film sensors resistance verses temperature. All the sensors are from the same type (100 KΩ). Some of them responded by a continuous increasing in their resistance value as T was decreasing, while others saturated at certain T value.

4.4 Thermal Conductivity (κ) measurement description

4.4.1 Mounting the samples

Figure 4.8 is a schematic of the kappa mount loaded with a sample. As mentioned in the previous section, during the design of κ mount, the ease of mounting the sample has been considered. One end of the sample is soldered to the silver block which represents the cold point or the I^-, while the other end of the sample is attached to the heater using silver paint glue, that terminal would represent the I^+ for the sample. Once this step is finished attaching the thermometers is the next step, the sensor close to the cold point would represent the V^-, while the other one will be the V^+. Since most of the samples used in this kind of experiments are very small and delicate, the better way to deal with it is by soldering four silver wires prior to mounting it, this will make attaching the other components easy and more convenient later on. Once we have made all the required connections, the attachment points must be checked by measuring the sample resistance. If the sample resistance is approximately what we should expect at room temperature then every thing should be fine, other wise a problem with the connections or with the attachments must exist. One can do the same with the sensors by measuring their

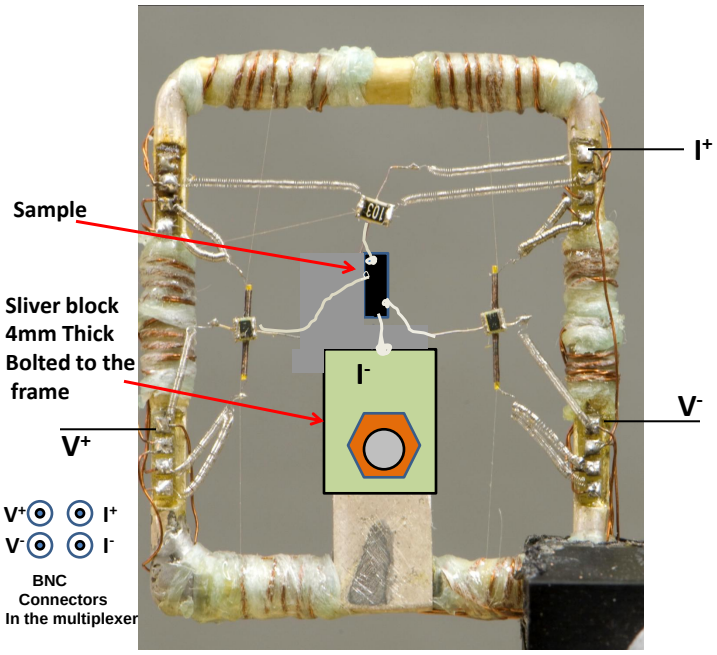

Figure 4.8: κ mount loaded with a sample. The sample is attached to the heater from one side and to the cold point from the other side, theses two terminals should represent the I^+ and I^- respectively. Then two thermometers are attached to the sample and these two terminals would represent the V^+ and the V^-. Once the terminals are marked and identified, they are connected to the LR-700 in order to get the sample resistance or the sensor resistances.

resistance value at room temperature to find any unexpected problem before the proceed in the cooling down process.

4.4.2 Calibration of the thermometers

The most important part of measuring thermal conductivity is to calculate the temperature gradient across the sample ΔT. At equilibrium the temperature gradient is measured by two thermal sensors and $\Delta T = T_+ - T_-$, where T_+ is the hot sensor temperature and T_- is the temperature of the cold sensor, also one can calculate T_{avrg}, where $\mathrm{T}_{avrg} = \dfrac{(T_+ + T_-)}{2}$. Since a resistance value for the sensor is measured, we need to convert these values into temperature values, and that is by calibrating both thermometers against some temperature reference values. In fact, because we don't have a standard values for the sensors, in

each run we might get different readings, therefore we have to have each thermometer to get calibrated for the specific run. We have used a longitudinal steady state method for this measurement in which for every temperature step the temperature of the sample is stabilized at a certain fridge temperature T_o, then by using the heater connected to one end of the sample, we apply a constant heat to the sample. Figure 4.9 shows the resistance value of the thermometers during the process of turning the heater on and off when the experiment is running. Ideally the two thin film sensors-if they are from the same type-should have very close values when no heat is applied (unless if there is some noise affecting them or due a bad contact points). One of them is connected to the sample close to the fridge T_- or T^{cold} while the other one is close to the heater T_+ or T^{hot}. Thus, the sensors resistances will read different values.

The values of the sensors are recorded in a log file along with the fridge temperature and time. At each temperature step, when the applied heat is off and when the sensor resistance gets equilibrated, a certain last values are averaged and recorded in another average file. This value will represent the last resistance value measured at that step before turning the heater on. The same process is applied to the same sensor when the heater is turned on and also the average value is recorded in the same average file, see the inset in figure 4.9. Meanwhile, all the above steps will be applied to the hot sensor as well. At the end, we will have four columns of data, two for each sensor, when the heater is off and when the heater is on.

Next is to plot these averaged values for the cold sensor (when the heater is off) against the fridge temperature using a logarithm of theses values, because the plain values are very steep, therefore one needs to transform them to relation that a fitting can be applied to it. KaliedaGgraph software has been employed to plot the date and to find the fitting equation, see figure 4.10. Once this fitting is obtained, one can use it to calibrate the same sensor resistance when the heater is on. By repeating the same process to the hot sensor one can obtain the temperature reading for each thermometer, i.e. T^- and T^+, hence ΔT and T_{avrg} can be calculated.

4.4.3 Analysis process

The thermal conductivity is given by

$$\kappa = \frac{\dot{Q}}{\alpha\, \Delta T} \tag{4.6}$$

where $\dot{Q} = I^2 R_{heater}$ is the heat flowing through the sample, in section (4.2.2) the method of calculating the amount of heat has been explained. $\alpha = A/\ell$ is the geometrical factor of the sample (A is the cross-section area, ℓ is the length), ΔT is the temperature gradient across

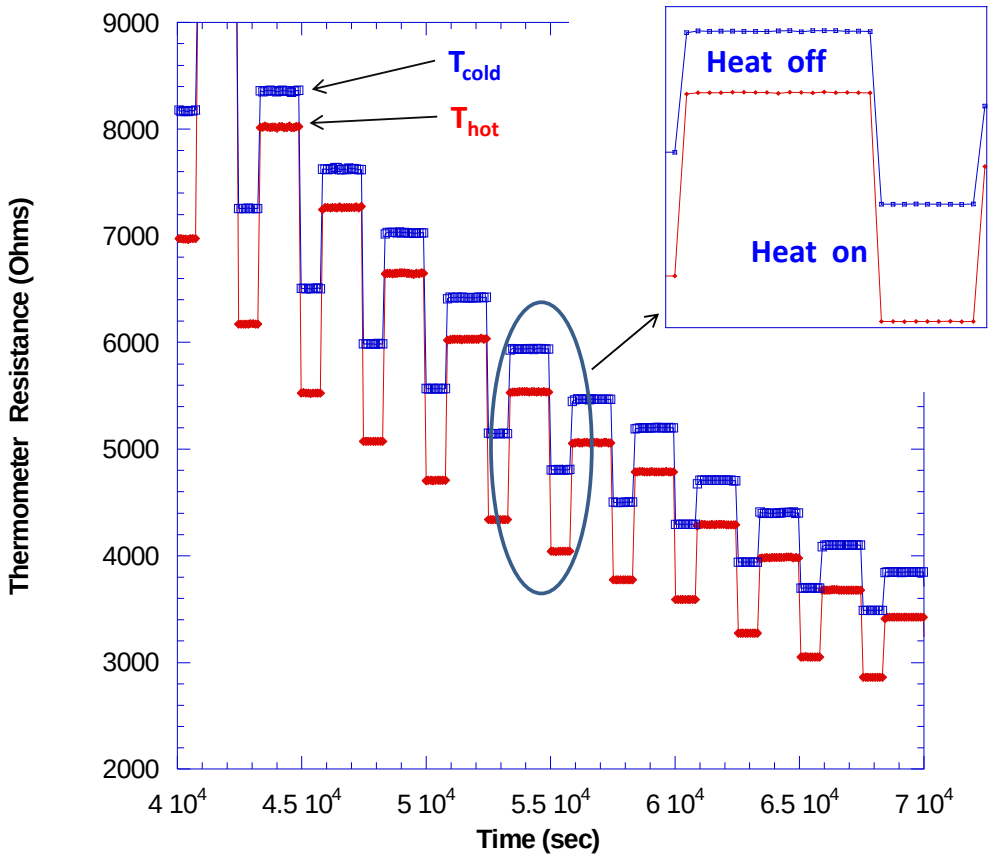

Figure 4.9: Thin film resistor's value vs temperature when no heat (Q) is applied, and when its applied across the sample, inset: the averaging of the sensors values at different base temperatures when the heater is on and off for the cold and hot thermometers respectively. Its very clear from the rapid change in the resistance values that the response time for both thermometers is very short which indicted that both thermometers are thermally anchored very well.

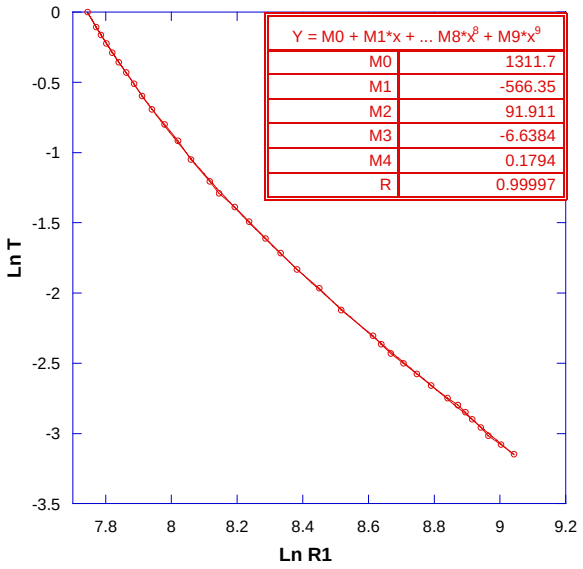

Figure 4.10: A polynomial of 4^{th} degree is been fitted to the sensor average resistance values.

the sample. In the average file all the data for the fridge temperature, sensors resistance value, voltage applied to the heater, and the time is recorded. Using the KaliedaGraph software the other information is extracted. By calibrating the thermometers each time as was mentioned in the previous section, ΔT and T_{avrg} (temperature at which thermal conductivity is measured) can be calculated. The conductance G is calculated, where

$$G = \frac{\dot{Q}}{\Delta T} \quad (\frac{W}{K}) \tag{4.7}$$

The thermal conductivity is given by

$$\kappa = \frac{G}{\alpha} \quad (\frac{W}{cm.K}) \tag{4.8}$$

And finally the Lorenz value L_o is calculated from

$$L_o = \frac{\kappa * R_{sample} * \alpha}{T_{avg}} \tag{4.9}$$

4.4.4 LabView Interfacing program

This software was written to control the thermal conductivity measurement process. It starts by setting up all the parameters like the resistance range, excitation voltage to the

desired values, and the fridge temperature, the applied voltages, and the timers to zeros. From the PID file (Proportional, Integral, Deferential values, these values are determined empirically to maximize the stability of the fridge temperature), the fridge temperature is set at T_o for a certain time, and for a given time the average temperature of the fridge will be measured and recorded. Then the heater is turned on for a certain time, and for a given time an averaging is done to the data. During the two steps when no heat is applied to the sample and when the heat is applied to the sample, the sensors resistance is measured and recorded in a log file then plotted, while the average values in each step is measured separately and recorded in a different average file and plotted. Also the standard deviation for the fridge temperature and sensors reading is measured during the two cases. Then, the PID value is changed to set up the temperature of the fridge at different temperature, and the over all process start again until it reaches the final temperature assigned to the program then stops.

4.5 Tests on the Thermometers

4.5.1 Using the LS-370AC to control the temperature

Oxford cryomagnetic system came with temperature controller system with an uncalibrated temperature sensor (generic thermometer), this sensor is used as a reference or as a guide during the fridge cooling down process. For accuracy we must use a calibrated one, therefore a calibrated sensor type RuO_2 with a resistance value of 2.21KΩ at room temperature and the LS-370 temperature controller have been used instead of the Oxford sensor, the precision we were aiming was 1 part in 1000 or (0.1%) scatter in the temperature values. Also a home made heater has been added to the mixing chamber with a resistance value of 560Ω made from constantan insulated wire to be used as a heat source. In figure 4.11 the temperature measured by Oxford and the LS-370 with the discrepancy in their reading is displayed. We observed a difference of 7 mK higher in the LS-370 reading comparing to Oxford one at the range from 20 up to 400 mK. The difference expands to 11 mK when the temperature is 1K. However, this discrepancy in the two temperatures does not have a significant impact on the thermometers behaviour, also regarding the calculation of κ because it is approximately a constant difference, but on the other hand it will shift the Lorenz values L_o down if the LS-370 is used because L_o is inversely proportional to T,

$$L_o = \frac{\kappa\rho}{T} \tag{4.10}$$

Figure 4.12 depicts the calculated values for κ using the two temperature controllers fittings. The main reason required the use of the LS-370 is to control the fridge temperature. In order to have a precision measurement, one needs to consider the fluctuation in the

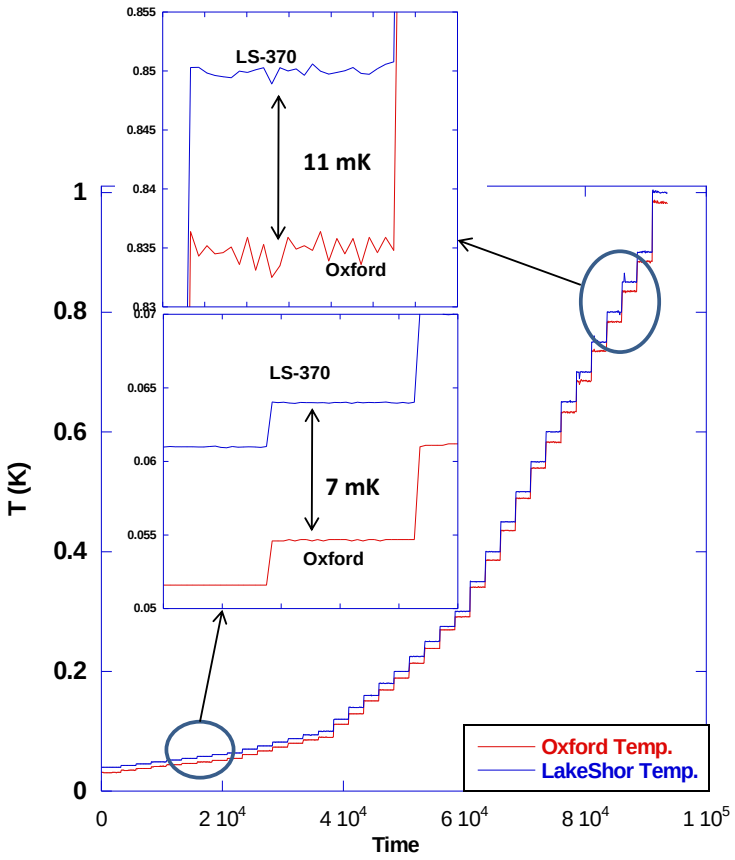

Figure 4.11: The temperature discrepancy in the reading of LR700 and LS-370 controllers. The lower inset shows at 40 to 400mK range the discrepancy between the two devices is approximately 7mK, but at higher temperatures range(the upper inst) the discrepancy is increased to 11mK

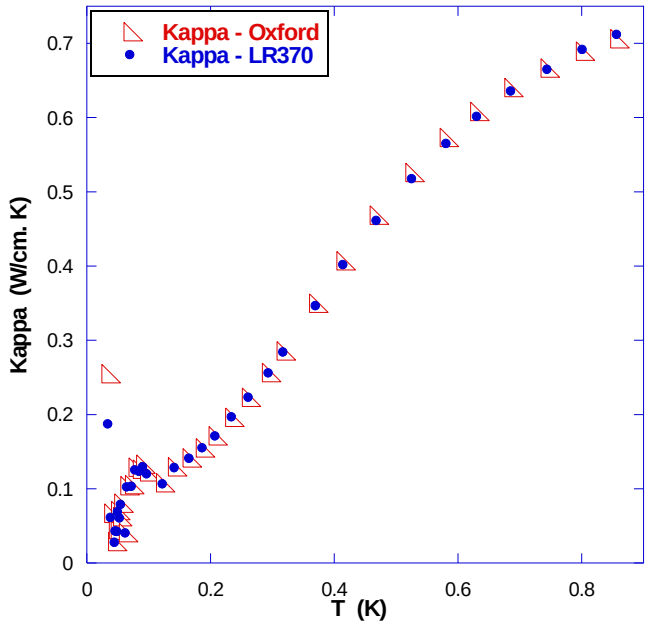

Figure 4.12: κ measured using the Oxford and the LS-370 temperature controllers, the effect is not significant.

temperature within an acceptable range (about 1μK of the fridge temperature). With LS-370 we were able to achieve this range which allow us to concentrate on the other sources of noise that affects the thermometers. Whereas with the Oxford temperature controller, this was not possible especially for the rang of 400K up to 1K. In figure 4.13 and figure 4.14 the scatter in temperature readings for both Oxford and LS-370 temperature controllers respectively are shown.

4.5.2 Comparison between using different types of sensor

Another test has been conducted to find how the type of the thermometers would affect the measurements results, by mean of the resolution in the their calibration. Two types of RuO_2 thin film has been used, the first type has a high resistance value with response of 100KΩ at low temperatures, and 1KΩ at room temperature. Whereas the second type has a response of 10KΩ at low temperature and also 1KΩ at room temperature.

In the beginning, one needs to identify the type of noise both sensors are introduced to during their operation. For example, if the fridge temperature is not stable, this could be one of the main source of generating some noise in the sensors. In order to compare

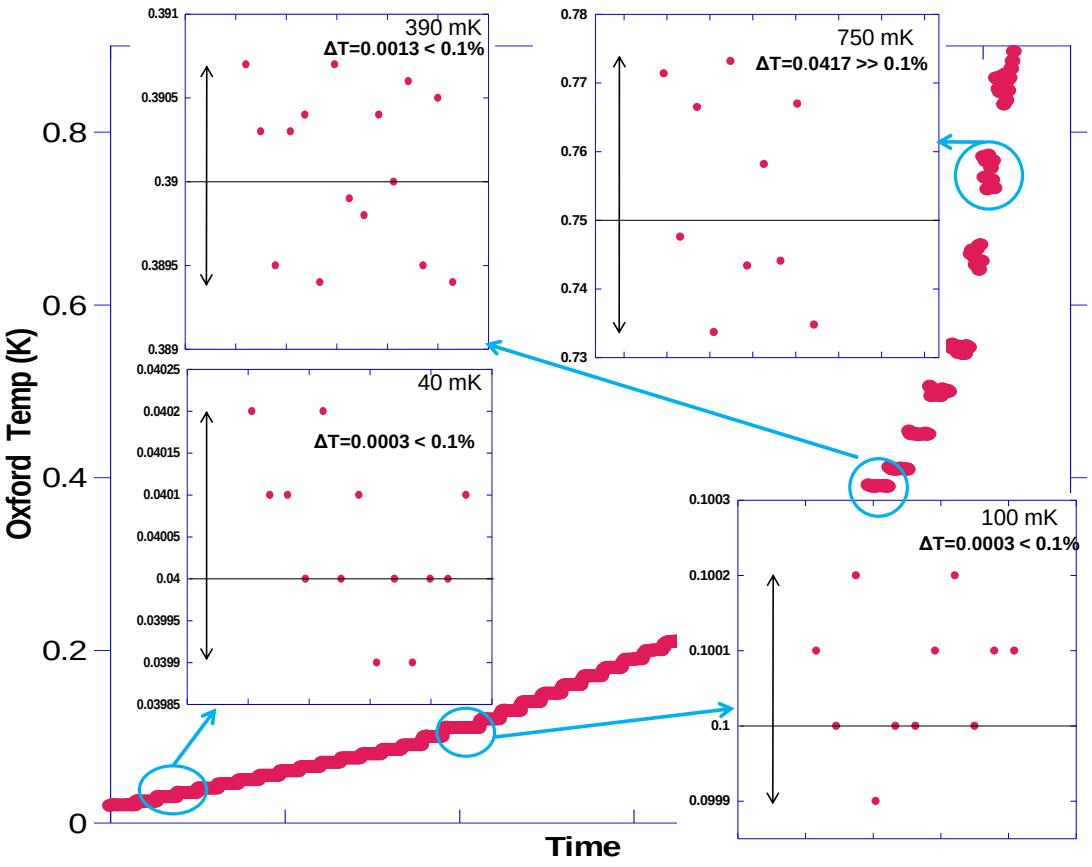

Figure 4.13: Temperature scatter in Oxford temperature controller, the scatter was acceptable in the range between 20mK up to 300mk (around 25μK), but above that the scatter gets very noisy, approximately 40mK.

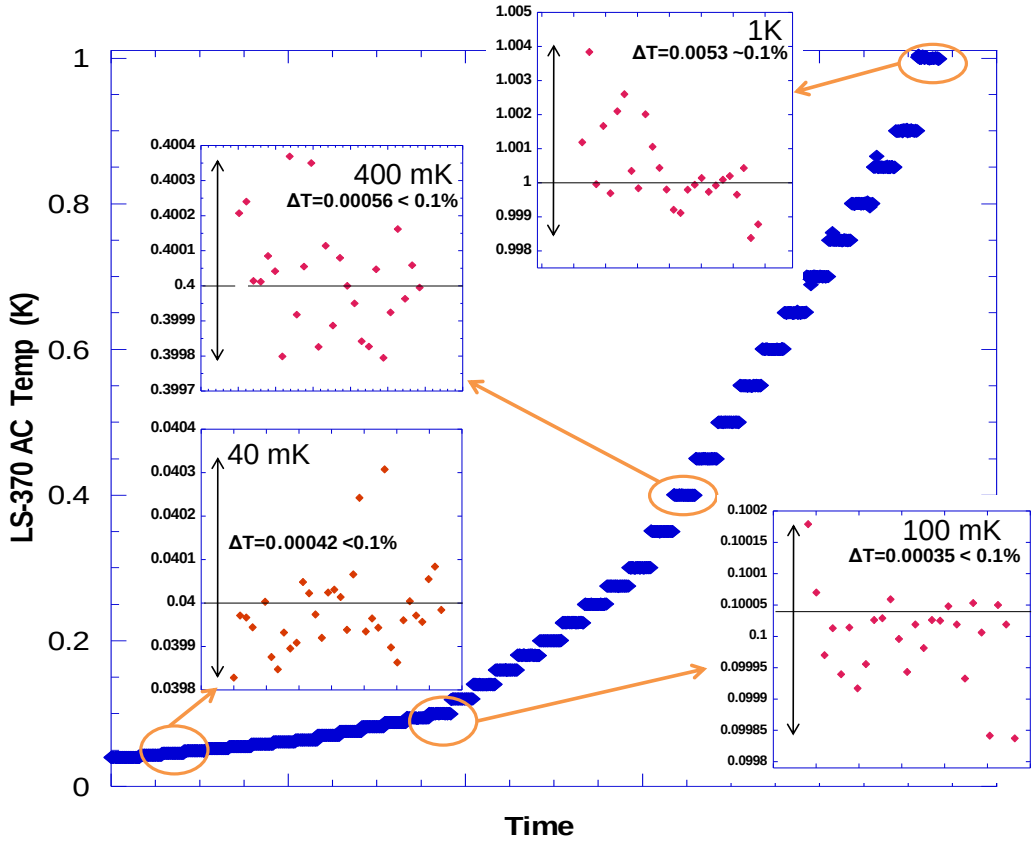

Figure 4.14: Temperature scatter in LS-370 controller, the scatter in temperature is around the acceptable value which is 0.1% for most of the temperature ranges.

between the resolution of the two sensors types one has to choose a certain temperature for both types and calculate the value of ΔR from peak to peak, that is by recording the maximum value and the minimum value of that sensor at that particular temperature, then convert them to temperature values using the polynomial fitting curve (the same one used to calibrate the same sensor). The ΔR value would correspond to ΔT value, hence the amount of error or the temperature fluctuation can be obtained.

For example, at 170 mK base temperature and at 0 Tesla magnetic field, from the average file one can get the maximum and the minimum value for the low resistance thermometer, i.e., from the fluctuation of these values (peak to peak),

$R_{1,max} = 3841.8\ \Omega$ corresponds to $T_{1,max} = 0.16651$ K

$R_{1,min} = 3837.6\ \Omega$ corresponds to $T_{1,min} = 0.16691$ K

i.e, $\Delta T = 0.4$ mK for $\Delta R = 4\Omega$. This tells us that a 1Ω fluctuation in the sensor resistance value would corresponds to 0.1 mK fluctuation in temperature.

One can repeat the same procedure for the other thermometer with the high resistance value. At 170 mK and 0 Tesla we get:

$R_{2,min} = 7826\ \Omega$ corresponds to $T_{2,max} = 0.16824$ K

$R_{2,max} = 7796\ \Omega$ corresponds to $T_{2,max} = 0.16904$ K

i.e, $\Delta T = 0.62$ mK for $\Delta R = 30\Omega$. This tells us that a 5Ω fluctuation in the sensor resistance value would corresponds to 0.1 mK fluctuation in temperature.

Now, by doing the same calculations for the same two sensors At 170 mK and 2 Tesla we get:

$R_{1,max} = 3895\ \Omega$ corresponds to $T_{1,max} = 0.1704$ K

$R_{1,min} = 3877\ \Omega$ corresponds to $T_{1,min} = 0.16855$ K

with $\Delta T = 0.19$ mK for $\Delta R = 18\Omega$. This tells us that a 9Ω fluctuation in the sensor resistance value would corresponds to 0.1 mK fluctuation in temperature.

and,

$R_{2,max} = 7865\ \Omega$ corresponds to $T_{2,max} = 0.16968$ K

$R_{2,min} = 7852\ \Omega$ corresponds to $T_{2,min} = 0.17003$ K

with $\Delta T = 0.35$ mK for $\Delta R = 13\Omega$. This tells us that a 4Ω fluctuation in the sensor resistance value would corresponds to 0.1 mK fluctuation in temperature.

If we are to compare these results, one deduces an interested conclusion: There is no significant difference in the resolution of the two thermometer types. Although, one of them has very high resistance value compared to the other type, the effect of this high

resolution has no impact on the temperature resolution conversion, and this fluctuation has no dependence on the magnetic field. Also, converting the resistance values using the calibration fitting equation will give the same temperature reading despite the different in their resistance values. Eventually, both of them will give exactly the same temperature value despite the large difference in their readings and in their fluctuation, i.e., the ratio of ΔR to ΔT is going to be the same for both types.

Chapter 5

Results On Wiedemann-Franz law in Silver

5.1 Introduction

In order to test our experimental set-up we measured the thermal conductivity of a silver sample. These experiments have been conducted using two methods: First, by using a regular solder to join the sample to the heater and to the two thermometers. Second, by using an indium solder. In order to compare our experimental results with theory, the Lorenz value L_o or the ratio of the charge to thermal conductivities in the limit of T=0 has been calculated. Since this value is constant for all metals at low temperatures, it will be a good reference to compare with the measured values which would show how accurate is the experimental data as well as defining any other potential problems in the experiment like the amount of heat used or the value of the temperature gradient generated across the sample. Two different resistance samples have been used in order to compare the power needed, ΔT, and the quality of contact resistance points of the sample, since we are going to deal with a very small resistance samples (superconductors), one needs to explore the effect of theses parameters and how would they affect the experiment set-up or the other set-ups in case of using three experiments simultaneously. Figure 5.1 shows the L_o measured value which indicates recovering the real value at some temperatures range but not over the whole range.

5.2 Low resistance sample

In this experiment, a silver wire of 100μm diameter and 0.9cm length has been used, the geometrical factor is (8.35×10^{-5} cm). An indium solder is used to connect the sample

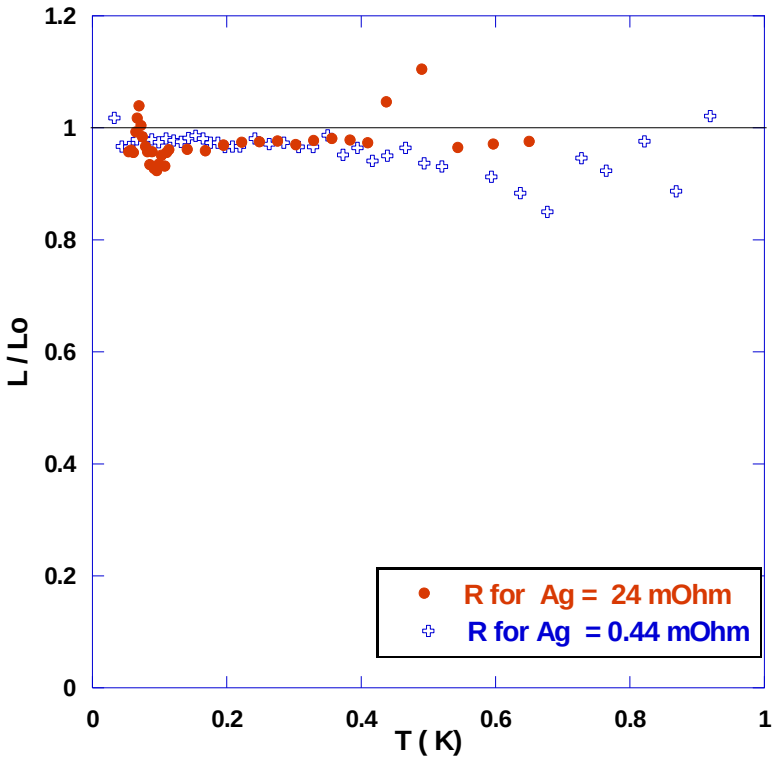

Figure 5.1: L_o measured value for high resistance sample compared with low resistance sample. The measured Lorenz value for a small resistance sample has been recovered within 2.5%, while for the high resistance sample the L_o was recovered within 3%.

to the thermometers and to the heater, the Lorenz value has been recovered within 2.5% error. It is important to point out that a small magnetic filed has been used during this experiment for the reasons to be explained in section (5.5). The discrepancy in L_o values can be explained by studying the plot in figure 5.1, its obvious that the associated error is systematic not randomly, where we could have under estimated the value of ΔT or over estimated the amount of the applied heat in which we did not included the part going through the Pt-Tungsten coil in our calculations. This error also might come from not using the exact resistance values for the heater or for the sample. The sample resistance was very small (40mΩ at T_{room} and 0.44mΩ at T=100mK) which made the sample very conductive and yet made the thermometers better cool down. In order to get a noticeable temperature gradient ($\Delta T \sim 5$ - 10% of T), the power applied to the heater has to be large because $\kappa \Delta T = \dot{Q}$. Thinking of applying more heat to increase the temperature gradient across the sample was not a good idea because that will lead to warming up the fridge and the other set-ups considering the lowest calibrated T_{avrg} we can get is 40mK. On the other hand, applying small amount of heat would cause the pickup noise to be very big due to the self heating of the thermometers themselves, this is why one prefers to apply 10% of the required power from the theoretical calculation of κ. Another important factor that added this error to the data is the ratio of the contact resistance to the sample resistance, since the sample resistance is very small, this leads to have all the ΔT developed at that contact point instead of being across the sample. (More details are given in the next section, see figure 5.4).

5.3 High resistance sample

In this experiment we used a silver paint glue to attach the sample to the thermometers and to the heater instead of using regular or indium solder, therefore there is no need to worry about the contact points and the superconducting concern. When the sample resistance is high it means the sample is less conductive, and to get the thermometers cold will be the major issue. This could happen only if the contact points and the grounding has been improved (providing that the temperature fluctuations is minimized). The reason for increasing the Ag sample resistance is to make the sample less conductive, then less heat is used in which the other two experiments can run simultaneously. Measuring L_o for Ag sample has been repeated when the fridge was completely installed and hanged on the pillars. The L_o has been recovered within 3% as it is shown in figure 5.1. The Ag wire sample is 3.9cm length with 25μm diameter. Its resistance at $T_{room} = 1.6\Omega$, and at $T_{100mK} = 0.024\Omega$ (which is 50 times in magnitude larger than that of the small one), the geometrical factor is (1.24×10^{-6} cm). In this experiment, one of the thermometer didn't cool down very well as the other one did, figure 5.2 depicts these results. It looks that some RF source was heating the thermometers, but since (the T^-) is very close to the cold

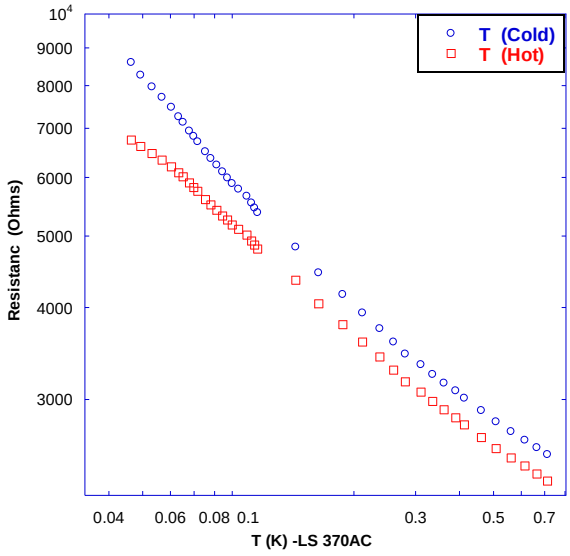

Figure 5.2: Thermometers resistances during the cooling down process for a high resistance sample

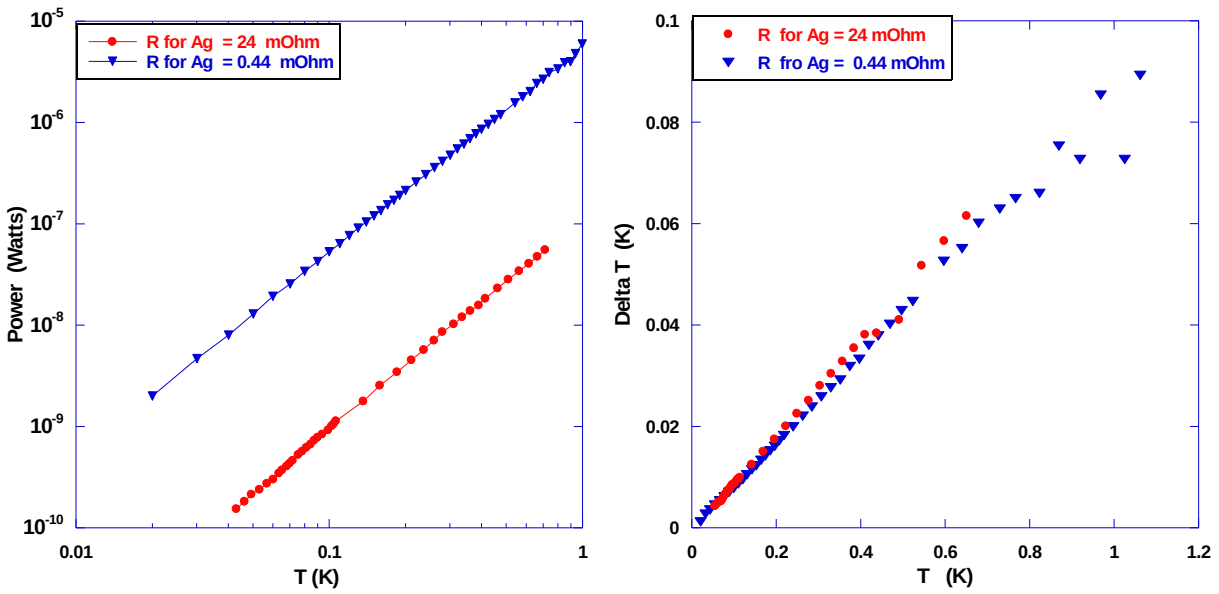

Figure 5.3: (left plot)Power used in heating Ag samples vs T, the power is dropped significantly when the high resistance sample is used. (right plot)ΔT across the samples vs T, it is obvious for the high resistance sample that we have got the same ΔT with much less amount of applied heat.

point, it was less affected by this source of noise. On the other hand, T^+ is connected to cold point thought the sample, it was more affected by this noise. It is clear from figure 5.1 that below the 100mK there is some noise introduced to the system, while from the range of 450mK and up the problem of controlling the fridge temperature become very serious, where the PID values used in the program were not the proper one. At this range one needs to think about turning the roots pump off in order to decrease the cooling power of the fridge, also because the phase change of ^{3}He happens at the range of 600mK which will add instability to the fridge temperature, therefore we considered using LS-370AC bridge to control the fridge temperature, see figure 4.13.

The power needed in the high resistance sample is much less compared with the low resistance, which will allow the measurements of the other experiment simultaneously without having any effect of over heating the whole system, this result is shown in figure 5.3. In the same figure, it shows also the temperature gradient for the two samples is approximately the same in which $\Delta T \sim$ 5-10% of T_{avrg}, this will enable us to get the ΔT with much less applied heat to the sample.

The other important point we need to investigate is the contact thermal resistance, we

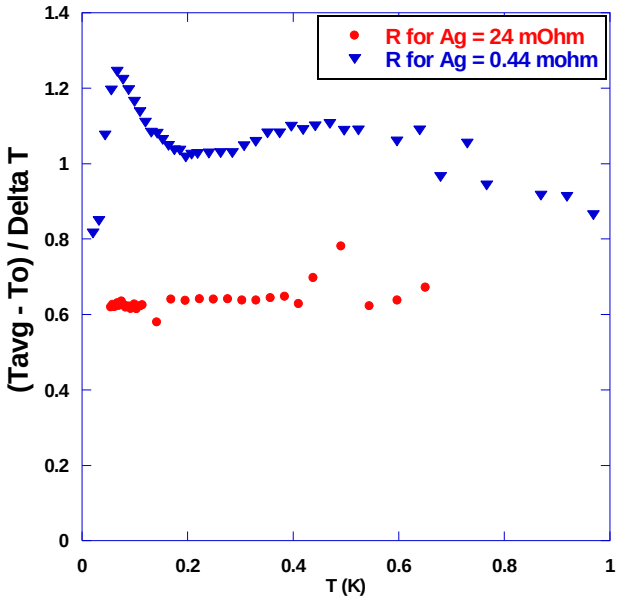

Figure 5.4: The contact thermal resistance of the two samples. Its clear that the contact resistance for the low resistances sample is much larger than the high resistance one. This will lead to the conclusion that the temperature gradient is developed at the contact point but not across the sample. Whereas for the High resistance sample the result is different, most of the temperature gradient is developed across the sample.

can estimate that value from the plot of $(\frac{T_{avrg} - T_o}{\Delta T})$ vs T with more details given in the next section, see figure 5.4.

5.3.1 Sources of Error-Induced electrical and Grounding loop noise

Types of noise

Noise from environment could be either from electric field (E-field), magnetic field (B-field), or ground loops. The electric field noise capacitively couples into measurement leads or to the resistor being measured, hence, voltage is induced as a source of noise. A cable shield is the line of defence against electric field noise, also the connection adaptors between the cables and the experiment or between the cables and the electronic devices are susceptible to this kind of noise, therefore a metal connectors with tight holding at theses contact points screens significantly the RF noise.

Magnetic field noise couples into measurement leads or other conductive loop, current is induced in the leads as a source of noise. Tightly twisted pairs of leads inside the shielded cable reduce the total loop area and minimize the effect of magnetic field.

Ground loops produce noise that acts similar to induced noise but the cause of the noise is different. Current is generated in any conductive circuit or loop when that loop contains changing current or magnetic field, they are usually a result of using an improper grounding method. Isolation reduces ground loops noise by breaking the circuit or the loop.

How to mitigate the above issues

To mitigate the E-field noise: at the very beginning of this research, we used two types of cables. The first type is a 24 wires wrapped with aluminium foil shield with a single ground wire, the second type is a 24 wire cable with a separated pairs wrapped with aluminium foil and a separate single ground wire for each pair. The D connectors connected to these wires are covered with a cases made of plastic. The results were not encouraging because RF was penetrating into theses contact adaptors directly, the noise was at very high level in which it had a significant influence on the measurements. Another issue needs to think about is, the cables themselves, because they are long (about 10 feet long each) running from the fridge to the cabinet, we were sceptic about them being as another source of noise. Therefore, a metal braided shield with a metal cases for the D-connectors at the end of each cable have been used. The connections of the metal braided shield with the metal D-connectors covers have been improved using a silver tape with zip ties for both ends.

To mitigate the B-field noise: a twisted pairs wires have been used all the way from the experiment to the fridge, it will reduces the amount of the external signal which interferes with the signal transported on the wires. Also all the cables used are constructed from twisted pairs which presumably reduces the pick-up noise to a minimum.

To mitigate the grounding loops: in order to minimize of the effect of grounding loops, we have tried different configurations, each configuration worked with specific test depending on the circumstances of that run, especially at the starting of this research until we have got the most ideal situation that can be reproduced at each run. The progress of this development was according to following steps:

We found that by connecting the cables grounding wire (of each one of the three cables) to a particular point on the fridge improves the noise and enhances the measurements. Then by connecting the fridge grounding to a separate ground (not the main one that is already with the building electrical wiring system, did not help very much. Later, we have decided to use an isolation transformer to isolate the electrical cabinet (that holds the electronic devices) from the main building ground, this provided a good improvement to

our measurements but it was not reproducible. Also using an optical isolation devices has been used to break the grounding between the computer and the electronic devices. The LR700 and the LS-370 are connected to one optical device via a GBIP interfacing cables, then a fibre optic cables used to connect the first optical device to a second one which is connected to the computer that controls the experiments, this process helped improving the measurement. Another attempt to improve the measurements has been done was through isolating the main ground totally from the fridge by disconnecting the ^{4}He and N_2 liquid levels meter, and by isolating the winch cables from the fridge, i.e., making the fridge float with no coupling to any grounding. Isolating the electronic cabinet from the main ground totally, then by connecting the fridge to the electronic cabinet, then connecting them together to the ground post in the pit. Trying to reconnect the main ground to the cabinet did not have any important impact on the experiment this time at all.

With all the above mentioned trials, we have got some improvements but it was not reproducible. However, the more interesting issue that improved the overall reading of the thermometers is the coupling between the still line and the braided shield cables.

5.3.2 Minimizing the temperature fluctuation

In section (4.3), the specs of the LR-700 bridge resistor have been discussed, which implies that there is a minimum level of associated noise due to Johnson noise that we can not avoid, it is always existed and would have some direct effect on the measurements. For example, using the results from section(4.5.2), at room temperature, for a 1KΩ resistor with 30μV and 2KΩ scale the fluctuation in the resistance value is ΔR = 30 mΩ corresponds to 3μK fluctuation in T. But in actuality when the measurement is done on the sensor with a 1KΩ at room temperature at the same scales we found ΔR = 60 mΩ which correspond to 6μK fluctuation in T. This implies that there is an additional pick up noise equals to Johnson noise in which doubles the fluctuation in the Temperature values.

In order to find the amount of noise in any sensor we need to use the LR-700 method of calculation. For a 3 sec filter time the amount of fluctuation In R value (or the noise) is given by

$$Noise = \frac{R_{peak\ \ to\ \ peak}}{\sqrt{5} \times \sqrt{3}} \tag{5.1}$$

In this equation the convention that peak to peak magnitude equals 5 times RMS noise magnitude is used. Also the noise decreases by the square root of filter time constant increase. We found the ΔR value for both sensor types is around 45 to 65 mΩ at room temperature, which confirms the above statements regarding the additional noise.

When cooling down, the Johnson noise is supposed to reduce significantly because it is temperature dependent ($\sqrt{RT}$). From Eq.(4.5), one can show how the Johnson noise is

varied by changing T. At T = 300K, R for the sensor = 1000Ω, then $\sqrt{RT} = \sqrt{3 \times 10^5}$, whereas at T = 50mK, R = 60000Ω, $\sqrt{RT} = \sqrt{3 \times 10^3}$. From this direct example we see how the Johnson noise is reduced by a factor of 2. But in our case the fluctuation in the sensors resistance values is still in the range of several Ohms ($\simeq$ 0.5mK as its shown in the figure 5.8.

One needs to point out that this fluctuation in R value is also magnetic field independent, i.e., no vibration issue is coupled to the system. Hence, this would suggests that there must be another reason causes this fluctuation which could be either from an external RF source interferes with the measurement or it could be from the temperature fluctuation. To justify this problem, we needed to think how to eliminate one of them in order to focus on the other source. If this external source of noise is an RF, then we need to know how it is affecting the experiment, we assumed there is a 1 MHZ frequency in effect on an impedance of 100KΩ, then $Z_c \sim \dfrac{1}{2\pi f C}$, or $C \sim \dfrac{1}{2\pi \times 10^6 \times 10^5} = 1.6$ pF.

From this straight calculations we have considered that the RF in effect is lower than 100MHz and therefore a capacitor with a value of 180 pF has been attached in parallel to the sensor, see figure 5.6. However, this attempt did not improved the fluctuation in the resistance values because we were still having ΔT= 6μK which is the same compared with the values at room temperature. Whereas at low temperatures, ΔT reading is in the range of millikelvins. This suggests that this source of noise could be due to other factors that we have not considered, because we know the temperature controller has a fluctuation in the fridge temperatures within 1 part in 1000 of the base temperature, and there is no RF in the chosen range affecting the system. Hence, it could be due to choosing the wrong frequency range to be filtered, or, the existed RF is affecting the heater used in supplying heat to the sample which produces additional heat in the heater itself. Also adding the capacitor to the sensor directly as it was shown in 5.6 might not be the proper position because it might heat the frame as it is filtering, one need to think about remove this direct coupling between the capacitor and the mount by putting it some where else.

5.4 Superconducting Contacts

If one needs to use a high resistance sample, then it is better to have an excellent contacts in order to get both thermometers cold. Because we have mentioned earlier that if the sample resistance is small and the contact points has a small resistances then both thermometers will get cold despite of any external source of noise, both of them will be susceptible to this source in the same way. But if the sample resistance is high, then one of the thermometers will be more susceptible for the same source of noise because its connected to the cold point across the sample resistance. In section (5.1) it was mentioned

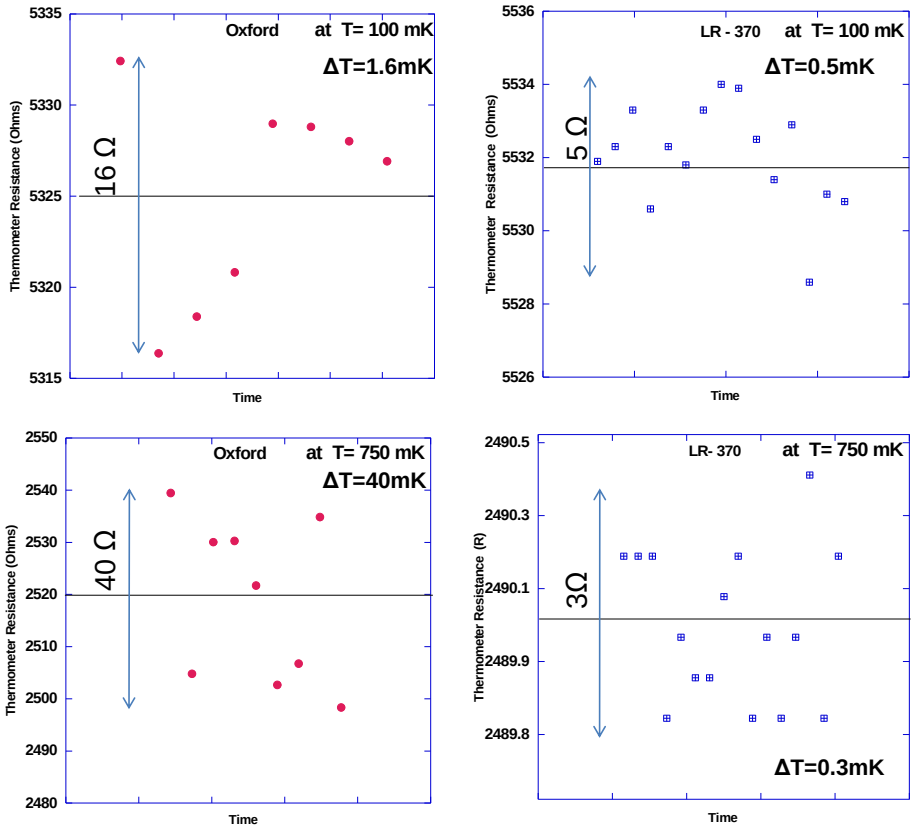

Figure 5.5: The fluctuation in the sensors resistance values using both LR-700 and LS-370AC temperature controllers. its Obvious the scatter is in the range of 1.6mk to 0.4mk using the Oxford controller. While with the LS-370 the scatter is in the range of 0.5mk. However, with using the LS-370 a reduction in the fluctuation is very clear but its not 0.1% as it is suppose to be, it is about 0.5% (5 times the 1 part in 1000). Note that an approximation is used to calculate the ΔT where its assumed the conversion of 1Ω is equivalent to 0.1mK.

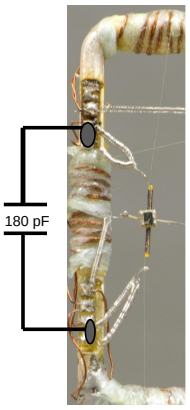

Figure 5.6: 180 pF capacitor connected in parallel with the thermometer in order to filter the RFs in the range of 100 MHz.

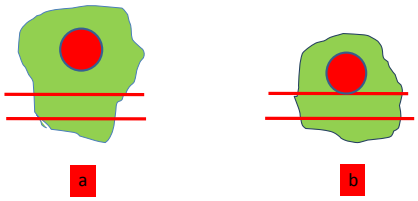

Figure 5.7: a) The solder is joining the two wires which adds its resistance to the thermal resistance of that contact point. b) The solder is holding the two wires and no resistance is added to the combination.

that a magnetic field has been used during that experiment. At Zero magnetic field the indium becomes superconductor when cooling it down which makes the contact points very poor against transferring heat, therefore a magnetic field of 200 mTesla has been used to terminate the superconductivity in Indium. If one thinks more about this issue by assuming the contact points to be as shown in figure 5.7, In figure 5.7-a if the solder is joining the two wires then there will be some resistance in that contact, and as we cool down if the solder material turns to a superconductor, the material will be poor against transferring heat. Once the magnetic field is applied we expect to see a significant field dependence in the measurements. Comparing with situation in figure 5.7-b, If the solder is holding the two wires then a small field dependence is expected to be seen. As a demonstration for this argument, a test on the thermometers behaviour has been conducted using different soldering materials, a regular solder and an indium solder and both of them become superconductor at low temperatures, hence a bad heat conductors. We will use this approach

in analysing this issue, assume the thermal resistance of the contact point is $R^C_{thermal}$ and for the sample is $R^S_{thermal}$, also we know that $\mathrm{R}_{thermal} = \dfrac{\Delta T}{\dot{Q}}$. Since $\dot{Q}$ is the same at any point across the sample, therefore $\mathrm{R}_{thermal} \sim \Delta T$ and hence

$$\frac{R^S_{thermal}}{R^C_{thermal}} \sim \frac{\Delta T_{sample}}{\Delta T_{contact}} \sim \frac{\Delta T}{T_{cold} - T_{fridge}} \tag{5.2}$$

if the contact is superconducting, this implies that $R^C_{thermal}$ is large, then $\dfrac{\Delta T}{T_{cold} - T_{fridge}}$ will be small. This will happen in zero field.

Whereas if the contact is normal, $R^C_{thermal}$ is small, then $\dfrac{\Delta T}{T_{cold} - T_{fridge}}$ will have a large value and this will happen with the existence of a magnetic field. In figure 5.8 results for this test are displayed.

5.5 The outstanding or the unknown issues

During the investigation of the previous issues part of these grounding loops broke, but not completely, causing the fluctuation in the sensor reading to be improved slightly. However, some other outstanding issues remain unexplained, because we could not find how they coupled together or with other sources of noise. One of these puzzles was the impact of the contact between the experimental cables and the liquid helium trap pipes or the still line. This happened just by coincidence when we were looking for a good grounding configuration. When the cables were in contact with the side of the fridge this led to an improvement of all of the thermometer sensitivities. The sensitivity of the LS-370 was also improved but the Oxford thermometer showed little improvement. On the six thermometers, the low resistance sensors were reading almost $11K\Omega$ and the high resistance sensors, $100K\Omega$. The LS-370 was reading $120K\Omega$. Another issue occurs when we make any changes in the configuration which have a negative effect on the LS-370 and a positive effect on the Oxford thermometers or the vies versa. This is a big paradox. We could not find the coupling between these two thermometers or the real reason behind this behaviour. Although, there is an ultimate situation where both read a maximum value. The final issue we have found occurs when there was coupling between the three experiments as they ran simultaneously. This coupling has huge effect on the experiments when they are running, but once we isolated them and let them run separately the effect disappears. The reasons behind all of these issues are not yet understandable which suggest more work on them to find out an optimum situation.

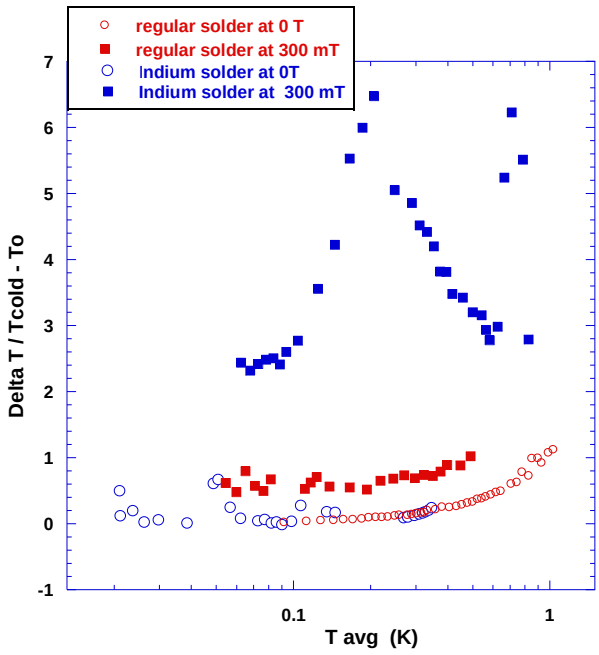

Figure 5.8: The improvement in the quality of the contact point between the sample and the fridge or T_o. Two solder types are used to connect the sample to T_o, Lead solder and Indium solder. In zero field at low temperatures, both points have a poor quality against conducting heat, but as the magnetic field is turned on a significant improvement occurs especially with the Indium solder.

5.6 Summery

In conclusion, we have recovered the Sommerfeld of the Lorenz number L_o at low temperatures using a sliver sample with two resistance values. Since, in the future we are going to deal with very low resistance samples (superconductors) it will be very instructive knowing the effect of the sample resistance parameter. We have used a LS-370 temperature controller to provide a fluctuation in the fridge temperature (within 0.1% of T) in order to eliminate one possible source of noise that has a significant effect on the thermometers behaviour. A calculation of the scattering in the sensors resistance values has been conducted in order to determine what type of noise those sensors are susceptible to. We found the fluctuation in the sensor resistance is independent of the magnetic field which implies that it is not vulnerable to vibrations. Although, even with controlling the temperature fluctuation the sensors are still susceptible to another type of noise which causes them to fluctuate in a range higher than they should. A 100MHz RF has been considered as an external noise, to filter it, a capacitor has been added in parallel to the sensor. However, no major difference has been detected and still the fluctuation was in the high range.

Using the high resistance sample requires the contact points to have a very low resistance in order to get both of the thermometers cold. The quality of this contact point depends on several factors, like the material used for joining the two parts or the quality of the sample surface, etc. Hence applying a small magnetic field makes a significant effect on the results in case the contact point turns to superconductor.

Chapter 6

Review on $PrOs_4Sb_{12}$ and Background

The discovery of superconductivity in the heavy fermion compounds has attracted a lot of experimental and theoretical activity. $PrOs_4Sb_{12}$ (which does not occur naturally, but its synthesized in the labs) is the first Pr- based filled skutterudite that exhibits the heavy fermion behaviour with m $\sim 50m_e$ where m_e is the mass of a free electron [12], the superconductivity occurs at 1.85 K. The natural skutterudite structure has two voids in each unite cell that are large enough to accommodate a variety of atoms including most of the light are lanthanides (La,Ce,Pr,Nd,Sm,Eu,Gd,Tb) and Yb [36], see figure 6.1.

From the previous different experimental studies on the $PrOs_4Sb_{12}$ compound have shown the following results:

In the normal state:

1- From the magnetic susceptibility measurements, the data shows both $\Gamma 3$ doublet and $\Gamma 1$ singlet could be the ground state, but $\Gamma 3$ doublet appeared to be most likely ground state due to fits to specific heat [22] and [21]. Both of these two ground states are non-magnetic which implies that the coupling in the superconducting state is related to some other mechanism but not the magnetic coupling.

2- From the specific heat measurements, shows that $\gamma = \dfrac{C}{T} = 607\frac{mJ}{mol.K^2}$, this value is much bigger comparing "for example" with Cu about $(1\frac{mJ}{mol.K^2})$ which is an evidence for the heavy fermion state [12],[5].

3- The existing of a high field induced antiferro-quadrupolar ordered phase above 5 Tesla near the superconducting phase, the high ordering phase (HOP) also is seen by means of large peaks in specific heat [22] and [20]. Suggesting that in the absence of magnetic ordering, Pr ions play an important role in this unusual superconductivity.

In the superconducting state: experimental evidence is conflicting with some measurements indicating a fully-gapped BCS state, others constitute with a superconducting

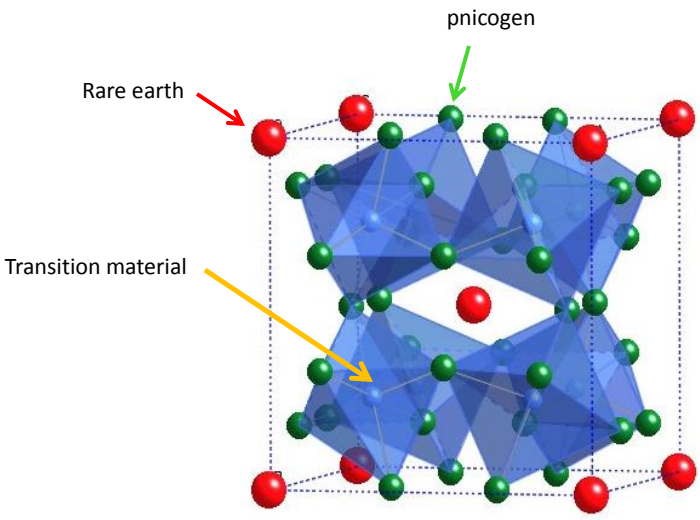

Figure 6.1: Model of the filled skutterudite structure. The transition metal atoms (Fe, Ru, or Os -small light blue spheres) are at the center of distorted octahedra formed by the pnicogen atoms (P, As,Sb- green spheres). The rare earth or the lanthanide atoms (red spheres) are located at the center of a cage formed by 12 pnicogen atoms. from [36].

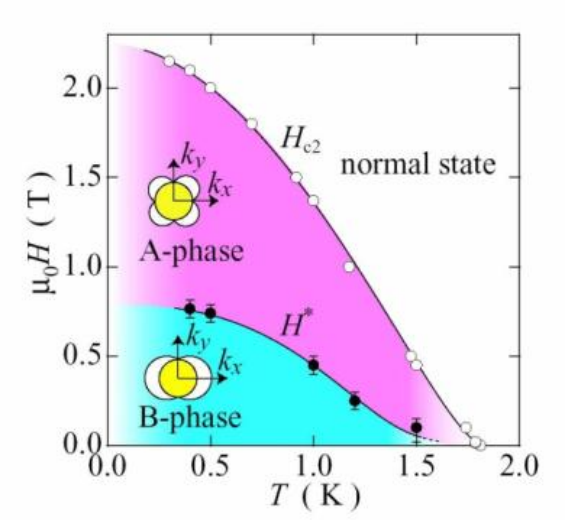

Figure 6.2: The phase digram of the superconducting gap, the filled circles represents the magnetic field H^* at which the transition from fourfold to two fold symmetry takes place. In this research we are only interested in the very low temperature region with a low magnetic field where only the phase B is existed.

energy gap with nodes suggests more exotic nature of superconductivity.

4- From the specific heat measurements, double superconducting transition is happening (unknown origin) [22]. This feature was also found when $PrOs_4Sb_{12}$ is probed by local magnetization measurements [16].

5- From the angle-resolved magneto-thermal conductivity experiments, a change in the symmetry of the small anisotropy in the conductivity is interpreted as evidence for a multiphase superconducting phase diagram with structure in the energy gap [11], see figure 6.2.

6- From the low temperature thermal conductivity measurements experiment, shows a multi-band superconductivity and a residual electronic conductivity when extrapolating the fit to T=0, see figure 6.3, [14].

From All the experiments above, they show that this compound has an exotic features and its behaviour is **unconventional superconductor**, where they indicate existing of nodes in the energy gap.

While on the other hand and from the following experimental results They show evidence that $PrOs_4Sb_{12}$ behaves as a **conventional superconductor** with an isotropic energy gap or fully gapped BCS superconductor:

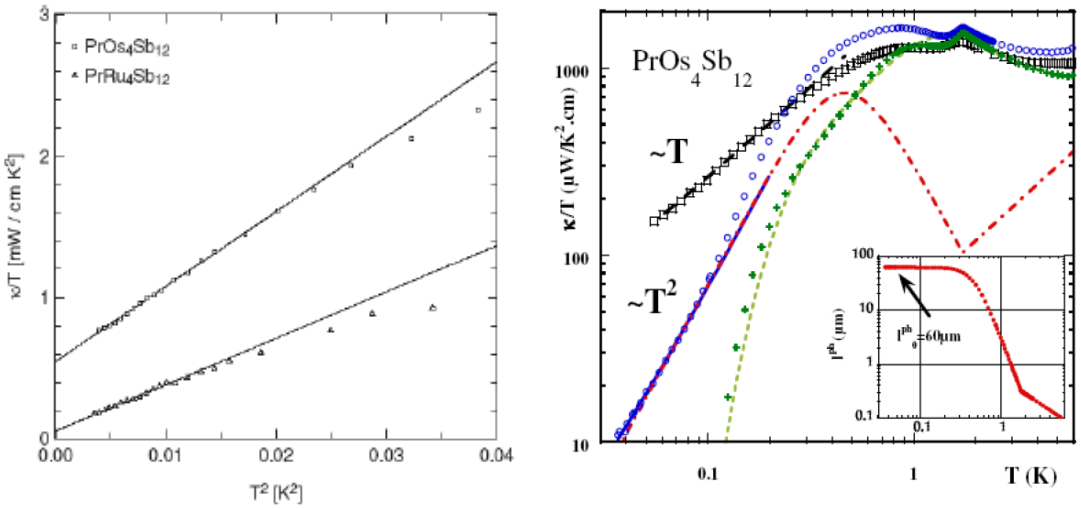

Figure 6.3: (Left plot), Thermal conductivity divided by temperature T versus T^2 in zero field for $PrOs_4Sb_{12}$ and $PrRu_4Sb_{12}$, from [14]. (Right plot) $\kappa(T)/T$ in zero field. The dashed line is in fit of κ_{el} within the Multi Band superconductivity scenario, with exponential behaviour (fully open gaps), from [7]. Note that the axis are plotted in log scale and by converting them to liner scale the difference will be more obvious, the residual term will look very tiny as compared with the left plot where the residual term is finite.

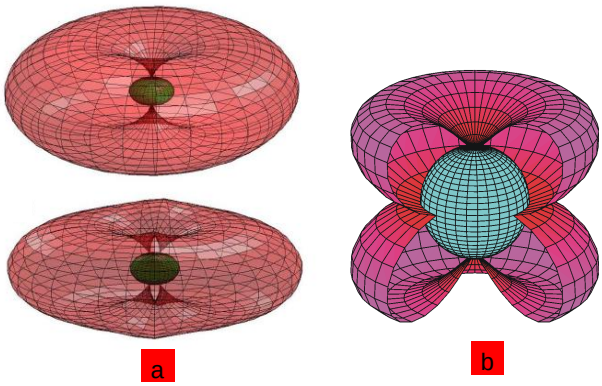

Figure 6.4: Three dimension hypothetical plot for the energy gap and the Fermi surface in $PrOs_4Sb_{12}$. This energy gap could have point nodes (a), or a hybrid (B).

7- From the other low temperature thermal conductivity measurements [7] and [8], see figure 6.3-right plot.

8- The transverse-field muon spin relaxation experiment [6].

9- The Scanning Tunnelling Microscope (STM) [10].

From the above results an important questions have to be addressed: how can we identify the superconducting state and provide a comprehensive theory that can explain all the above features about this material? and what is the nature of superconducting state that can give a complete picture for the energy gap in this material? and how can thermal conductivity reconcile the κ measurements in figure 6.3?

Two works ([17],[18]) relate more closely to the research presented here. In these references, the result of a strict analysis of symmetry breaking described by landau theory was considered. According to this approach, for $PrOs_4Sb_{12}$ the order parameter which describes the normalto-superconducting phase transition must belong to one of the irreducible representation of the crystallographic point group. Also, it has been shown in [11] that the superconducting gap structure in heavy fermion $PrOs_4As_{12}$ using thermal transport measurements in magnetic field rotated relative to the crystal axis, a change in symmetry of the superconducting gap function occurs deep inside the superconducting state. A clear indication has been demonstrated regarding the presence of two distinct superconducting phases with twofold and fourfold symmetries, see figure 6.2. One needs to emphasize the fact that we are only interesting in the very low temperature region with a low applied magnetic field where only the phase B is existed. This phase has nodes located at a polar of hypothetical spherical Fermi surface, see figure 6.4.

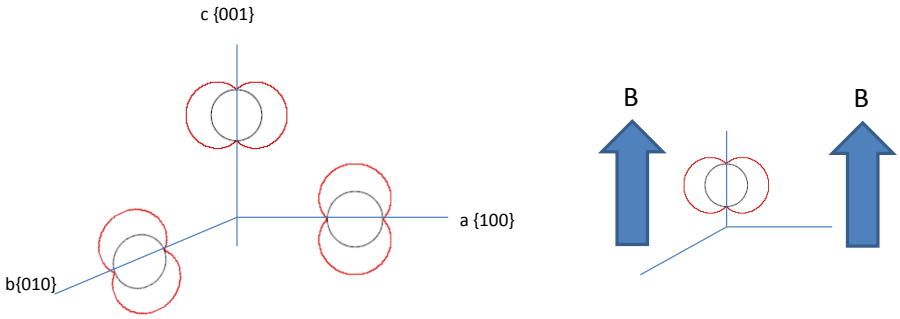

Figure 6.5: In Phase B at low temperatures the order parameter is two folds with polar point nodes, they can be presented along any of the three axis symmetry when no magnetic field is presented. But as a small magnetic field is applied one of the three symmetries will be in favoured than the other two and more likely will be along the magnetic field. This direction can be determined by measuring the thermal conductivity.

Thermal conductivity can detects the presence of these nodes along the heat current axis by registering a linear in thermal conductivity as T$\rightarrow$ 0, see theory section (2.6). The B phase has three possible directions which could exist in three separate domains (1,0,0), (0,1 0), and (0,0,1), in which in the absence of unusual crystal shape or external fields are all expected to be present, and will lead to the observation of the full tetrahedral symmetry. Six degenerate nodes will be observed in the directions <00$\pm$1>. If we introduce an external effect (for example) along the Z direction, because the crystal symmetry of $PrOs_4As_{12}$ is tetrahedral to begin with, any axial perturbation will lift the degeneracy of all three domains in which any of these domains could be favoured. Therefore, only one domain is present; the symmetry will be with two nodes. It is not likely that two out of three domains would be present in the B phase, but could be possible if they were very close in energy, see figure 6.5. When the Magnetic field is $\parallel$ to the thermal current direction then, there will be a residual coefficient (κ_0/T) that can be measured by thermal conductivity. Other wise if the Magnetic field is $\perp$ to the thermal current direction then (κ_0/T) is expected to be Zero, see figure 6.6.

Regarding the states of this experiment, many attempts have been repeated to get a reasonable data but unfortunately many obstacles have deterrent these attempts. One of the problems is the contacts of the sample which never let the thermometers get cold. The suggestion to overcome this problem is by redoing the contacts or may be if it is possible by etching the surface of the sample to remove the oxide layer that is giving a large resistance.

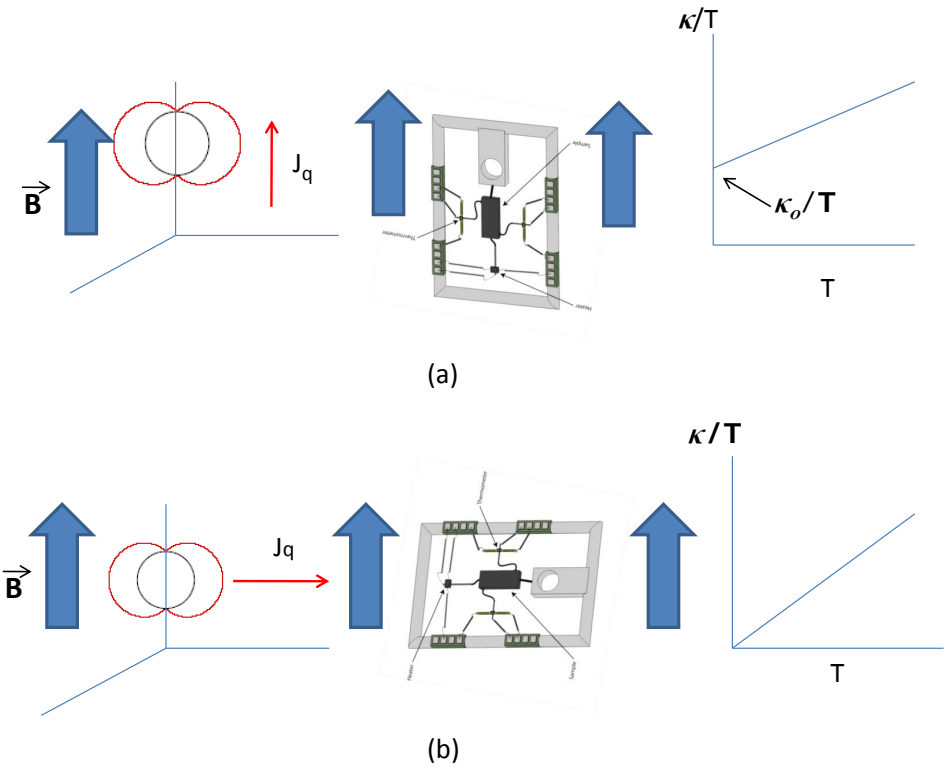

Figure 6.6: (a) Magnetic field is applied parallel to sample thermal current. (b) The magnetic field is perpendicular to sample thermal current. Note that the two mounts are supposed to be used simultaneously in conjugation of a magnetic field. Using two samples with two mounts mounted in different directions provide more convenient in extracting the results.

Appendix I

Through put test when the fridge temperature is at 4 K:

a- Close the 1 Kpot N/V and vent it to the helium bath by opening 1A.

b- valve 6 must be closed.

c- Fully open 12A, open V9, V3, then G1 must go to zero.

d- Open 13A periodically, G1 must go to some value then close 12A and let G1 settle to some value 60 mbar or 76 mbar.

e- Close V3, then open V5 to let G1 go to zero.

f- Open V1, then open the ^{4}He trap manual valve on the fridge, in the same time run a timer to measure the flow of gas into G1 per 1 minute.

First test,

G1= 60 mbar, starting flow measure was at 0. By opening the manual valve the rate was 26 mbar/min

$I(impedance) = \frac{P}{\Delta P} = \frac{26}{60} = 0.47$

Second test,

G1= 77 mbar, starting flow was 0 By opening the manual valve the rate was 22 mbar/min

$I(impedance) = \frac{P}{\Delta P} = \frac{22}{77} = 0.36$

So the idea is to put a certain amount of a pressure (gas mixture) in the fridge through valve 3 and measure the back flow of the gas mixture through valve 1 after opening the manual valve.

Trouble shooting problems in the fridge and how to solve them

[**1**]- Gas Mixture leaks into the IVC can

Symptoms: in the condensing state, usually G1 and G2 readings should come close together at 80 mbar, this has to be done by throttling 12A, open 13A, 3, and 9. We use to condense through the still line instead of the condensing big line where the first one has a big diameter comparing to the second one. Although, we can condense through both lines in the same time. In this process most of the gas mixture has to be condensed in the mixing chamber, but what is happing is still there is some gas left in the dump and cant be condensed. By running the circulating step, usually would continue the condensing and would suck all the gas mixture from the dump to use it in cooling the fridge where the temperature of the mixing chamber should go from 1k to 16 mK. But what we are observing is, the temperature goes down to a certain value at 800 mK and starts to rise up, it can't go down further.

This means that either there is a heat load or He leak in the IVC where the charcoal is saturated and can't suck any more He gas.

Diagnosing:
a- Pump out all the gas mixture into the dump and warm up the fridge.
b- Make sure there is no touch or heat load in the mixing chamber.
c- Put the IVC can on and pump it over night, let some gas mixture go into the mixing chamber while a leak detector is hooked up to the IVC.

We found a small leak in one of the condensing plates on mixing chamber. It was ^{3}He and ^{4}He leaking out of that part into the IVC and causing this problem.

[**2**]- 1 Kpot needle valve doesnt open properly

a- Usually after transferring He to the Dewar we run the 1 Kpot before starting the condensing. Some times when opening the N/V valve no pressure is seen on G3.

b- To solve this problem, check the power going to the motor, if its OK and you notice the motor is working, then we need to open the N/V manually by undoing the screw of the motor mount and turning it to left and right till it starts open and G3 value rises up.

[3]- N_2 or He trap blocked

Symptoms:
a- Usually, the pressure on G1 and G2 during a normal run of the fridge while circulating should be 130 to 170 mbar respectively.
b- We start noticing that G1 is reading 250 mbar, and G2 368 mbar

This an indication that, there is either a blockage in the N_2 trap (liquid nitrogen-LN_2) or in the He trap. To solve this problem,

*****Cleaning the N_2 trap (LN_2) while the fridge is cold.***

1- Close 13A and 1 while the fridge is running and cold.

2- Open 3, 2, 7 ,12A is opened already. let the rotary pump suck and clean the lines through V6 till G1 goes to 0.

3- Close 3, 11A and 2 then take the N_2 trap out and heat it up. Since 12A is still opened, you can watch the pressure or the amount of dirt collected in the trap on G1.

4- Using an external pump hooked up to the vent line at the back of the IGH, open 2, 7 and 11A. Use a heat gun to warm up the trap, that will make sure you have got rid of all the dirt in the trap.

Notice we are doing this procedure during the fridge is cold, therefore 1 Kpot needs to be kept cold and running so the pressure in the still side will not go very high.

*****Cleaning the He trap (LHe) while the fridge is cold.***

1- 1 Kpot must be running during this process too.

2- Close 12A and the manual valve of the condensing line. then pump the gas mixture back into the still line, that is through V3 and by keeping 6 fully opened as well as 1 should be open.

3- Once G1 goes to 0, take the He trap out of the fridge and warm it up using heat gun.

4- Since we will be able to see the pressure on G1 which shows the amount of unwanted molecules in trap, an external pump must hooked up to the vent line at the back of IGH.

5- Once G1 gets saturated, open 7, 2 and clean out all this dirt from the gas mixture.

6- Put the tarp back in the fridge slowly. Open the manual valve then open 3. Throttle 12A gradually until the pressure on G1 and G2 goes to normal, 130 and 175 mbar respectively.

[4]- After pumping the gas mixture back to the dump, G2 reads more than the expected value which is 681 mbar at room temperature with ^{3}He rotary pump running. G2 is reading 780 mbar.

This problem indicates either developing a leak in system allows air to enter. Or, it could be H_2 evaporation from the pumps oil, entering the system through the oil mist. So what is this extra stuff, and where is it coming from??

a- First thing need to think about is to start purifying the gas mixture using N_2 trap to take out all the extra stuff which is supposed to be air if the system is leaking from the PVC pipes or from the glue used to connect these pipes, or some where from one of the connections. After several times of repeating this process, we still end up with 740 mbar in G2. This suggests that the extra stuff could be H2 or a leak from the IHG system itself. Because when we purify the gas mixture, this process required to isolate all the external lines connected to IGH including the PVC pipe lines and all the other hoses, except the lines that connects the N_2 trap and the ^{3}He rotary pump. By running the fridge with this new amount of gas mixture, it will not run properly and soon or later a block will be developed in the fridge for sure.

b- How to locate this leak and cure it?

* if the fridge is cold, for instance, with these reading values: Still line= 23 mbar, Mix-Chamber= 1.9 K, 1 Kpot= 2.5 K.

* pump the gas mixture into the still line through the N_2 trap back to the dump. G2 is reading now 803 mbar.

* empty the cold trap line from by opening 12A or 2 and 11A and let all the stuff go to the dump.

* close all valves, then open 3 to monitor still line with G1, immediately G went to 106 mbar.

* mix-Chamber is at 4K, let the fridge sit to the next day to see G1 how further it will increase?

* next day, G1 was still reading 107 mbar, no further increase.

* leave the dump closed, turn on the ^{3}He rotary pump, pump the 107 mbar and all the mixture left in the pipes using N_2 trap, put it in the front of the pump. Then close V6 and V1.

* since V1 and V6 are closed , P1 did not showed any leak in PVC pipe lines or the fridge side.

Having done this test, we are sure now the source of this leak in the fridge is either the IGH or the ^{3}He rotary pump.

To check which one is causing this problem, we need first, to warm up the fridge. Second, to cryopump all the gas mixture from the IGH and the rotary connection lines in order to be able to identify the source.

Connect the cryopump to the back of the IGH via the vent line. Clean the lines using external pump or the ^{3}He rotary pump then close rotary valve (but leave the one that connects the cryopump opened).

Make sure all the valves are closed. We need to cryopump the front and the back lines of the ^{3}He rotary pump. Starting at 740 mbar on G2, the cryopump holds 200 mbar when its inserted in liquid He dewar, this means that we need to repeat this process several times to make sure that no mixture is left in the lines. The process of cryopumping the gas mixture from the lines is performed as following:

- insert the cryopump into a liquid He dewar, open 12A, 13A, 2, and 7. Or, 12B, 13B, 2, and 7 if you want to use N_2 trap number 2.

- close 12A, 13A, 7, then open 3. Take the cryopump out of the dewar and warm it up using heat gun.

- close 3, put back the cryopump in the dewar and open 2, 7 12A, 13A, repeat this operation several times until the G2 reads 0 (this is an ideal case usually if there is no leak, otherwise G2 will sit at some value which is in our case 45 mbar), in the same time P1 must read some value rather than 0 because of the stuff we cryopumping in the still line where it has a very large volume.

- Now, in ^{3}He rotary pump and its lines,it's suppose to be empty (no gas mixture), G2 is still reading 45 mbar, by just running the ^{3}He rotary pump with 13A, 13B both closed, G2 starts to increase immediately from 45 to 250 mbar in 1 minute,(its only air not He).

This result has one interpretation; the problem is only in the ^{3}He rotary pump, not in the IGH. Also it suggests that the leak is from the rotary shaft seal or from the shaft it self. To cure this problem, we need to do a check on the ^{3}He rotary pump, or by changing the pump if that is possible. In our case we changed the pump with a new one.

The new pump oil has a lot of air dissolved in it, we must get rid of it. By pumping on the rotary pump using another efficient pump and by keep the new pump running, this will make sure the new oil would get hot, thus any unwanted dissolved particles would come out. We have do a leak check on the new pump using the vent line. Then we let the gas mixture go through the new pump using LN_2 trap and throttling V6 gradually, till the pressure on G2 goes to original value (with the extra stuff). We purify the gas mixture to go back to almost to 680 mbar which is the true value of the gas mixture, that is by letting it to go back and forth through the LN_2 trap to the still line and then pump it back to the dump. Usually its done by following these steps:

1- Use both LN_2 traps, A and B, V6 is closed, push the gas to the still line by opening V3 then throttle V10 till we empty the dump.

2- Close V6, V3, then open V4 and throttle V6 to fill the dump.

Appendix II

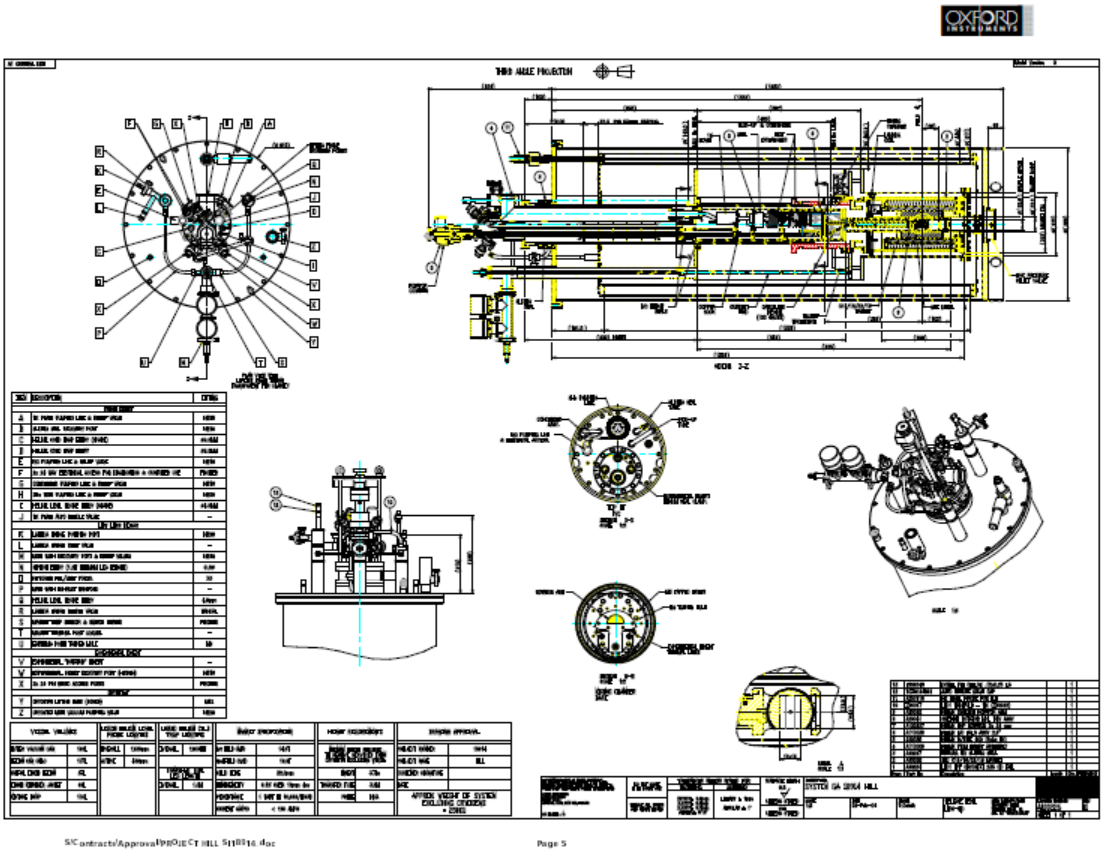

Figure 6.7: Schematic diagram of the fridge specs and dimensions.

Appendix III

To find the electron density of states

Starting from the number of states inside a sphere with radius k in k space.

The volume V of the sphere is $V = \frac{4}{3}\pi k^3$

The volume V_k of one unit cell (containing two states: spin up and spin down) is

$V_k = (\frac{2\pi}{L})^3$

This give the total number of states

$$N_s = 2\frac{V}{V_k} = \frac{4^3}{3\,.\,8\,.\,\pi^3} = \frac{k^3.L^3}{3\pi^2}$$

The density of states g(E) is primarily a density on the energy scale, and only secondarily a density in space, i.e.

$$g(E) = \frac{1}{V}\frac{dN_s}{dE} = \frac{1}{L^3}\frac{dN_s}{dE}$$

The wave vector is expressed in terms of energy as

$$E = \frac{\hbar k^2}{2m} \quad and \quad k = \pm(\frac{2Em}{\hbar^2})^{(\frac{1}{2})}$$

Insertion in the formula for N_s yields

$$N_s = \frac{L^3}{3\pi^2}(\frac{2Em}{\hbar^2})^{(\frac{3}{2})} = \frac{L^3}{3\pi^2}\frac{(2m)^{\frac{3}{2}}}{\hbar^3}E^{\frac{3}{2}}$$

Dividing by L^3 and differentiating with respect to E gives the density of states g

$$g(E) = \frac{1}{L^3}\frac{dN_s}{dE} = \frac{1}{2\pi^2}(\frac{2m}{\hbar^2})^{\frac{3}{2}}E^{\frac{1}{2}}$$

To fined the **density of electrons per unite volume n**, we start with Fermi energy and with the aid of the information from the previous derivation

$$E_F = \frac{\hbar^2 k_F^2}{2m} = \frac{\hbar^2}{2m}(\frac{3\pi^2 N}{V})^{\frac{2}{3}} = \frac{\hbar^2}{2m}(3\pi^2 n)^{\frac{2}{3}}$$

where N is the number of electrons in the state.

Thus total number of orbitals of energy $<$ E will be

$$\mathrm{N(E)} = \frac{V}{3\pi^2}(\frac{2mE}{\hbar^2})^{\frac{3}{2}}$$

And the density of state is then

$$g(E) = \frac{dN}{dE} = \frac{V}{2\pi^2}(\frac{2m}{\hbar^2})^{\frac{3}{2}} E^{\frac{1}{2}}$$

or equivalently

$$g(E) = \frac{3N}{2E}$$

Thus $n = \frac{2}{3} g(E) E_F$, where n= (N/V).

Bibliography

[1] A. A. Abrikosov. *Reviews of Modern Physics*, 76, Page 974-978, 2004. x, 17, 18

[2] N. W. Ashcroft and N. David Mermin. *Solid State of Physics*. 1979. 4, 7, 9, 10, 11, 17

[3] J. S. Blakemore. *Solid State Physics*. W. B. Saunders Company, Philadellphia, London, Toronto, 1969. 9, 12

[4] E. G. D. Cohen. *Journal of Science*, 197, No 11-16, Page 4289, 1977. 25

[5] B. Andraka et. al. *Phys. Rev. B*, 81, 054509, 2010. 95

[6] D. E. Maclaughlin et. al. *Physica B*, 403, Page 1132-1134, 2008. 99

[7] G. Seyfarth et. al. *Phys. Rev. Lett.*, 95, 107004, 2005. xv, 98, 99

[8] G. Seyfarth et. al. *Phys. Rev. Lett.*, 2006. 99

[9] H. Shakeripour et. al. *New Journal of Physics*, 11, May 2009. x, 2, 20, 21, 22

[10] H. Suderow et. al. *Phys. Rev. B*, 69, 060504(R), 2004. 99

[11] Izawa et. al. *Phys. Rev. Lett.*, 90, 117001, 2003. 97, 99

[12] M. B. Maple et. al. *ACTA PHYSICA POLONICA B*, 34, No 2, 2003. 95

[13] M. J. Graft et. al. *Phys. Rev. B*, 53, No 22, Page 15147, 1996. 21

[14] R. W. Hill et. al. *Phys. Rev. Lett.*, 101, 237005, 2008. xv, 2, 97, 98

[15] S. N. Ehrlich et. al. *Journal of Low Temperature Physics*, 68, No 1-2, July, 1987. 30

[16] Shigeru Kasahara et. al. *Physica C 460-462*, (2007) 696-697. 97

[17] T. R. Abu Alrab et. al. *Phys. Rev. B*, 76, 184511, 2007. x, 19, 99

[18] T. R. Abu Alrab et. al. *Phys. Rev. B*, 76, 054514, 2007. 99

[19] W. Steinwarz et. al. *Nuclear engineering and Design*, 78, 267-272, 1984. 25

[20] Y. Aoki et. al. *Jour. Phys. Soc. Jap.*, 71, Page 2098, 2002. 95

[21] Y. Karaki et. al. *Journal of Physics: Conference Series 150*, 2009 (052094). 95

[22] M. B. Maple et.al. *Journal of Superconductivity and Novel Magnetism*, 19, No 3-5, July, 2006. 95, 97

[23] Frolich. *Phys. Rev.*, 79, Page 845, 1950. 15

[24] T. Hirata and Y. Asada. *Journal of Superconductivity*, 4, Page 171, 1991. 16

[25] Oxford Instruments. *Oxford Manual*. 2007. xi, 34, 35, 37

[26] L.N. Cooper J. Bardeen and J. R. Schrieffer. *Phys. Rev.*, 108, Page 1175, 1957. 15

[27] J. Batchelor J. P. Harris, B. Yates and P. J. Garrington. *Journal of Materials Science*, volume 17. 59

[28] Charles Kittel. *Introduction to Solid State Physics. eighth Edition.* University of California, Berkeley, November, 2004. 4, 10

[29] Charles G. Kuper. *An Introduction to the Theory of Superconductivity.* Clarendon Press, Oxford, 1968. 17

[30] P. A. Lee. *Phys. Rev. Lett.*, 71, Page 1887, 1993. 21

[31] Kendall White Philip J. Meeson. *Experimental Techniques in Low Temperature Physics.* Oxford Science publication, by Oxford University Press Inc., New York. xi, 27, 30, 33, 42, 62

[32] Frank Pobell. *Matter and Methods at low Temperaturres - 2nd Edition.* Springer, Germany, 1995. xi, xii, 8, 25, 26, 27, 28, 29, 31, 59, 60, 61, 62

[33] C.H. Watson et. al. Q. Li. *Cryogenics*, 26, Page 467-470, August/September 1986. 60

[34] H. M. Rosenberg. *The Thermal Conductivity of Metals at low Temperatures*, volume 247, No. 933, Page 441-497. The Royal Society, 1955. ix, 13

[35] H. M. Rosenberg. *Low Temperature Solid State Physics.* Oxford at the Calerndon press, 1965. ix, 8, 9

[36] Brian C. Sales. *Filled Skutterudites*. Oak Ridge National Laboratory, Oak Ridge, Tennessee, 2002. xv, 95, 96

[37] C. B. Satterthwaite. *Phys. Rev.*, 125, No. 3, Page 873, 1962. x, 20

[38] J. R. Schrieffer. *Nobel Lecture, Physics Today*, 23, 1973. 20

[39] Steven W. Van Sciver. *Helium Cryogenics*. Plenum Press, New York, N. Y. 10013, 1986. 25

[40] Michael Tinkham. *Introduction to Superconductivity*. Dover Publications Inc., Mineola, N.Y. 11501 Oxford, 1996. 16, 17, 19

[41] Terry M. Tritt. *Thermal Conductivity. Theory, Properties, and Applications*. Kluwer Academic/Plenum Publishers, New York, N. Y. 10013, 2004. 6, 9, 10, 12

[42] D. R. White and S. P. Benz. *Metrologia*, 45, Page 93-101, 2008. 65

[43] G. Wiedemann and R. Franz. *Ann. Phys.*, 89, 479-531, 1853. 12

[44] J. M. Ziman. *The Theory of Transport Phenomena in Solids*. Oxford at the Claredon press, 1960. 4, 5, 8